



저작자표시-비영리-변경금지 2.0 대한민국

이용자는 아래의 조건을 따르는 경우에 한하여 자유롭게

- 이 저작물을 복제, 배포, 전송, 전시, 공연 및 방송할 수 있습니다.

다음과 같은 조건을 따라야 합니다:



저작자표시. 귀하는 원저작자를 표시하여야 합니다.



비영리. 귀하는 이 저작물을 영리 목적으로 이용할 수 없습니다.



변경금지. 귀하는 이 저작물을 개작, 변형 또는 가공할 수 없습니다.

- 귀하는, 이 저작물의 재이용이나 배포의 경우, 이 저작물에 적용된 이용허락조건을 명확하게 나타내어야 합니다.
- 저작권자로부터 별도의 허가를 받으면 이러한 조건들은 적용되지 않습니다.

저작권법에 따른 이용자의 권리는 위의 내용에 의하여 영향을 받지 않습니다.

이것은 [이용허락규약\(Legal Code\)](#)을 이해하기 쉽게 요약한 것입니다.

[Disclaimer](#)

Master's Thesis

Design and Analysis of a 2kW Wind Turbine with a Flange Type Velocity Booster for Low Wind Speeds

Supervisor: Professor Young-Ho LEE, Ph.D



August 2018

**Department of Mechanical Engineering
Graduate School of Korea Maritime and Ocean University**

P. Chanaka Hasitha Weerasena

We certify that we have read this thesis and that, in our opinion, it is satisfactory in scope and quality as a thesis for the degree of Master of Mechanical Engineering, submitted by **Pandigamage Chanaka Hasitha Weerasena**.

THESIS COMMITTEE

Chairperson: Prof. Dr. Dong-Woo Sohn

Devision of Mechanical Engineering, Korea Maritime and Ocean University


.....

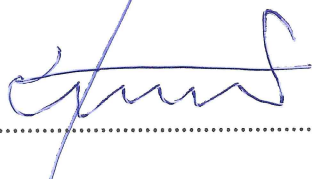
Co-Chairperson: Dr. Byung-Ha Kim

Devision of Mechanical Engineering, Korea Maritime and Ocean University


.....

Supervisor: Prof. Dr. Young-Ho Lee

Devision of Mechanical Engineering, Korea Maritime and Ocean University


.....

June 2018

Department of Mechanical Engineering

Graduate School of Korea Maritime and Ocean University

본 논문을 P. Chanaka Hasitha Weerasena 의
공학석사 학위논문으로 인준함



위원장: 손 동 우



위 원: 이 영 호



위 원: 김 병 하



2018 년 06 월 28 일

한국해양대학교 대학원

기겨공학과

Table of contents

List of figures.....	iv
List of tables.....	viii
Abstract.....	x
Nomenclature.....	xii
Abbreviations.....	xiv
Chapter 1. Introduction.....	1
1.1. Background.....	1
1.2. Generation of wind	2
1.3. Classification of wind turbines	3
1.3.1. Rotor size and scale.....	3
1.3.2. Drag and lift wind machines	3
1.3.3. Horizontal and vertical axis wind turbines.....	4
1.4. Wind turbines with velocity augment devices	8
1.5. Purpose of the research	11
Chapter 2. Theory behind wind turbine design	12
2.1. Introduction.....	12
2.2. Actuator Disc Model.....	12
2.3. Angular Momentum.....	15
2.4. Blade Element Theory	17
2.4.1. Tip Losses	19
2.5. Blade Element Momentum (BEM) Theory.....	20
Chapter 3. Design of 2kW wind turbine and flange type velocity boosters	22
3.1. Determining the design wind speed	22

3.2.	Calculating the Rotor Diameter and Rated Rotational Speed	23
3.3.	Tip loss correction.....	23
3.4.	Flow induction factors	24
3.5.	Air foil selection	26
3.6.	Chord length calculations.....	31
3.7.	Twist angle calculations.....	32
3.8.	Optimized blade parameters.....	34
3.9.	Flange type velocity booster designs	36
Chapter 4.	CFD analysis.....	42
4.1.	Computational fluid dynamics	42
4.1.1.	Introduction.....	42
4.1.2.	Governing equations	42
4.1.3.	Creating the geometry	43
4.1.4.	Defining the simulation settings and boundary conditions	43
4.1.5.	Mesh generation.....	44
4.1.6.	Solving the simulation	45
4.1.7.	Post processing.....	46
4.2.	NREL Phase VI Turbine analysis	46
4.3.	2 kW wind turbine analysis.....	53
4.4.	Flange type velocity booster analysis	58
4.5.	2 kW wind turbine analysis with flange type velocity boosters.....	62
Chapter 5.	Results and Discussion	72
5.1.	NREL Phase VI turbine	72
5.2.	2 kW turbine	76
5.3.	Flange type velocity booster models.....	82

5.4.	Wind tunnel experiment.....	87
5.5.	2 kW turbine with different flange type velocity booster models.....	98
5.6.	Scaled down turbine-booster system.....	108
Chapter 6.	Conclusions.....	110
	Acknowledgement	112
	References.....	113



List of figures

Figure 1.1 Global cumulative installed wind capacity 2001-2017	2
Figure 1.2 Global wind circulation patterns	2
Figure 1.3 Savonius rotor wind turbine	4
Figure 1.4 Vertical axis wind turbine configurations	5
Figure 1.5 Horizontal axis wind turbine configurations	6
Figure 1.6 Components of a large scale HAWT	7
Figure 1.7 Shrouded turbine developed by Kyushu University	9
Figure 1.8 Ogin (FloDesign) wind turbine	10
Figure 1.9 Vortec 7 turbine	10
Figure 2.1 Actuator disk model of a wind turbine	13
Figure 2.2 Velocity behind the turbine disc	16
Figure 2.3 Definition of blade element according to the theory	18
Figure 2.4 Velocities and forces acting on a blade element	19
Figure 3.1 Average wind capacity in Sri Lanka	22
Figure 3.2 Prandtl's Tip Loss Coefficient	24
Figure 3.3 Axial flow induction factor.....	25
Figure 3.4 Tangential flow induction factor	26
Figure 3.5 NACA 634421 airfoil	27
Figure 3.6 FX 76 MP 140 airfoil	27
Figure 3.7 Air foils and their span wise locations.....	28
Figure 3.8 Lift coefficient variation with angle of attack	29
Figure 3.9 Cl/Cd variation with angle of attack.....	30
Figure 3.10 Distribution of chord length at each section	32
Figure 3.11 Twist angle distribution	33
Figure 3.12 Isometric view of the blade	35
Figure 3.13 Isometric view of the turbine rotor	35
Figure 3.14 Parameters of flange type velocity booster.....	36
Figure 3.15 Sectional 2-D drawing of booster model 1	38
Figure 3.16 Isometric view of booster model 1	38
Figure 3.17 Sectional 2-D drawing of booster model 2	39

Figure 3.18 Isometric view of booster model 2	39
Figure 3.19 Sectional 2-D drawing of booster model 3	40
Figure 3.20 Isometric view of booster model 3	40
Figure 3.21 Sectional 2-D drawing of booster model 4	41
Figure 3.22 Isometric view of booster model 4	41
Figure 4.1 3-D cell-centered control volume	45
Figure 4.2 NREL phase VI turbine	47
Figure 4.3 Sectional view of the blade.....	48
Figure 4.4 3-D blade model	48
Figure 4.5 3-D model of the NREL phase VI turbine.....	49
Figure 4.6 Numerical domain of NREL phase VI turbine case	50
Figure 4.7 Sectional view of the volume mesh	51
Figure 4.8 Zoomed sectional view of the volume mesh closer to the turbine region ...	51
Figure 4.9 Surface mesh of the blade.....	52
Figure 4.10 Y plus values on blade surface	52
Figure 4.11 Sectional view of the blade.....	53
Figure 4.12 3-D blade model	53
Figure 4.13 3-D model of the 2 kW turbine.....	54
Figure 4.14 Numerical domain of 2 kW turbine case	55
Figure 4.15 Sectional view of the volume mesh	56
Figure 4.16 Zoomed sectional view of the volume mesh closer to the turbine region .	56
Figure 4.17 Surface mesh of the blade.....	57
Figure 4.18 Y plus values on blade surface	57
Figure 4.19 Numerical domain of flange type velocity booster analysis.....	59
Figure 4.20 Sectional view of the volume mesh	60
Figure 4.21 Zoomed sectional view of the volume mesh closer to the booster region .	60
Figure 4.22 Surface mesh of the booster model 1.....	61
Figure 4.23 Surface mesh of the booster model 2.....	61
Figure 4.24 Surface mesh of the booster model 3.....	62
Figure 4.25 Surface mesh of the booster model 4.....	62
Figure 4.26 2 kW turbine with booster model 1	63
Figure 4.27 2 kW turbine with booster model 2	63

Figure 4.28 2 kW turbine with booster model 3	64
Figure 4.29 2 kW turbine with booster model 4	64
Figure 4.30 Numerical domain of turbine and booster combine systems	66
Figure 4.31 Sectional view of the volume mesh	67
Figure 4.32 Zoomed sectional view of the volume mesh closer to the turbine region .	67
Figure 4.33 Surface mesh of the 2 kW turbine and booster model 1	68
Figure 4.34 Y plus values on 2 kW turbine and booster model 1	68
Figure 4.35 Surface mesh of the 2 kW turbine and booster model 2	69
Figure 4.36 Y plus values on 2 kW turbine and booster model 2	69
Figure 4.37 Surface mesh of the 2 kW turbine and booster model 3	70
Figure 4.38 Y plus values on 2 kW turbine and booster model 3	70
Figure 4.39 Surface mesh of the 2 kW turbine and booster model 4	71
Figure 4.40 Y plus values on 2 kW turbine and booster model 4	71
Figure 5.1 Thrust comparison	73
Figure 5.2 Torque comparison	74
Figure 5.3 Power comparison	75
Figure 5.4 Velocity distribution in the plane perpendicular to turbine rotation.....	76
Figure 5.5 Velocity distribution in the plane of the turbine rotation.....	76
Figure 5.6 Thrust variation with TSR	77
Figure 5.7 Torque variation with TSR	78
Figure 5.8 C_p variation with TSR	79
Figure 5.9 Power variation with TSR	80
Figure 5.10 Velocity distribution in the plane perpendicular to turbine rotation.....	81
Figure 5.11 Velocity distribution in the plane of the turbine rotation.....	81
Figure 5.12 Velocity distribution in the middle region.....	83
Figure 5.13 Velocity distribution in the critical region.....	84
Figure 5.14 Velocity distribution in the total area	85
Figure 5.15 Average velocity distribution	86
Figure 5.16 Wind tunnel facility	87
Figure 5.17 Velocity measuring point and booster placement in the wind tunnel	88
Figure 5.18 Booster orientation in the wind tunnel.....	88
Figure 5.19 Velocity measuring points inside the booster	89

Figure 5.20 Percentage velocity increase through booster model 3 at free stream wind velocity of 5 m/s	90
Figure 5.21 Percentage velocity increase through booster model 3 at free stream wind velocity of 7.5 m/s	91
Figure 5.22 Percentage velocity increase through booster model 3 at free stream wind velocity of 10 m/s	92
Figure 5.23 Percentage velocity increase through booster model 3 at free stream wind velocity of 12.5 m/s	93
Figure 5.24 Percentage velocity increase through booster model 4 at free stream wind velocity of 5 m/s	94
Figure 5.25 Percentage velocity increase through booster model 4 at free stream wind velocity of 7.5 m/s	95
Figure 5.26 Percentage velocity increase through booster model 4 at free stream wind velocity of 10 m/s	96
Figure 5.27 Percentage velocity increase through booster model 4 at free stream wind velocity of 12.5 m/s	97
Figure 5.28 Torque comparison	99
Figure 5.29 Comparison of power coefficient	101
Figure 5.30 Power comparison	103
Figure 5.31 Velocity distribution of turbine with booster model 1 in the plane perpendicular to turbine rotation	104
Figure 5.32 Vorticity around booster model 1	104
Figure 5.33 Velocity distribution of turbine with booster model 2 in the plane perpendicular to turbine rotation	105
Figure 5.34 Vorticity around booster model 2	105
Figure 5.35 Velocity distribution of turbine with booster model 3 in the plane perpendicular to turbine rotation	106
Figure 5.36 Vorticity around booster model 3	106
Figure 5.37 Velocity distribution of turbine with booster model 4 in the plane perpendicular to turbine rotation	107
Figure 5.38 Vorticity around booster model 4	107
Figure 5.39 Power variation of scaled down turbine with wind velocity	109

List of tables

Table 1.1 Classification of wind turbines by rotor size	3
Table 3.1 Aerodynamic characteristics of chosen airfoils	31
Table 3.2 Geometric parameters of the blade	34
Table 3.3 Non dimensional parameters of the flange type velocity booster	37
Table 4.1 Basic settings for NREL phase VI turbine simulation	49
Table 4.2 Boundary conditions for NREL phase VI turbine	50
Table 4.3 Basic settings for 2 kW turbine simulation	54
Table 4.4 Boundary conditions for 2 kW turbine	55
Table 4.5 Basic settings for flange type velocity booster simulations	58
Table 4.6 Boundary conditions for flange type velocity booster simulations	58
Table 4.7 Basic settings for turbine and booster combine system simulations	65
Table 4.8 Boundary conditions for turbine and booster combine systems	65
Table 4.9 Cell count in the mesh	66
Table 5.1 Thrust comparison	73
Table 5.2 Torque comparison	74
Table 5.3 Power comparison	75
Table 5.4 2 kW turbine overall results	77
Table 5.5 Average velocity distribution	86
Table 5.6 Velocity distribution through booster model 3 at free stream wind velocity of 5 m/s	90
Table 5.7 Velocity distribution through booster model 3 at free stream wind velocity of 7.5 m/s	91
Table 5.8 Velocity distribution through booster model 3 at free stream wind velocity of 10 m/s	92
Table 5.9 Velocity distribution through booster model 3 at free stream wind velocity of 12.5 m/s	93
Table 5.10 Velocity distribution through booster model 4 at free stream wind velocity of 5 m/s	94
Table 5.11 Velocity distribution through booster model 4 at free stream wind velocity of 7.5 m/s	95

Table 5.12 Velocity distribution through booster model 4 at free stream wind velocity of 10 m/s.....	96
Table 5.13 Velocity distribution through booster model 4 at free stream wind velocity of 12.5 m/s.....	97
Table 5.14 Torque comparison	99
Table 5.15 Comparison of power coefficient.....	100
Table 5.16 Power comparison.....	102
Table 5.17 Power variation with wind velocity	108



Design and Analysis of a 2kW Wind Turbine with a Flange Type Velocity Booster for Low Wind Speeds

P. Chanaka Hasitha Weerasena

*Department of Mechanical Engineering
Graduate School of Korean Maritime and Ocean University*

Abstract

Demand for the energy is raising with the population growth and technological advancement. There is a global trend to invest in renewable sources of energy to fulfil that demand due to increasing environmental effects which fossil fuels cause on earth. Other than this, renewable energy sources are ideal for places where there is no reliable electrical access.

Similar situation occurred in Sri Lankan dairy industry, where small scale dairy farmers need a reliable source of power for their milk cooling systems, wind-PV hybrid system was proposed to fulfil their energy needs.

This study is focused on designing a wind turbine for above project. Region where this wind turbine is to be installed is subjected to low wind conditions. Thus, wind speed augment device is also needed, and designed.

First NREL pulse VI turbine was modelled and analyzed in Star CCM+ which is a finite volume based commercial CFD code. Then the available experimental data was used to compare numerical results. Comparison indicates satisfactory similarity. Thus, numerical code can be considered as valid and later used for wind turbine analysis of this project.

Then, a 2 kW horizontal axis wind turbine was designed using NACA 634421 and FX 76 MP 140 air foils according to Blade Element Momentum theory. Then the performance characteristics of the turbine was evaluated using star CCM+. Power output of the turbine at designed wind velocity 7.5 m/s and TSR 7.5 was 2273.4 W. Power coefficient is 0.48 at this point which indicates the success of design.

Next, four flanged type velocity booster models were designed with size constraints considering manufacturing and handling easiness. Flow behavior through these booster

models were numerically analyzed. Scaled down models of 2 of these boosters were tested in a wind tunnel and numerical data were validated against those experimental results.

Finally previous turbine was again analyzed numerically for its performances with each of four booster models. All four models indicated significant improvement in performances of the turbine. Turbines with booster model 1 and booster model 3 indicated similar behavior and improve the power output by a factor of 2 compared to the stand-alone turbine, while turbine with booster model 2 indicated slightly lower performance with power output increase by a factor of 1.98. Booster model 4 indicated even lower performances, but still increased the power output by a factor of 1.7. Both booster model 1 and 3 are recommended to use for smaller turbines considering their higher performance. Booster model 4 is also suitable, despite its comparatively lower performance due to its compact design. Considering the power requirement and size of this turbine, booster model 4 was selected due to its size and performance. Required power output was achieved using scaled down turbine and booster by 25% of its original design size. This was an additional advantage which leads to lower structural loads and lower material usage.

Key words: Small scale wind turbine, Wind augment device, Computational Fluid Dynamics, Flange type velocity booster

Nomenclature

A_1	Upstream cross sectional area	$[m^2]$
A_4	Downstream cross sectional area	$[m^2]$
a	Axial induction factor	$[-]$
a'	Tangential induction factor	$[-]$
A_d	Cross sectional area of the actuator disc	$[m^2]$
B	Number of blades	$[-]$
C	Chord length	$[m]$
C_d	Drag coefficient	$[-]$
C_l	Lift coefficient	$[-]$
$C_{l/d}$	Lift to drag ratio	$[-]$
C_p	Coefficient of power	$[-]$
D	Rotor diameter	$[m]$
F	Force on blade	$[N]$
f	Prandtl's tip loss factor	$[-]$
\dot{m}	Mass flow rate of wind	$[kg/s]$
N	Number of blade sections	$[-]$
N_{rpm}	Rated rotational speed	$[rpm]$
P_1	Upstream pressure	$[Pa]$
P_2	Pressure before actuator disc	$[Pa]$
P_3	Pressure after actuator disc	$[Pa]$
P_4	Downstream pressure	$[Pa]$
R	Turbine radius	$[-]$
r	Radial position on blade	$[m]$
U_2	Upstream wind velocity	$[m/s]$
U_2	Wind velocity before actuator disc	$[m/s]$
U_3	Wind velocity after actuator disc	$[m/s]$
U_4	Downstream wind velocity	$[m/s]$
V_D	Design wind velocity	$[m/s]$
W_1	Tangential induced velocity in turbine region	$[m/s]$

W_2	Tangential induced velocity after turbine	[m/s]
α	Angle of attack	[°]
β	Pitch angle	[°]
η	Efficiency of the generator	[-]
θ	Twist angle	[°]
λ	Tip speed ratio	[-]
μ	Local position of the blade	[-]
ρ	Density of air	[kg/m]
ϕ	Inflow angle	[°]
Ω	Rotational rate	[rad/s]



Abbreviations

2-D	Two dimensional
3-D	Three dimensional
BEM	Blade element momentum
CAD	Computer aided design
CFD	Computational fluid dynamics
CV	Control volume
FVM	Finite volume method
HAWT	Horizontal axis wind turbine
ITCZ	Inter-tropical convergence zone
PV	Photovoltaic
SST	Shear stress transport
TSR	Tip speed ratio
VAWT	Vertical axis wind turbine



Chapter 1. Introduction

1.1. Background

There is a higher tendency in the world to shift into renewable sources of energy due to the huge effect which fossil fuels are having on environment. Growth of energy demand, shrinking the fossil fuel resources and increase of fuel price also forcing the world to do more research on alternative sources of energy.

According to the International Energy Agency “Renewable energy is derived from natural processes that are replenished constantly. In its various forms, it derives directly from the sun or from heat generated from the earth. Electricity and heat generated from solar, wind, ocean, hydropower, biomass, geothermal resources, bio fuels and hydrogen derived from renewable resources” [1].

It is very important to develop techniques in order to harness energy from all above sources. Wind energy, which is the focus in this study, has a tremendous development in both research and commercial sector compared to the other sources of renewable energy. According to the Global Wind Statistic- 2017 report published by Global Wind Energy Council [2] worldwide wind energy capacity reached to 539,581 MW. It is expected to increase up to 817,000 MW by the end of 2021 [3]. Global annual installed wind capacity is higher than 40 GW until 2017 from 2011 [2]. It is also expected to increase annually with the improvement of the technology and reduction of the cost.

Wind energy has become one of the most economical renewable energy technology in recent years. Today, wind turbines provide secure and sustainable supply of energy due to its proven and tested technology. At windy sites wind energy can successfully compete with conventional energy production. Recent development of technology caused to develop bigger, reliable and more efficient wind turbines. Especially the increase of offshore employment of wind turbines has lead the wind energy sector to expand their territory and capacity.

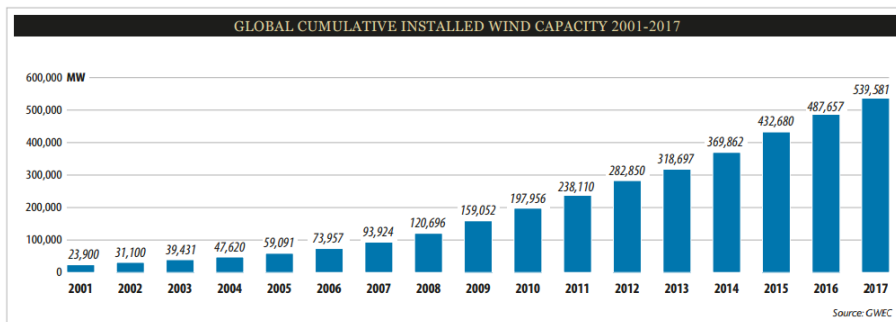


Figure 1.1 Global cumulative installed wind capacity 2001-2017 [2]

1.2. Generation of wind

Atmospheric pressure differences occur due to the uneven heating of the earth by sun, causes the wind generation. In a simple model, air would rise from the equator and sink at the poles due to the fact that more solar radiation is absorbed in the equator than in the poles. But due to the seasonal variation, the circulation of the wind is more complex. Figure 1.2 shows the typical patterns of the wind. In addition to the above affects, internal forces of the wind itself and the friction of the earth's surface also affects the wind patterns [4].

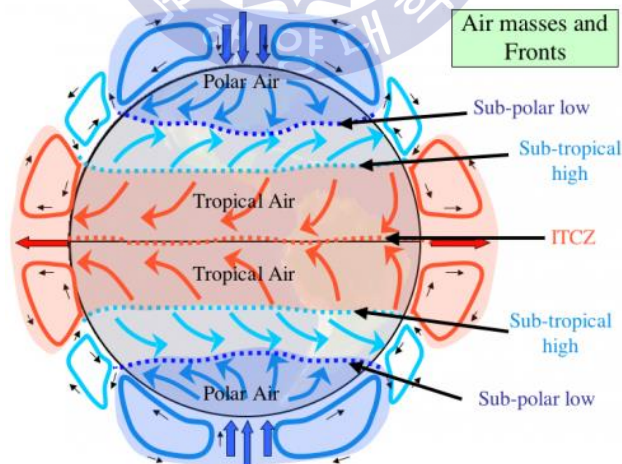


Figure 1.2 Global wind circulation patterns [5]

1.3. Classification of wind turbines

Few methods are used to classify wind turbines. They are based on the size and scale, lift or drag type and horizontal or vertical axis type.

1.3.1. Rotor size and scale

Wind turbines have a wide scale and size variation. Because of that a classification system according to the various sizes is very important. Table 1.1 shows the classification of wind turbines based on its size and scale. [6].

Table 1.1 Classification of wind turbines by rotor size

Scale	Power Rating	Rotor Diameter
Micro	50 W to 2 kW	less than 3m
Small	2 kW to 40 kW	3m to 12 m
Medium	40 kW to 999 kW	12m to 45m
Large	More than 1 MW	larger than 46m

1.3.2. Drag and lift wind machines

Drag type wind machines will be discussed first. In these turbines the force of the wind pushes against a surface like in an open sail, which were used in ancient Persia where this technique started. Savonius rotor is a simple drag based wind turbine which is used nowadays. Since the vertical rotor moves along the wind, it is impossible for the turbine to rotate faster than the wind. This results in a very low efficiency. An example for this type of wind turbine is indicated in figure 1.3.

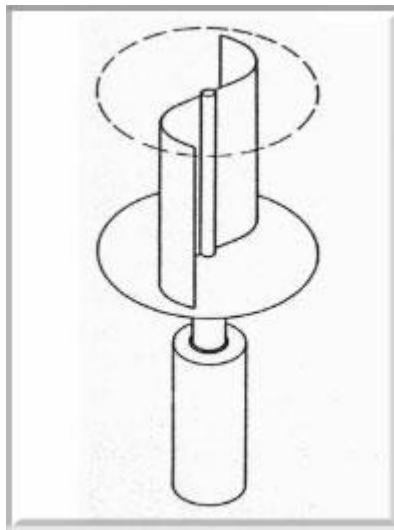


Figure 1.3 Savonius rotor wind turbine [7]

Lift type wind turbines have blades that are similar to wings of an airplane. These blades move at a higher speed than the actual wind. They work with the wind unless against the wind, as drag type machines do. This type of wind turbines need less materials compared to the drag type wind turbines, due to its blades cover only a fraction of the rotor surface. Furthermore these turbines have a higher efficiency compared to the drag type wind turbines. [8, 9]. Due to all these reasons, lift type wind turbines are widely used around the world.

1.3.3. Horizontal and vertical axis wind turbines

Horizontal Axis Wind Turbines (HAWT) and Vertical Axis Wind Turbines (VAWT) are classified based on the axis of rotation of the wind turbine. As indicated in their names HAWT spins parallel to the ground while VAWT rotates perpendicular to the ground. Most of the early stage wind turbines were VAWTs, due to their relative simplicity and their ability to capture wind from any direction without an additional mechanism to orient them for wind direction. But most of them were not successful.

There are three current popular design of VAWTs namely, curved- blade Darrieus VAWT, Savonius VAWT and Straight-blade VAWT.

Several configurations of VAWTs are indicated in figure 1.4.

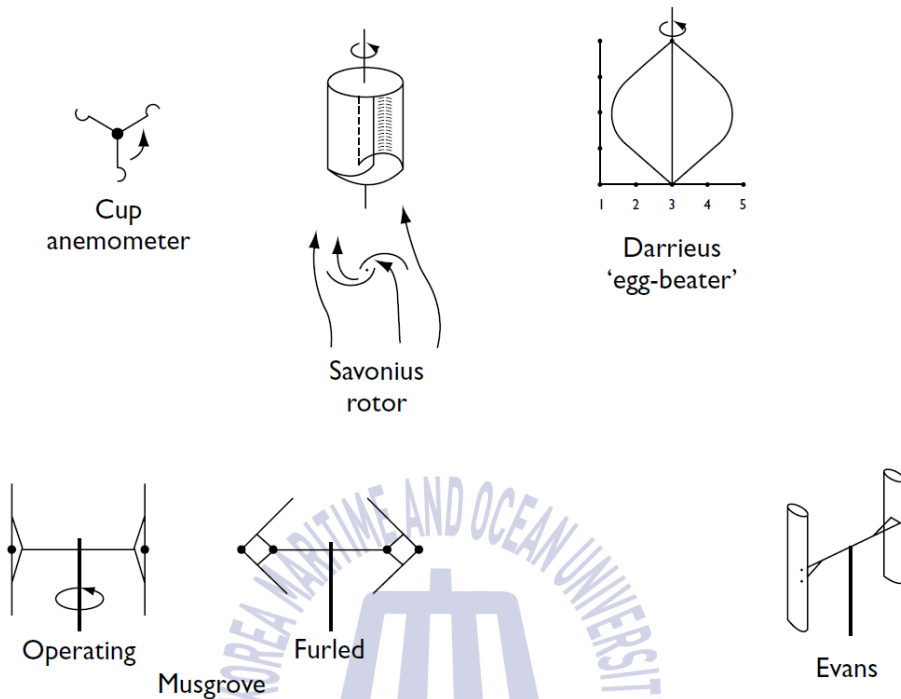


Figure 1.4 Vertical axis wind turbine configurations [10]

HAWT are the most popular among all types of wind turbines at present. Main reason behind this is the higher efficiencies that HAWTs' can achieve. These HAWTs can be further categorized into sub categories as shown in figure 1.5.

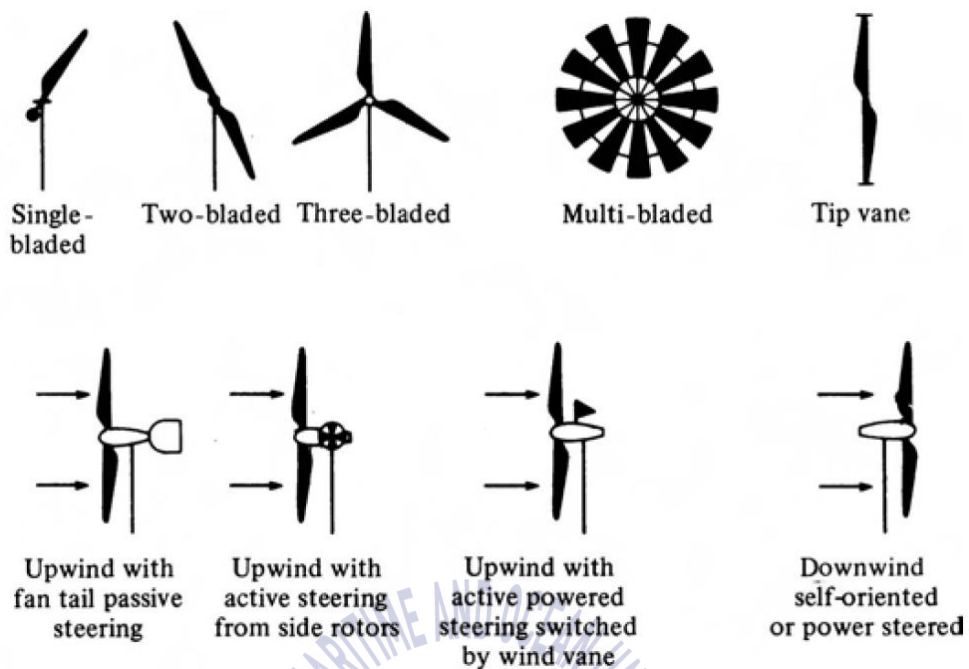


Figure 1.5 Horizontal axis wind turbine configurations [10]

HAWTs are highly sensitive to changes in blade profile, design and surface roughness because they are lift type wind turbines. Other drawback of this type of wind turbine is their inability to catch the wind from all directions without a yaw system. Yaw system is responsible to orient the turbine rotor to the wind direction. Small size wind turbines use “Passive yaw system”. It comprises with simple roller bearing connected between the tower and nacelle and a tail with a fin which is mounted back of nacelle which produces corrective moment to turn the wind turbine rotor into the wind.

Larger scale wind turbines on the other hand have “active yaw system” which equipped with a wind sensor and servo motor, which allows it to sense the wind direction and orient accordingly. Components and their functions of a large scale HAWTs are indicated in figure 1.6 since this type is the most widely used wind turbine nowadays.

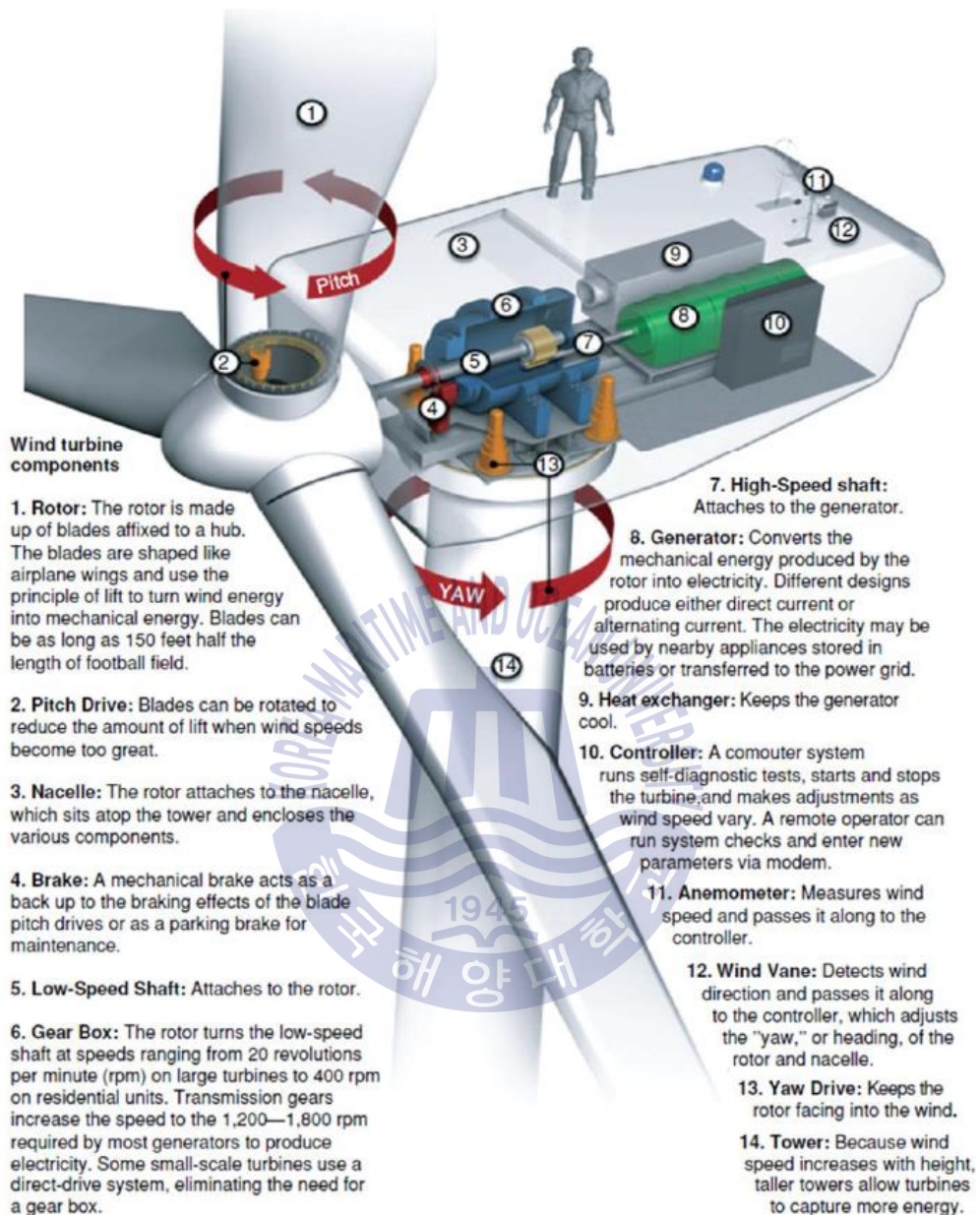


Figure 1.6 Components of a large scale HAWT [11]

1.4. Wind turbines with velocity augment devices

These wind turbines use a mechanism to draw more wind in to the turbine. There are various designs and types of these turbines. But most of them are under research and development stage.

Since the power generation from wind is proportional to the wind speed cubed, it is clear that even a slight increase of wind velocity can contribute for higher power output of the turbine. So, that is the main concern behind these types of devices. Additionally, these devices can increase the wind velocity even in very low wind conditions. This enable their ability to operate in very low wind conditions.

Turbine with flanged type diffuser which was developed in Kyushu University [12, 13] achieved four to five times increase in output power compared with conventional wind turbines. Due to the flange at the exit, diffuser automatically rotate accordingly to the change in the wind direction. Hence the requirement of an additional yaw mechanism also eliminated. Due to the vortices generated from the blade tips are considerably suppressed through the interference with boundary layer within the diffuser, aerodynamic noise is also reduced according to them. Additionally, safety of the wind turbine also increased to the fact that the diffuser acting as a guard wall from damaged or broken blades. Turbine which was developed by Kyushu University is indicated in figure 1.7.



Figure 1.7 Shrouded turbine developed by Kyushu University [12]

Main disadvantage of this turbine is its large structure. Its diffuser is twice the size of its turbine. This leads to huge support structures and practically hard to implement in many situations. Due to these reasons, one could simply increase the size of the rotor and accomplish the same increase in energy output with less material usage, since materials required for the rotor is much less than that needed for the diffuser. Some of the other attempts with similar diffuser type wind turbines are indicated in figure 1.8 and figure 1.9.



Figure 1.8 Ogin (FloDesign) wind turbine [14]



Figure 1.9 Vortec 7 turbine [14]

1.5. Purpose of the research

A milk cooling system with a wind-PV hybrid system is proposed to Sri Lankan milk farmers. Necessity of this system and the part which is covered under this thesis is explained below.

Sri Lanka, as a developing economy has a steady increase in their demand for the milk. On the other hand, 58 % of current milk supply is from small scale dairy farmers who are mostly located in remote areas of the country. 20% of their milk is rejected in collecting centers due to the bad quality [15]. Remaining milk price also varies from 43.25 to 77.25 Sri Lankan Rupees per litter depending on its quality. This is a huge economical loss for both local farmers as well as for the country. Main reason behind this milk waste is lack of cooling facilities. It takes a long time for farmers to transport their milk to milk collecting centers. They even have to keep their milk which they got in the evening, stored overnight until the collecting vehicle arrives next day morning. Sri Lanka being a tropical country, is always subjected to warmer weather conditions ranging from 20 °C to 37 °C throughout the year, which leads this milk to deteriorate very quickly. So, an affordable cooling system is proposed. An ice-making system, as the cooling method which is powered by a wind-solar hybrid system is proposed to address the above issue. Ice which will be made by the above system can later be used to milk cooling with a specially designed insulated milk collecting tanks.

Developing a wind turbine with a flange type velocity booster for the above system is carried out and presented here in this thesis. This method was chosen mainly, in order to increase the power output. However, increase the wind velocity and improve the ability to use the system even in lower wind conditions are also important aspects for choosing this method, for the reason that most of the small-scale dairy farms where this system will be employed are subjected to low wind conditions. Design of the wind turbine, numerical analysis of stand-alone turbine and turbine with flange type velocity booster is explained in coming chapters.

Chapter 2. Theory behind wind turbine design

2.1. Introduction

Wind turbines are used to convert kinetic energy into mechanical energy. The fundamental theory of design and operation of wind turbines are derived based on an approach conserving the mass and energy in a wind stream. This was first shown by Albert Betz. He showed the extractable mechanical energy of a certain cross-sectional area of an air stream is restricted to a proportion of the available energy in the stream. Additionally, he found out that the optimal point of highest power conversion can be determined by the ratio of the flow velocity behind the converter [16]. Classical analysis method is based on the Momentum theory and Blade Element theory. Combined theory is known as Blade Element Momentum Theory (BEM) which is described in this chapter.

2.2. Actuator Disc Model

Wind turbine is considered as an actuator disc in this concept. Following assumption are made to explain the concept with momentum theory. Flow is steady, homogenous and air is incompressible. Number of turbine blades is infinite and there is no frictional drag. The static pressure for upstream and far downstream of the actuator disk is taken as equal to ambient static pressure and wake is non-rotating.

Consider a stream tube of an air stream flowing through the actuator disc as shown in figure 2.1. Upstream of the stream tube has across sectional area of A_1 and a velocity of U_1 . This velocity of wind slows down to U_3 just after the actuator disc which has a cross sectional area of A_d , since it extracts the kinetic energy in the wind up to a certain level. Assuming incompressible flow, the cross-sectional area of stream tube should expand in order to accommodate the slower moving air. Then the downstream wind continues to expand up to A_4 of cross sectional area due to static pressure drop across the actuator disk and reach a final wind velocity of U_4 .

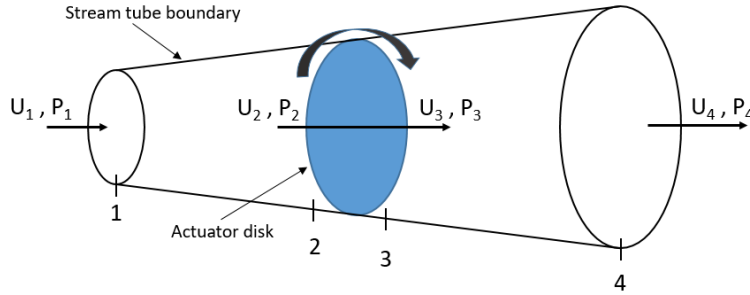


Figure 2.1 Actuator disk model of a wind turbine

According to the continuity equation, the mass flow rate of the wind flow through the stream tube, \dot{m} , can be written as,

$$\dot{m} = \rho U_1 A_1 = \rho U_2 A_d = \rho U_4 A_4 \quad (2.1)$$

Where ρ denotes the density of air.

Actuator disc induces velocity in the stream tube which is called the axial induced velocity. It is the difference between U_1 and U_2 . This velocity is non-dimensionalized with the free stream velocity and can be written as follows,

$$a = \frac{(U_1 - U_2)}{U_1} \quad (2.2)$$

This non-dimensional form of induces velocity a , is called axial induction factor. The stream wise velocity component U_2 , is then written as,

$$U_2 = U_1(1 - a) \quad (2.3)$$

The conservation of momentum across the actuator disk provides,

$$(P_2 - P_3)A_d = (U_1 - U_4)\rho A_d U_1(1 - a) \quad (2.4)$$

Pressure values can be expressed in terms of the upstream and downstream velocities according to Bernoulli's equation as follows,

$$U_4 = U_1(1 - 2a) \quad (2.5)$$

It is equivalent to,

$$U_2 = \left(\frac{U_1 + U_4}{2} \right) \quad (2.6)$$

Extracted power from the wind is obtained through equation 2.4,

$$Power = F U_d = 2\rho A_d U_1^3 a(1 - a)^2 \quad (2.7)$$

Ratio of power extracted to available power is called power coefficient,

$$\begin{aligned} Power\ Coefficient = C_p &= \frac{Power\ Extracted}{Power\ in\ the\ Wind} \\ &= \frac{2\rho A_d U_1^3 a(1 - a)^2}{\frac{1}{2}\rho U^3 A_d} \end{aligned} \quad (2.8)$$

Power coefficient variation with respect to the induction factor a , provides the value of the induction factor which maximizes the power,

$$\frac{dC_p}{da} = 4(1 - a)(1 - 3a) = 0 \quad (2.9)$$

Physically acceptable solution is $a = \frac{1}{3}$, since $a = 1$ makes $C_p = 0$. Then,

$$C_{p_{max}} = \frac{16}{27} = 0.593 \quad (2.10)$$

This maximum power coefficient is called Betz limit. Due to the other factor such as aerodynamic losses and friction, usually the power coefficient has a lower value than this.

2.3. Angular Momentum

Flow is assumed to be unidirectional in previous analysis. But in this analysis, rotary motion of the turbine is also included, since the rotation of the wind turbine generate angular momentum which can be related to the turbine torque.

When the turbine disc gains a torque while the air passing through it, an equal and opposite torque is acting on the air. As a result of this, the air passes the turbine rotates in a direction opposite to the turbine.

Air gains an angular momentum due to this effect. Those air particles which are in the wake, have a velocity that have two components as one in the direction parallel to axial free stream velocity and one in the direction tangential to the rotation of turbine. Due to this phenomenon, the kinetic energy of air increases while static pressure of air in the wake decreases [10].

The air entering the turbine has no rotational motion at all. But the flow exiting from the disc does have a rotation and transformation of the motion of air takes place entirely across the turbine region. This is shown in figure 2.2.

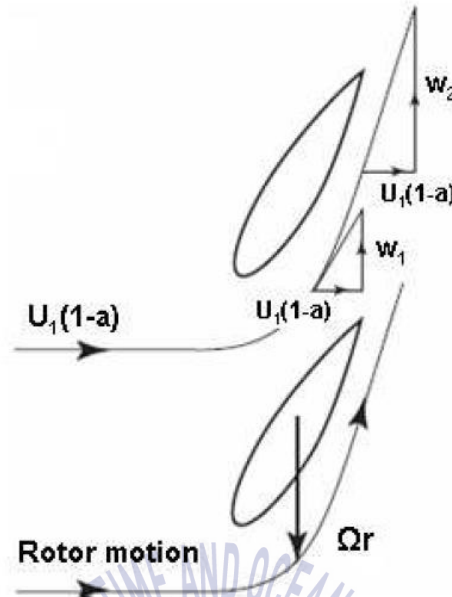


Figure 2.2 Velocity behind the turbine disc [10]

W_1 is the tangential induced velocity of air by the turbine and W_2 is the tangential induced velocity of air right after the turbine. These induced velocities are non-dimensionalized by the product of turbine rotational speed and radius, Ωr as follows,

$$\frac{W_1}{\Omega r} = a' \quad (2.11)$$

a' is called tangential induction factor. Form the conservation of angular momentum, it was found that W_2 is equal to half of W_1 [10,18]. Then,

$$W_1 = a' \Omega r \quad (2.12)$$

$$W_2 = 2a' \Omega r \quad (2.13)$$

An assumption for the pressure difference across the blades can be derived using a control volume that moves with the angular velocity of the blades. The angular velocity of air relative to the blades increases, from Ω to $\Omega+2\Omega a'$ across the turbine disc. Both tangential velocity and axial velocity are not the same in all radial positions.

Only an angular ring of the turbine disc which is radius r , and of radial width δr , with area δA is considered in order to allow both induced velocity components to vary. Torque on the ring is equal to the rate of change of angular momentum of the air passing through the ring. Thus,

$$\text{Torque} = \text{rate of change of angular momentum}$$

$$= \text{mass flow rate} \times \text{change of tangential velocity} \times \text{radius} \quad (2.14)$$

$$\delta Q = \rho \delta A U_1 (1 - a) 2\Omega a' r^2$$

Increment of the turbine shaft power output is,

$$\delta P = \delta Q \Omega \quad (2.15)$$

Detailed analysis and information about wake can be found in the references [10 and 18].

2.4. Blade Element Theory

Forces on the blades of a wind turbine, can also be declared as a function of angle of attack, lift coefficient and drag coefficient. Here, the blade is assumed to be divided into N number of sections which are called blade elements. Some assumptions are made in order to explain blade Element theory as follows.

The forces on the blade element are decided entirely by lift and drag characteristics of 2-D air foils of blade. Span wise velocity components on the blade are neglected. No aerodynamic interactions between blade elements.

Drag and lift components are parallel and perpendicular to the relative wind direction, in the blade element analysis. Consider a turbine of tip radius R with B number of blades, each with cord length of c and pitch angle β measured between the plane of disc and air foil zero lift line. Pitch angle and chord length may vary along the blade span.

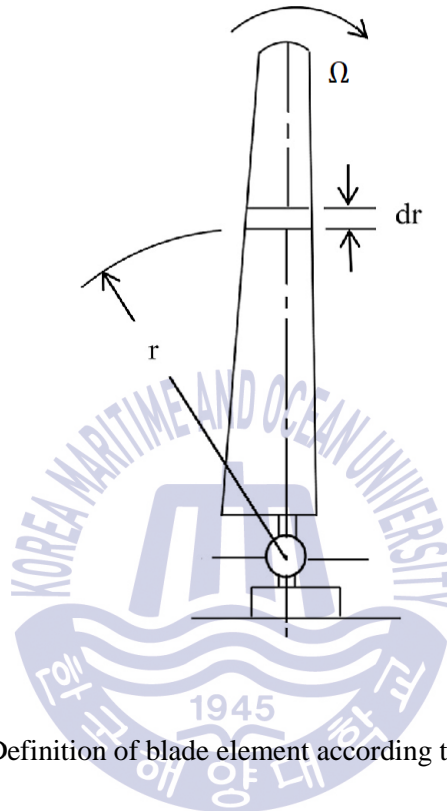


Figure 2.3 Definition of blade element according to the theory [10]

For a wind speed U_a and angular velocity Ω , the total tangential velocity experienced by the element is $(1+a') \Omega r$ and axial velocity is $(1-a) U_a$. Hence resultant relative wind velocity at the blade element is shown in equation 2.16.

$$W = \sqrt{U_a^2 (1-a)^2 + \Omega^2 r^2 (1+a')^2} \quad (2.16)$$

There is an angle between the plane of rotation and this relative velocity direction,

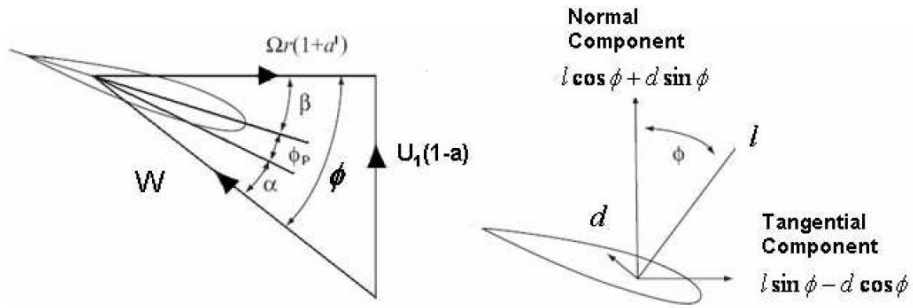


Figure 2.4 Velocities and forces acting on a blade element [10]

According to figure 2.4 and definitions, it can be derived that,

$$\tan \phi = \frac{U_{\infty}(1-a)}{\Omega r(1-a')} = \frac{(1-a)}{(1-a')\lambda r} \quad (2.17)$$

Net force normal to the plane of rotation for each blade element can be written as follows,

$$\delta F = B(l \cos \phi + d \sin \phi) \delta r \quad (2.18)$$

Resulting torque in each blade element can be expressed as follows,

$$\delta Q = Br(l \cos \phi + d \sin \phi) \delta r \quad (2.19)$$

These expressions will be used later when deriving axial induction factors and tangential induction factors in the Blade Momentum Theory.

2.4.1. Tip Losses

Pressure experienced by the pressure side of the blade is higher than the suction side of the blade. Air tends to leak around the tip from lower to upper surface due to this reason.

This effect is reducing the lift, which reduces the power production near the tip. This is similar to the tip losses of an aircraft wing.

These losses cannot be determined directly by blade element or momentum theory due to its 3D characteristics. But, there are some models which can be used to include the tip losses into the calculations. The most acceptable and commonly used tip loss model was developed by Prandtl [10]. The correction factor f must be introduced into the previously discussed equations which are used to calculate the net force and torque according to this model.

This factor is a function of the radius of the turbine, number of blades, the position of the blade element and the angle of relative wind.

$$f(R, B, r, \phi) \quad (2.20)$$

Final equation of the Prandtl tip loss factor is given below,

$$f = \frac{2}{\pi} \cos^{-1} \left(\exp \left(-\frac{B(R-r)}{2r \sin \phi} \right) \right) \quad (2.21)$$

2.5. Blade Element Momentum (BEM) Theory

Blade element momentum theory intend to model the axial induction factor and tangential induction factors by relating the torque and force equations derived from each blade element and momentum theories.

By equating the force relations in the theories, which are equation 2.7 and equation 2.18 with Prandtl tip loss correction, axial induction factor can be derived as follows,

$$2\rho AFU_1^2 a(1-a) = B(l \cos \phi + d \sin \phi) \delta r \quad (2.22)$$

$$\delta A = r \delta r \quad (2.23)$$

$$l = C_l \frac{1}{2} \rho W_c^2 \quad (2.24)$$

$$d = C_d \frac{1}{2} \rho W_c^2 \quad (2.25)$$

$$C_N = C_p \cos \phi + C_d \sin \phi \quad (2.26)$$

$$\rho = \frac{B_c}{2\pi r}; \text{Local solidity} \quad (2.27)$$

$$a = \frac{1}{\frac{4F \sin^2 \phi}{\rho' C_N} + 1} \quad (2.28)$$

By equating the rate of change of momentum in the annular disc by using equation 2.14 and equation 2.19, tangential induction factor can be derived as follows,

$$2\rho\delta AFU_1^2 a(1-a)2\Omega a' r^2 = Br(l \cos \phi + d \sin \phi)\delta r \quad (2.29)$$

$$C_{Tan} = C_l \sin \phi - C_d \cos \phi \quad (2.30)$$

$$a' = \frac{1}{\frac{4F \sin \phi \cos \phi}{\sigma' C_{Tan}} - 1} \quad (2.31)$$

These induction factors are used to predict velocities. Wind turbines can be analyzed for power and thrust outputs more precisely once induced velocities are modelled accurately.

Chapter 3. Design of 2kW wind turbine and flange type velocity boosters

3.1. Determining the design wind speed

It is very important to get accurate initial design values in order to complete a wind turbine which performs well in the site, where it will be operated.

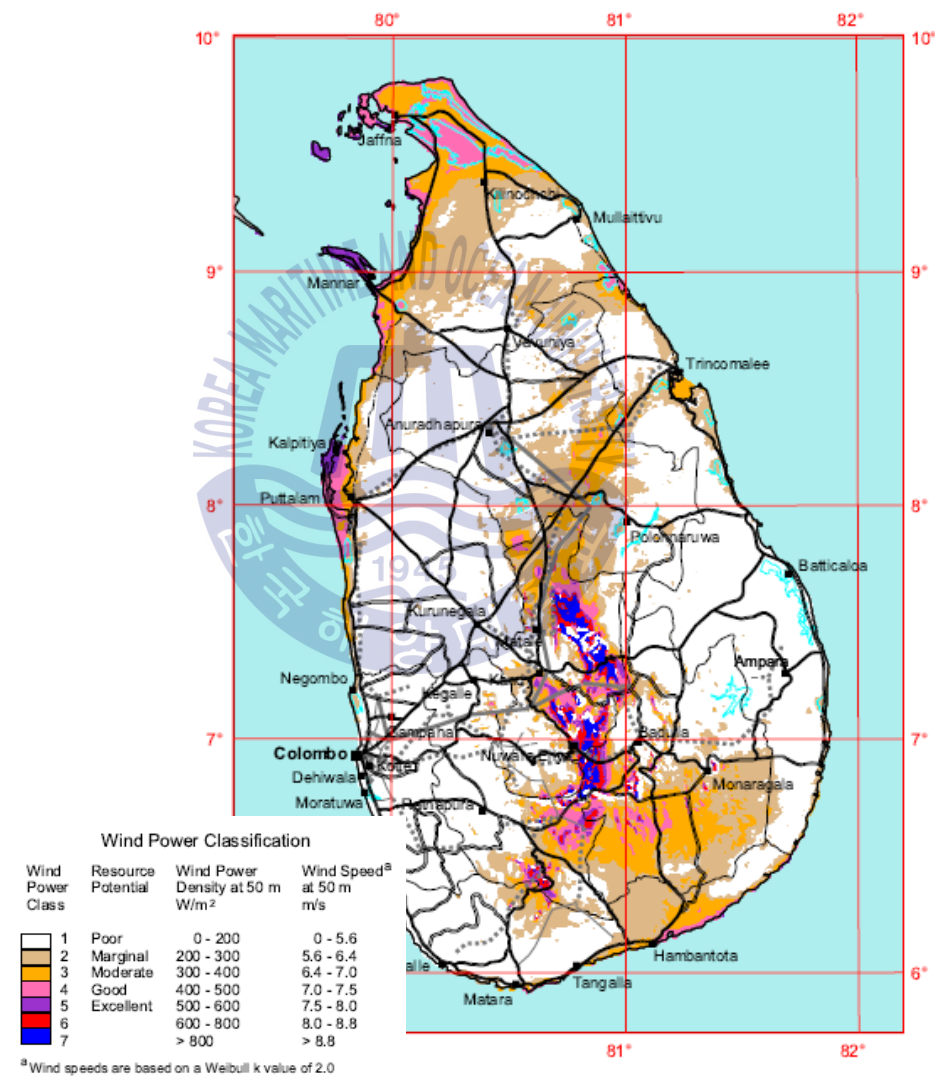


Figure 3.1 Average wind capacity in Sri Lanka [19]

Turbine, which is designed here is not for a single site but for a region which has a similar wind climate. Initial site data was obtained from “Wind Energy Resource Atlas of Sri Lanka and Maldives” published by the “National Renewable Energy Laboratory” [19]. Average wind velocity in the region is 5.5 m/s as indicated in figure 3.1. But it is expected to increase the wind conditions in the site using a booster. So 7.5 m/s was chosen as the design wind velocity V_D of the turbine.

3.2. Calculating the Rotor Diameter and Rated Rotational Speed

Equation 3.1 was used to calculate the rotor diameter. Estimated power coefficient C_P , was taken as 0.45 and the efficiency of the generator η , assumed to be 0.9. Air density ρ , is 1.225 kg/m³. Then the rotor diameter got a value of 4.83 m.

$$D = \sqrt{\frac{8Pr}{\eta C_p \rho \pi V_D^3}} = 4.83m \quad (3.1)$$

Then rated rotational speed can be calculated by equation 3.2. Tip speed ratio (TSR) was taken as 6. N_{rpm} was found as 178 rpm.

$$N_{rpm} = 60 \left[\frac{V_D}{\pi D} \right] \lambda = 178 \text{ rpm} \quad (3.2)$$

3.3. Tip loss correction

Tip loss correction is one of the most important factor in BEM analysis. This concept was introduced by Prandtl [20] to simplify the wake generated by the turbine. Momentum of the blade element momentum equations are modified by these corrections. Modified equation is indicated below in equation 3.3.

$$f = \frac{2}{\pi} \cos^{-1} \left[e^{-\left[\frac{\frac{B}{2}(1-\mu)}{\mu} \sqrt{\frac{1+(\lambda\mu)^2}{(1-a)^2}} \right]} \right] \quad (3.3)$$

Here, B is number of blades and μ denotes a variable that is, non-dimensionalized local position of the blade from the hub to tip, and it is set to increase from 0.05 (hub) to 1 (tip). Here axial flow induction factor a is assumed to be its maximum of $1/3$, which is derived from Betz theory. The calculated tip loss factor at each local location of the blade is shown in figure 3.2.

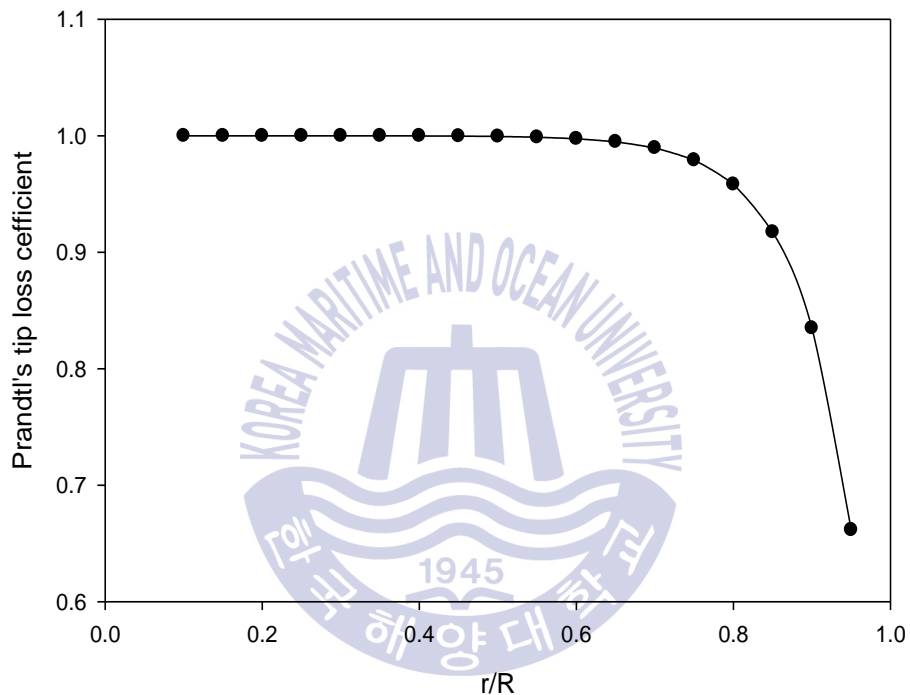


Figure 3.2 Prandtl's Tip Loss Coefficient

3.4. Flow induction factors

Blade tip losses with localized blade position was calculated using equation 3.3. That is the theoretical maximum value which can be obtained from the momentum theory.

Using equation 2.28, equation 2.31 and equation 3.3 axial flow induction factor and tangential flow induction factors can be re written with tip loss correction and expressed in equation 3.4 and equation 3.5 respectively as below,

$$a = \frac{1}{3} + \frac{1}{3}f - \frac{1}{3}\sqrt{1 - f + f^2} \quad (3.4)$$

$$a' = \frac{a(1-\frac{a}{f})}{\lambda^2 \mu^2} \quad (3.5)$$

Calculated axial induction factor and tangential induction factors are indicated against local position of the blade in figure 3.3 and figure 3.4 respectively.

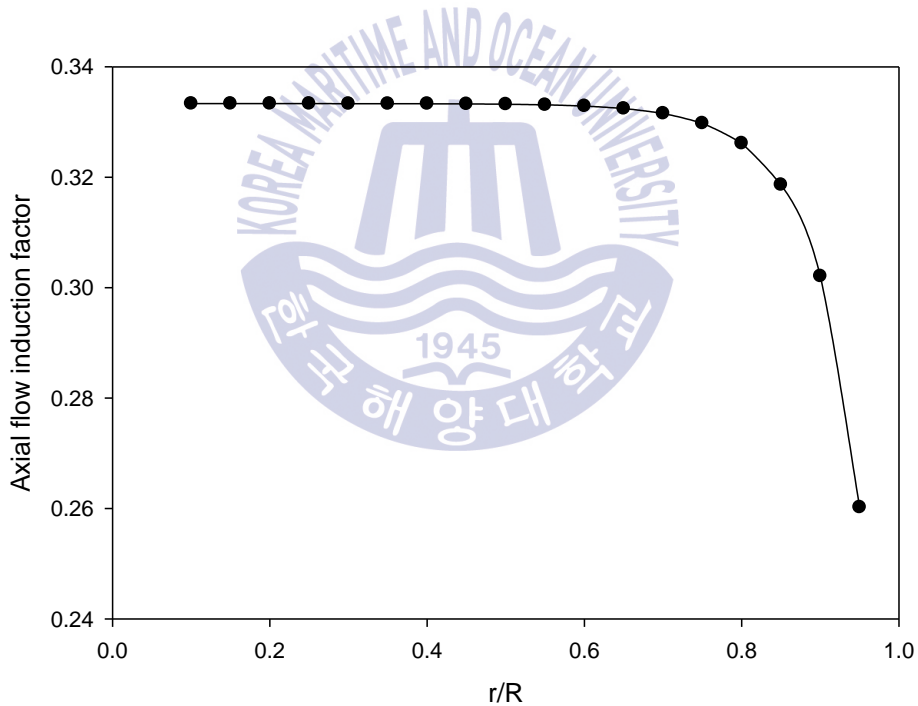


Figure 3.3 Axial flow induction factor

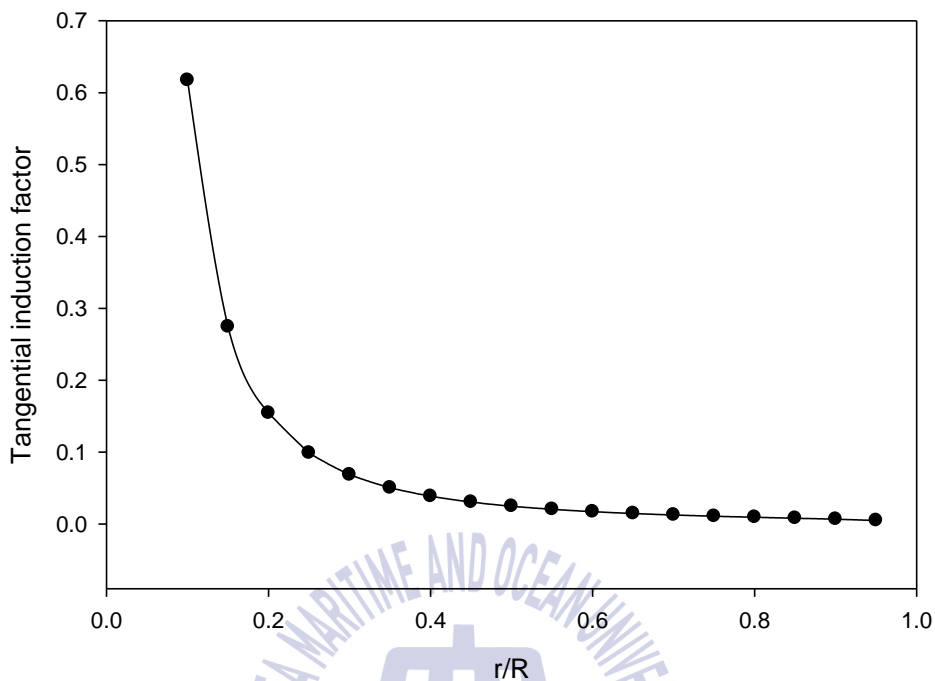


Figure 3.4 Tangential flow induction factor

3.5. Air foil selection

Chosen air foils have a direct impact on turbine performance. Several factors of the air foil, such as thickness, camber, lift, drag, lift to drag ratio and its performance at different Reynolds numbers should be considered. Generally, a turbine with thinner blades will cause to get higher power coefficient since they can use high performance air foils. But this will weaken their strength and stiffness. Blade strength can be improved by using thicker air foils to the blade. But this will lead for lower aerodynamic performance of the turbine. Beyond this, the blade of the wind turbine experiences different flow conditions over the blade geometry. Thus, air foils which are used in different parts of the blade are required to have different characteristics.

Several air foils namely, AH 93 W 257, FX 76 MP 140, NACA 634421, NACA 644421, Nasa NLF 1015, NREL S 823 were examined in order to choose the most suitable air

foils. Finally, NACA 634421 and FX 76 MP 140 foils were selected for 20% to 60% region of blade from root and 60% to 100% region of blade from root, respectively considering above conditions as shown in figure 3.7. Chosen airfoils are indicated in figure 3.5 and figure 3.6 below. Lift coefficient variation of the chosen air foils with angle of attack and lift to drag ratio variation of the chosen air foils with angle of attack at the estimated Reynolds number of turbine, which is 450,000, is indicated in figure 3.8 and figure 3.9 respectively.

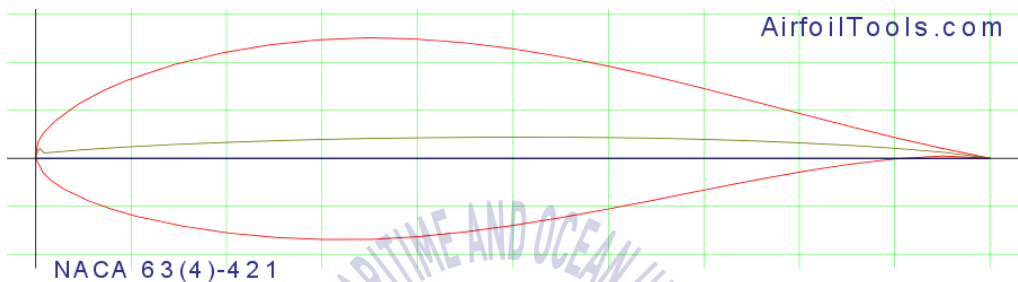


Figure 3.5 NACA 634421 airfoil [21]

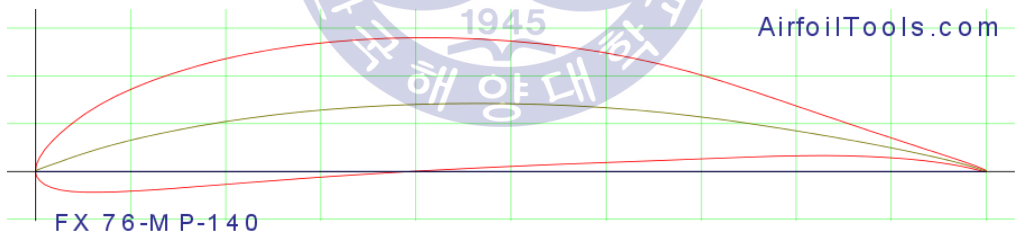


Figure 3.6 FX 76 MP 140 airfoil [21]

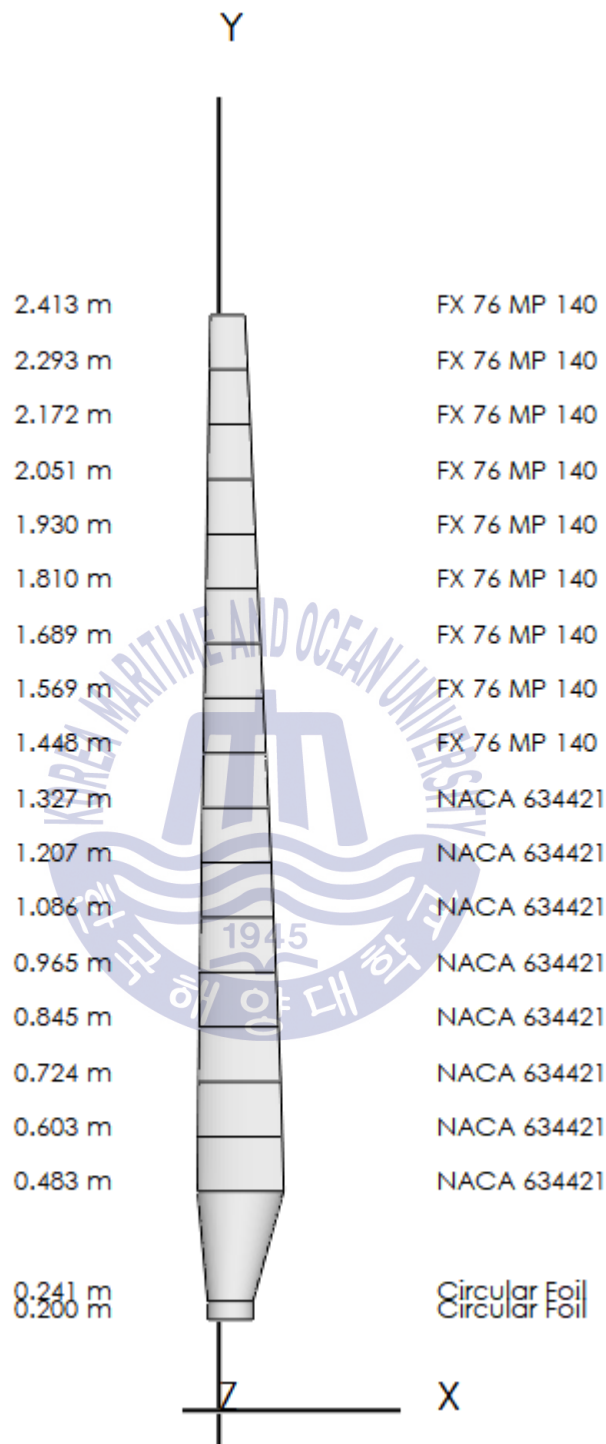


Figure 3.7 Air foils and their span wise locations

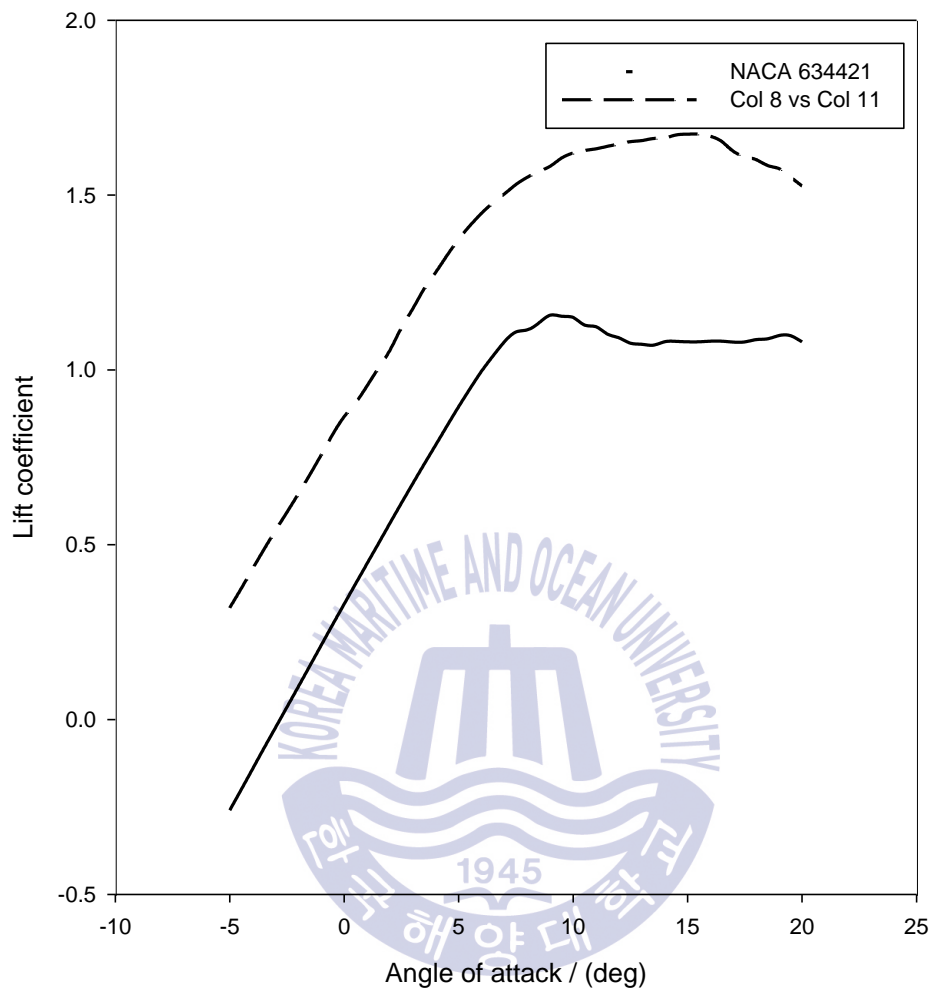


Figure 3.8 Lift coefficient variation with angle of attack

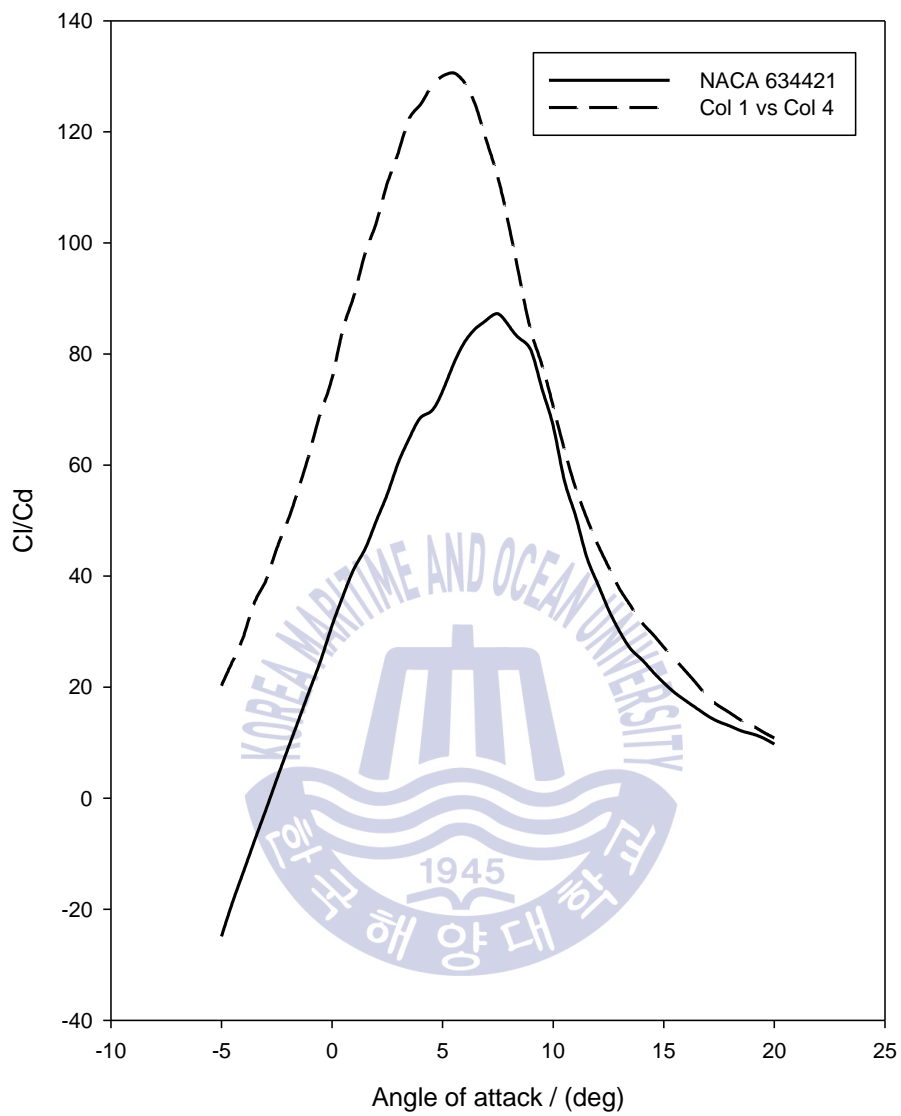


Figure 3.9 C_l/C_d variation with angle of attack

3.6. Chord length calculations

Chord length can be calculated using equation 3.6,

$$\frac{C}{R} = \frac{2\pi}{B\lambda C_l} \times \frac{4\lambda\mu^2 a^1}{(1-a)^2 + \sqrt{[\lambda\mu(1+a^1)]^2}} \quad (3.6)$$

Number of blades **B**, Tip speed ratio **λ** , tangential induction factor **a'** , axial induction factor **a** and lift coefficient of the airfoil **C_l** are already known from the previous steps. So, chord lengths of all locations were calculated. Aerodynamic characteristics of used airfoils NACA 634421 and FX 76 MP 140 are indicated in table 3.1.

Table 3.1 Aerodynamic characteristics of chosen airfoils

Airfoil	RE	α (deg)	C_l	$C_{l/a}$
NACA 634421	450,000	7.5	1.1075	87.2568
FX 76 MP 140	450,000	5.5	1.4135	130.6173

A broad variation of chord length observed in the region where air foils are changed due to different aerodynamic characteristics of two airfoils. Additionally, a sharp increase of chord length was observed towards the hub region as indicated in figure 3.9. But the region of blade which is closer to the hub does not highly effect on the overall performance of the turbine. But the region closer to the tip which over 65% from the hub has a higher effect on the turbine performance thus should be optimized. Considering the above region, the whole blade was optimized by linearizing chord lengths by extrapolating sections lies on 70% and 90% of the blade, to reduce the manufacturing cost while gaining on acceptable level of performance.

Final chord length distribution is indicated in figure 3.10.

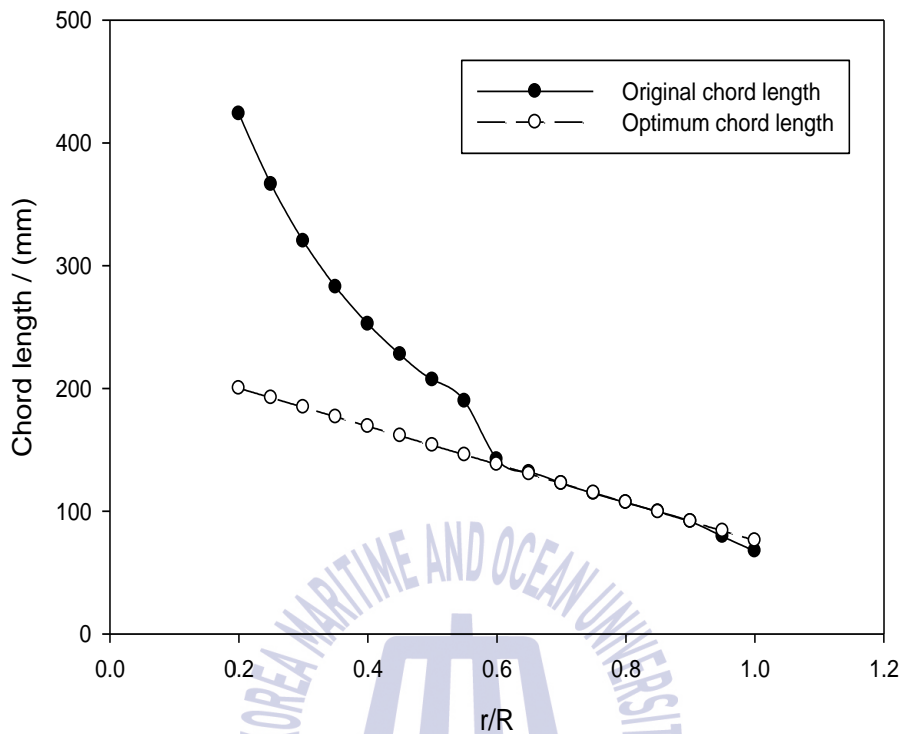


Figure 3.10 Distribution of chord length at each section

3.7. Twist angle calculations

Twist angle depends on inflow angle ϕ and angle of attack α . First inflow angle was calculated using equation 3.7 which is indicated below.

$$\tan \phi = \frac{1-\alpha}{\lambda\mu(1+\alpha^1)} \quad (3.7)$$

Above calculated inflow angle ϕ and optimum angle of attack were used to calculate twist angle θ as in equation 3.8.

$$\theta = \phi - \alpha \quad (3.8)$$

Twist distribution with blade position is indicated in figure 3.11.

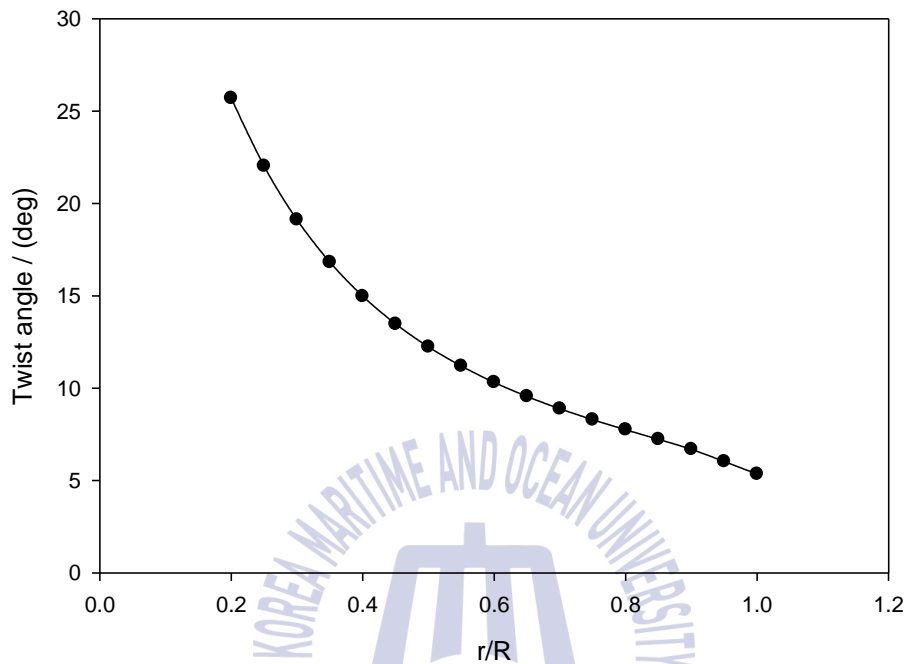


Figure 3.11 Twist angle distribution

3.8. Optimized blade parameters

Geometric parameters of the blade which were calculated in previous sections are presented below in table 3.2.

Table 3.2 Geometric parameters of the blade

Local Position	Radial Distance (mm)	Chord Length (mm)	Twist (Deg)	Air Foil
0.20	483	200.1	18.2	NACA 634421
0.25	603	192.3	14.5	NACA 634422
0.30	724	184.6	11.6	NACA 634423
0.35	845	176.8	9.3	NACA 634424
0.40	965	169.1	7.5	NACA 634425
0.45	1086	161.3	6.0	NACA 634426
0.50	1207	153.6	5.2	NACA 634427
0.55	1327	145.8	4.7	NACA 634428
0.60	1448	138.1	4.3	FX 76 MP 140
0.65	1569	130.4	3.9	FX 76 MP 141
0.70	1689	122.6	3.4	FX 76 MP 142
0.75	1810	114.9	2.8	FX 76 MP 143
0.80	1931	107.1	2.3	FX 76 MP 144
0.85	2051	99.4	1.7	FX 76 MP 145
0.90	2172	91.6	1.2	FX 76 MP 146
0.95	2293	83.9	0.5	FX 76 MP 147
1.00	2413	76.1	-0.2	FX 76 MP 148

Isometric view of the blade and rotor are shown in figure 3.12 and figure 3.13 respectively.

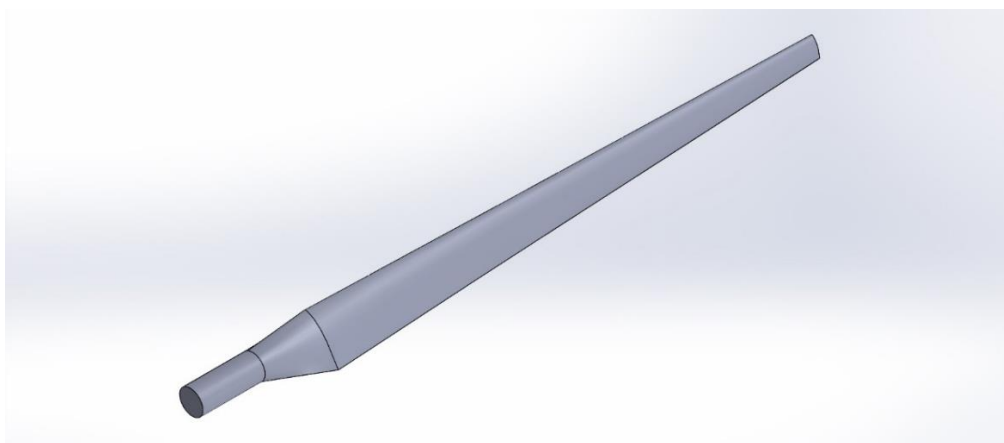


Figure 3.12 Isometric view of the blade



Figure 3.13 Isometric view of the turbine rotor

3.9. Flange type velocity booster designs

Diffuser design of Kyushu University which was discussed earlier looks promising [12 and 13]. The main drawback of this system is its size. This diffuser is larger compared to the turbine size and thus difficult to handle. New flange type velocity boosters are proposed in this study considering the size limitation. Here on words, this “flange type velocity booster” will be referred as “booster” or “velocity booster”. Initial booster is based on a similar design which was designed for a tidal current turbine [23]. So, the maximum diameter of the booster was limited to $1.433 D$, maximum length was limited to $0.4 D$ and flange height was fixed to $0.173 D$, where D is the minimum inner diameter of the booster. Four different flange type velocity boosters were designed and the basic non dimensional parameters are indicated in figure 3.14 and table 3.2 below.

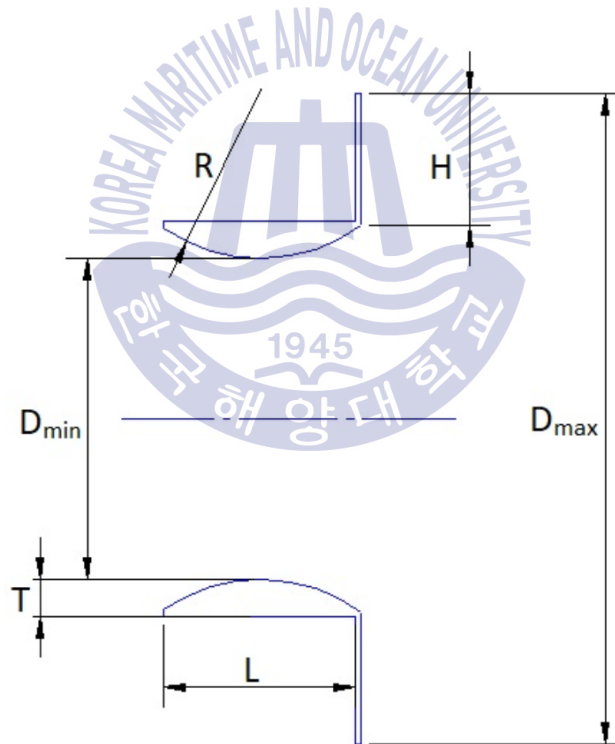


Figure 3.14 Parameters of flange type velocity booster

Table 3.3 Non dimensional parameters of the flange type velocity booster

Parameter	Booster 1	Booster 2	Booster 3	Booster 4
Minimum diameter / (D_{\min})	D	D	D	D
Flange height / (H)	0.173 D	0.173 D	0.173 D	0.173 D
Maximum diameter / (D_{\max})	1.433 D	1.433 D	1.433 D	1.433 D
Length / (L)	0.4 D	0.4 D	0.4 D	0.2 D
Booster curvature radius / (R)	0.5 D	-	0.5 D	0.136 D
Maximum thickness / (T)	0.008 D	0.008 D	0.046 D	0.046 D

Flow condition in case of “Booster only analysis” and “Booster, turbine complete system analysis” are different because the turbine resistance has an effect on the flow of the whole system. Thus, first boosters were analyzed without the turbine and a booster-turbine combined system was also analyzed later to understand the turbine effect on the booster. Booster models are indicated in figure 3.15 to figure 3.22.

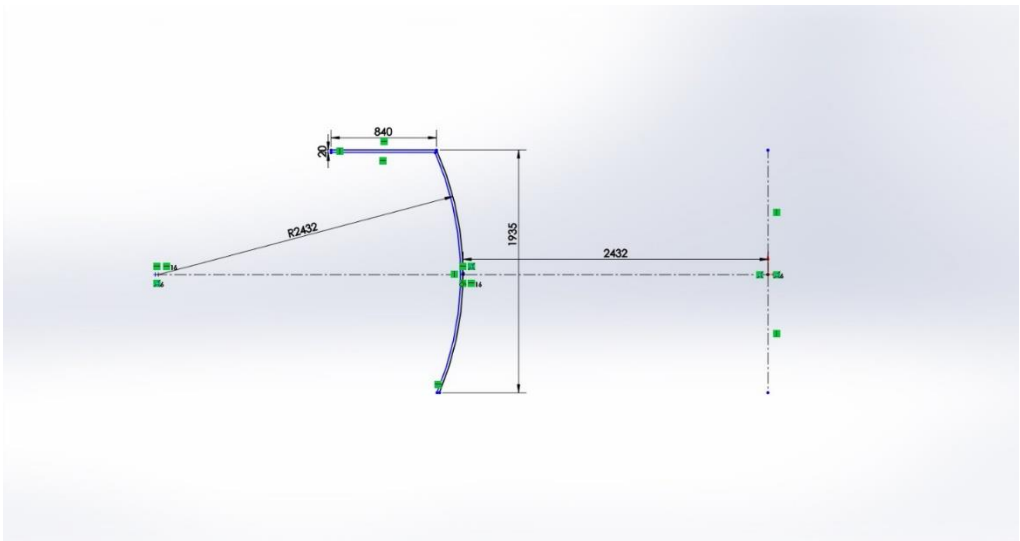


Figure 3.15 Sectional 2-D drawing of booster model 1



Figure 3.16 Isometric view of booster model 1

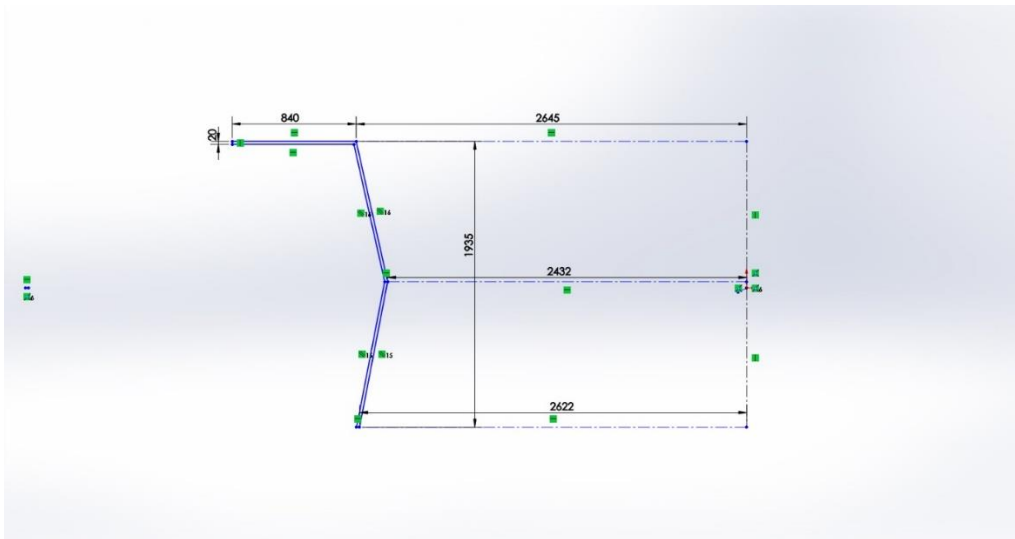


Figure 3.17 Sectional 2-D drawing of booster model 2



Figure 3.18 Isometric view of booster model 2

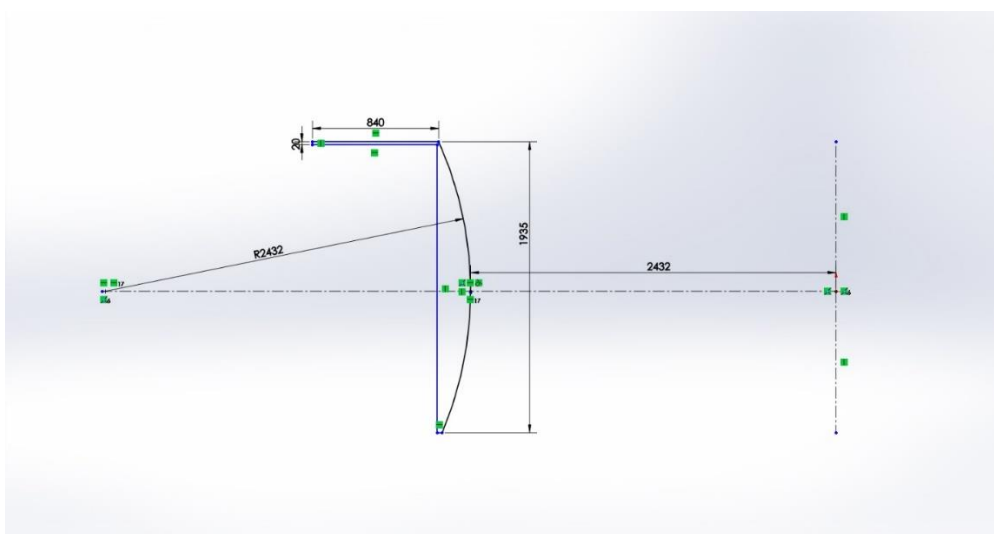


Figure 3.19 Sectional 2-D drawing of booster model 3



Figure 3.20 Isometric view of booster model 3

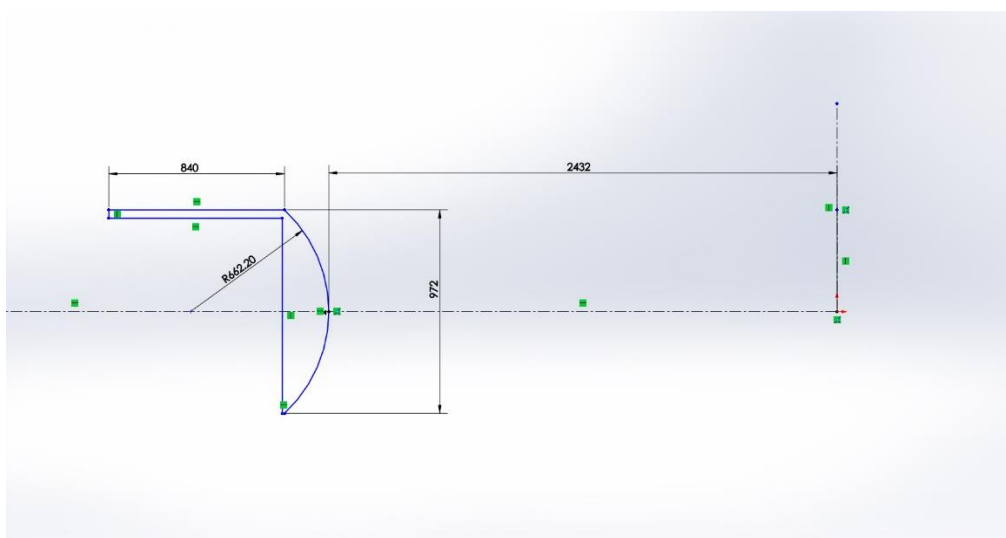


Figure 3.21 Sectional 2-D drawing of booster model 4



Figure 3.22 Isometric view of booster model 4

Chapter 4. CFD analysis

4.1. Computational fluid dynamics

4.1.1. Introduction

Computational Fluid Dynamics (CFD) is the science of describing and analyzing fluid flows by producing numerical solutions to a system of partial differential equations (PDEs). Use of CFD was first started by the airplane industry. But it has expanded its application over variety of fields, with the increase of computational power and the large economical advantage.

Due to the fact that extensive studies of fluid flows using experiments are expensive and time consuming, CFD plays a valuable role in many industries including wind power industry. In addition, CFD allows the study of ideal cases which practically impossible, as well as very small scales and time development (in slow motion) of phenomena that otherwise would not be visible. Computers are used to solve the problems due to the fact that the equations governing fluid flows are very complicated. Star CCM+ was used to analyze wind turbine and the total system which was designed in this study.

4.1.2. Governing equations

Governing equations of fluid flow, which describe the processes of momentum, heat and mass transfer, are known as the Navier-Stokes equations. Following are the core governing equations used in Star CCM+.

The continuity equation,

$$\frac{\partial p}{\partial t} + \nabla(\rho * U) = 0 \quad (4.1)$$

The momentum equation,

$$\frac{\partial(pU)}{\partial t} + \nabla * (\rho U \otimes U) = -\nabla_p + \nabla \sigma + S_M \quad (4.2)$$

σ indicates the stress tensor (including both normal and shear components of the stress). Navier-Stokes equations describe both laminar and turbulent flows. But that needs a fine mesh which is computationally expensive. Therefore, turbulence models are used to predict the effects of turbulence with comparatively lower computational effort. These models account for the effects of turbulence without the use of a very fine mesh. These turbulence models modify the transport equations by adding averaging and fluctuating components. Then, the transport equations are changed to equations below.

$$\frac{\partial p}{\partial t} + \nabla(\rho * U) = 0 \quad (4.3)$$

$$\frac{\partial(\rho U)}{\partial t} + \nabla * (\rho U \otimes U) = -\nabla_p + \nabla\{\sigma - \overline{\rho u \otimes u}\} + S_M \quad (4.4)$$

The mass equation is not modified but the momentum equation contains extra terms which are the Reynolds stresses, $\overline{\rho u \otimes u}$ and Reynolds flux, $\overline{\rho u \phi}$. These Reynolds stresses need to be modeled by additional equations. In this study, the model utilized was the Shear Stress Transport (SST) model. The advantage of using this model is that, it combines the advantages of other turbulence models.

4.1.3. Creating the geometry

First step in STAR, is to prepare the geometry for the case to be studied. This geometry can either be imported from external CAD-program or created directly using the 3-D CAD module which exist within the STAR-software.

In this study, 3-D model of a wind turbines and boosters were made in SOLIDWORKS which is a commercial computer aided design software and imported to Star CCM+.

4.1.4. Defining the simulation settings and boundary conditions

An essential part of the process in setting up a simulation is to define the relationship between geometry parts and regions, boundaries, and interfaces.

Geometry parts are used to define the edges, faces and vertices that make up the surfaces of the model. But the simulation domain on which mesh is generated, and for which physics is solved, is defined using regions, boundaries, and interfaces.

Imported CAD models were changed initially according to the required surface and feature curve definitions. Then those were assigned to the regions. Finally boundary conditions were applied before generating the mesh.

4.1.5. Mesh generation

Establishing a proper grid resolution is very important before attempting to solve any CFD problem. Star CCM+ offers powerful tools to establish a better quality mesh depending on the problem which is to be solved.

According to the Star CCM+ user guide [22] a mesh is a discretized representation of the computational domain, which the physics solvers use to provide a numerical solution. There are different meshing strategies in Star CCM+ and each one has its advantages and disadvantages. Thus it is important to choose the suitable strategies depending on the application.

In all cases “Surface Mesher” was used as the surface meshing technique. This remeshes the initial surface to provide a quality discretized mesh that is suitable for CFD. It is used to rectangular surface based on a target edge length supplied and can also omit specific surfaces or boundaries preserving the original triangulation from the imported mesh. Further refinement was done in to the surface mesh based on edges and specific surfaces. “Trimmer” was used as the volume mesh in all cases. This model was chosen due to its ability to model external aerodynamic flows accurately with its options to refine cells in wake region. This technique generates a volume mesh by cutting a hexahedral template mesh with geometry surface. Mesh was customized using volumetric controls in all three conditions to make the mesh finer in critical regions.

“Prism Layer Mesher” used as an optional mesh model in all cases. This technique adds prismatic cell layers next to wall boundaries. This technique projects the core mesh back to the wall boundaries to create prismatic cells. This aids to improve the accuracy of the flow solution as prediction of various flow features such as drag and pressure drop which are depend on velocity and temperature gradients normal to the wall. Twelve prism layers

were used next to the turbine boundary and five prism layers were used next to booster wall boundary in order to achieve better results in all cases.

4.1.6. Solving the simulation

Once all the boundary conditions defined in a domain where an adequate accurate mesh has constructed, Star CCM+ can solve for solutions.

There are several techniques which can be used to solve the governing equations described earlier. Star CCM+ uses the Finite Volume Method (FVM). Figure 4.1 indicates a typical cell- centered Control Volume (CV). There can be arbitrary number of cell faces (AS). The cell center, or computational node, is represented by C and the face centers are represented by (K). Finite Volume (FV) method describes the volumes not in terms of their computational nodes but in terms of CV boundaries.

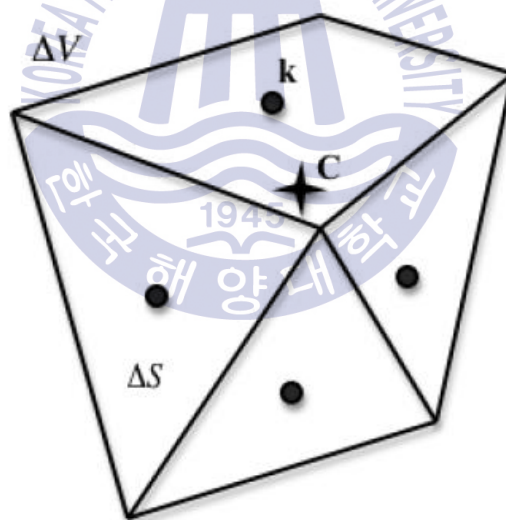


Figure 4.1 3-D cell-centered control volume

4.1.7. Post processing

Post processing is done after simulation completed. There are number of ways used here in order to analyze the results. Results can be exported in several forms such as graphs and spread sheets. Visualization of the results in different formats is another widely used method due to its simplicity and ability to understand easily. Hard copies of contours and vectors are available. Animations can also be made. The result obtained by the turbine simulations were analyzed in above manners and presented in next chapter.

4.2. NREL Phase VI Turbine analysis

The NREL phase 6 experiment was performed in 2001 by “The National Renewable Energy Laboratory (NREL)” in the NASA-AMES wind tunnel with a test section of 24.4×36.6 m. Wind turbine was stall-regulated and had a diameter of 10.058 m. The aim of the experiment was to provide data for validate flow models in the computation of wind turbines. Thus, aerodynamic quantities are well documented and available for the international science community on request and widely used by the CFD community. This data was obtained from the NREL and used to check the accuracy of the CFD analysis.

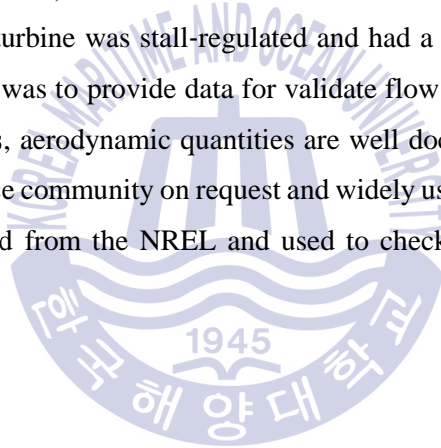




Figure 4.2 NREL phase VI turbine [21]

Geometric detail of the NREL phase VI turbine blade is available in related technical report [21]. Blade used NREL 5809 airfoil for the whole blade. All available chord length values and twist angle values which were given section wise were used to model the blade.

Figure 4.3, figure 4.4 and figure 4.5 indicate the 2-D sectional curves which were drawn using above data, the enclosed 3-D CAD model of the blade and the complete 3-D drawing of the NREL phase VI turbine rotor respectively.

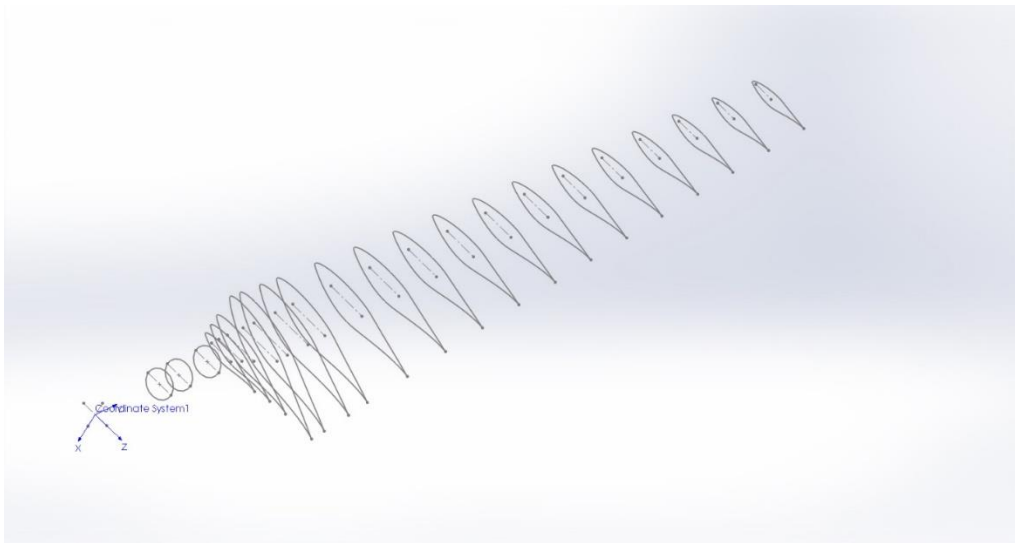


Figure 4.3 Sectional view of the blade



Figure 4.4 3-D blade model

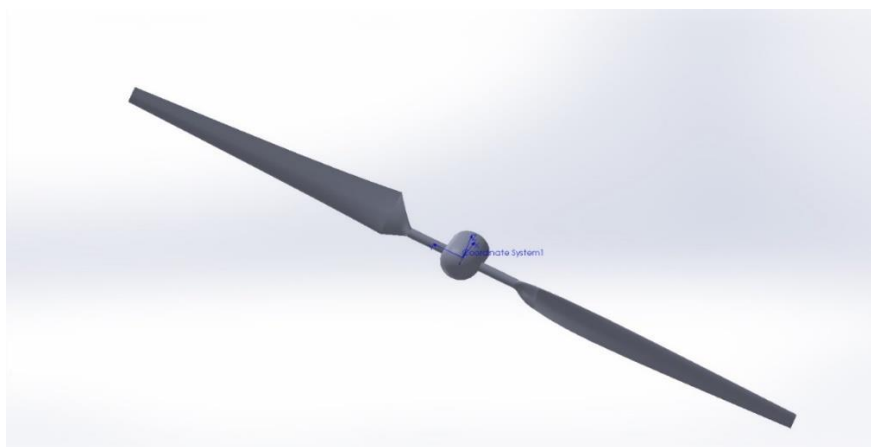


Figure 4.5 3-D model of the NREL phase VI turbine

An unsteady analysis was done for NREL phase VI turbine. K - Omega SST turbulence model was used in order to get accurate results with comparatively lower computational effect.

First simulation was run in steady state for 10,000 steps to gain more stability. Then it was run again for 15 s in transient conditions. Flow was defined as incompressible because there are no changes in density as air travels through turbine.

Basic setting of the simulation is indicated in table 4.1.

Table 4.1 Basic settings for NREL phase VI turbine simulation

Item	Specification
Simulation type	Unsteady
Turbulence model	K-Omega SST
Fluid	Air
Domain size	24.4 m X 36.6 m X 221.3 m
Turbulence intensity	0.01
Turbulence viscosity ratio	10
Reference pressure	101 k Pa
Blade tip pitch	3 deg
Simulation time	15 s
Velocity conditions (varies)	7, 10, 13, 15 m/s

Numerical domain and its boundary conditions are indicated in table 4.2 and figure 4.6.

Table 4.2 Boundary conditions for NREL phase VI turbine

Condition	Related boundaries
Wall	3 (side walls), 5 (turbine surface)
Velocity inlet	1 (inlet)
Pressure outlet	2 (outlet)
Interface	4 (interfaces between rotating and stationary domains)

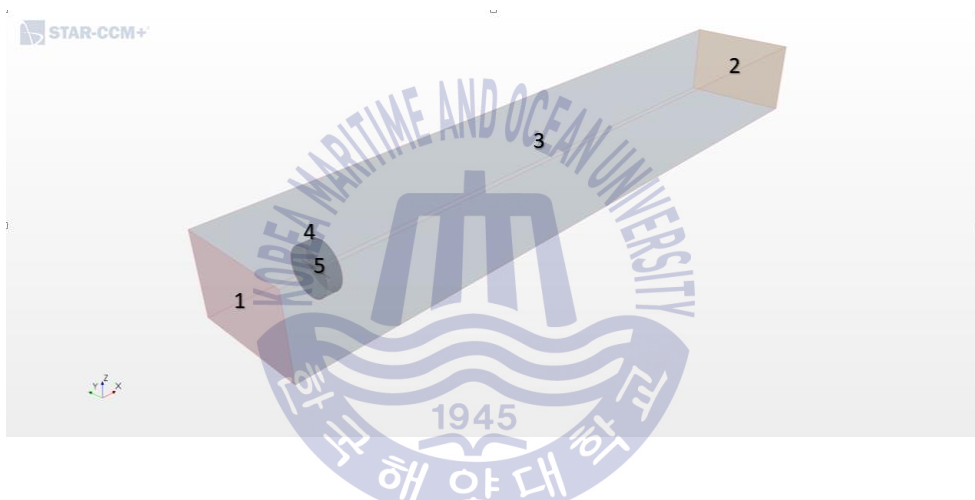


Figure 4.6 Numerical domain of NREL phase VI turbine case

Hexahedral mesh was used as the main type of mesh. It was fined close to the turbine and coarsened towards the tunnel walls. 15 layers of prism mesh was used near turbine surface to capture the boundary layer accurately. Total number of cells in the mesh is 7,055,603 with 2,276,726 cells in rotating domain and 4,778,877 in static domain.

Figure 4.7 indicates the cross sectional view of the volume mesh. Figure 4.8 indicates the zoomed view of the volume mesh close to the turbine. Interface between the rotational and stationary domains is also visible there. Figure 4.9 indicates the surface mesh on turbine blade suction and pressure sides and figure 4.10 indicates the y plus distribution along the turbine suction and pressure sides.

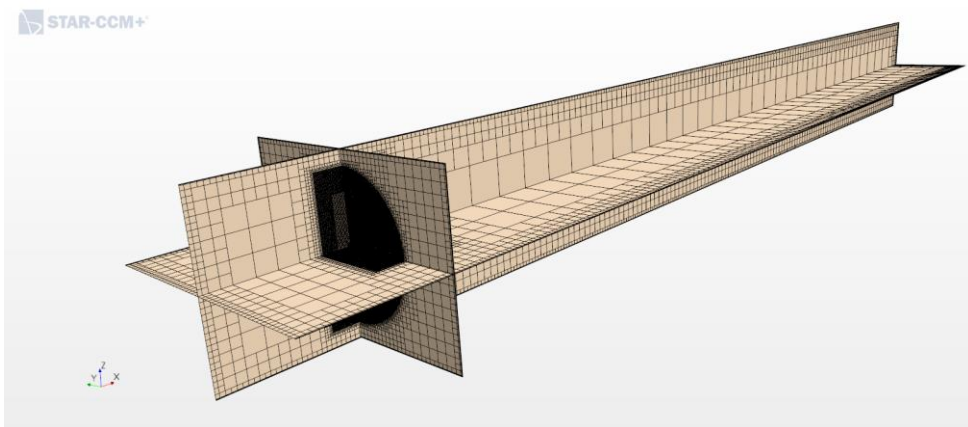


Figure 4.7 Sectional view of the volume mesh

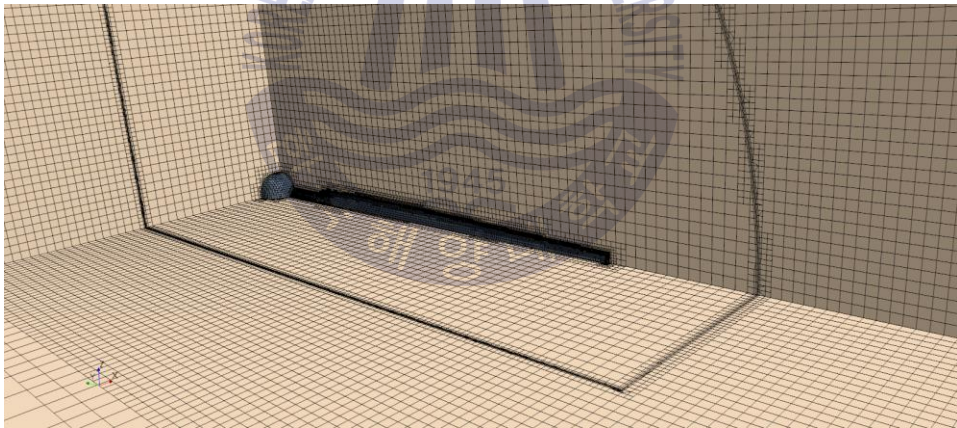


Figure 4.8 Zoomed sectional view of the volume mesh closer to the turbine region



Figure 4.9 Surface mesh of the blade

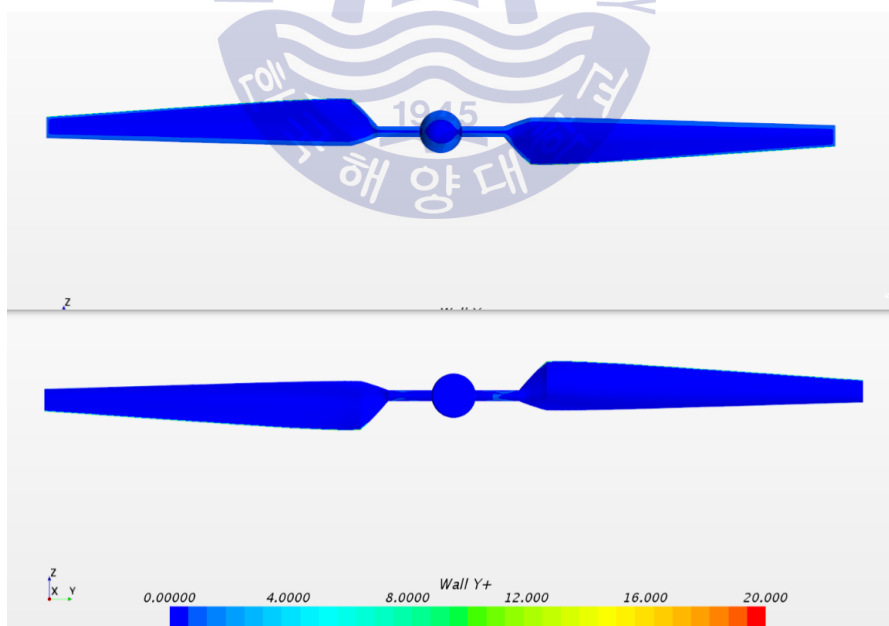


Figure 4.10 Y plus values on blade surface

4.3. 2 kW wind turbine analysis

Geometric details of the 2 kW wind turbine were calculated previously, as in chapter 3.

Finalized details of the turbine blade were taken from table 3.2.

Figure 4.11 indicates the 2-D sectional curves which were drawn using the table 3.2 data.

Figure 4.12 and figure 4.13 indicate the enclosed 3-D CAD model of the 2 kW wind turbine blade and the complete 3-D drawing of the 2 kW wind turbine rotor respectively.



Figure 4.11 Sectional view of the blade



Figure 4.12 3-D blade model



Figure 4.13 3-D model of the 2 kW turbine

Basic setting of the simulation is indicated in table 4.3. Numerical domain and its boundary conditions are indicated in table 4.4 and figure 4.14.

Table 4.3 Basic settings for 2 kW turbine simulation

Item	Specification
Simulation type	Unsteady
Turbulence model	K-Omega SST
Fluid	Air
Domain size	14.48 m X 107.27 m X 14.48 m
Turbulence intensity	0.01
Turbulence viscosity ratio	10
Reference pressure	101 k Pa
Simulation time	10 s
Tested wind velocities (varies)	5 m/s, 7.5 m/s, 10 m/s
TSR value (varies)	4, 5, 6, 7, 8, 8.5, 9, 10, 11, 12

Table 4.4 Boundary conditions for 2 kW turbine

Condition	Related boundaries
Wall	5 (turbine surface)
Symmetry	3 (side walls)
Velocity inlet	1 (inlet)
Pressure outlet	2 (outlet)
Interface	4 (interfaces between rotating and stationary domains)

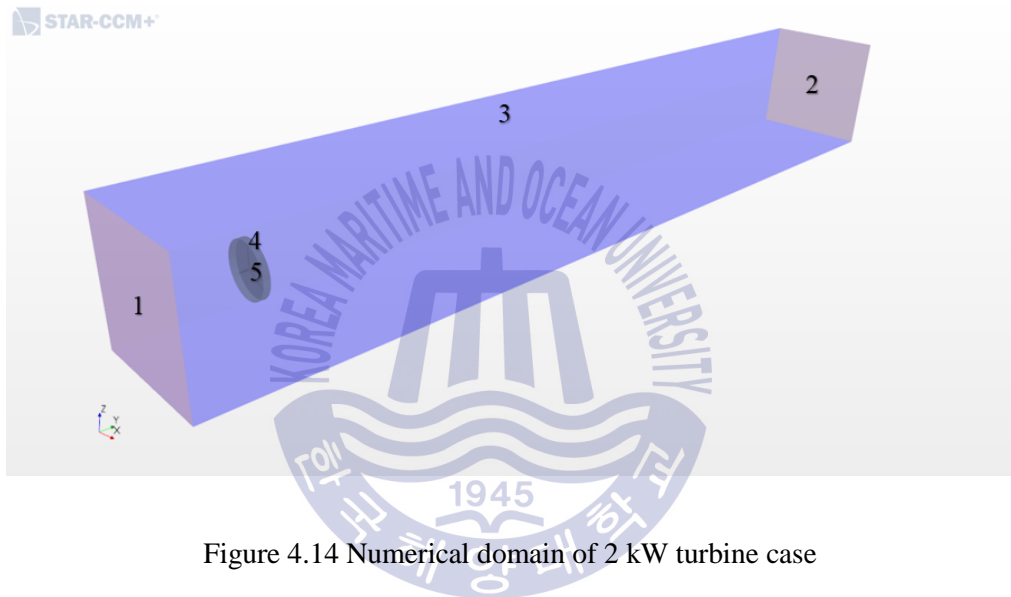


Figure 4.14 Numerical domain of 2 kW turbine case

Hexahedral mesh was used as the main type of mesh. It was fined towards the turbine and coarsened outwards. 12 layers of prism mesh was used near turbine surface to capture the boundary layer accurately. Total number of cells in the mesh is 3,153,571 with 3,087,561 cells in rotating domain and 66,012 in static domain.

Figure 4.15 indicates the cross sectional view of the volume mesh. Figure 4.16 indicates the zoomed view of the volume mesh close to the turbine. Interface between the rotational and stationary domains is also visible there. Figure 4.17 indicates the surface mesh on turbine blade suction and pressure sides and figure 4.18 indicates the y plus distribution along the turbine suction and pressure sides.

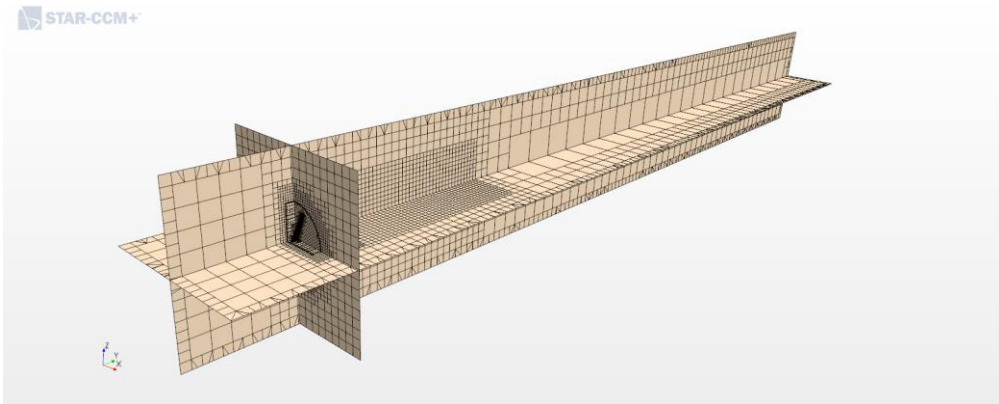


Figure 4.15 Sectional view of the volume mesh

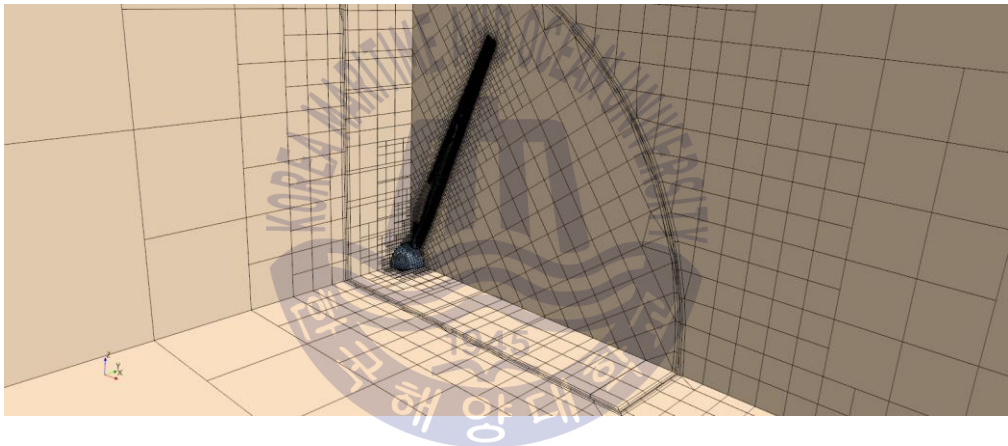


Figure 4.16 Zoomed sectional view of the volume mesh closer to the turbine region

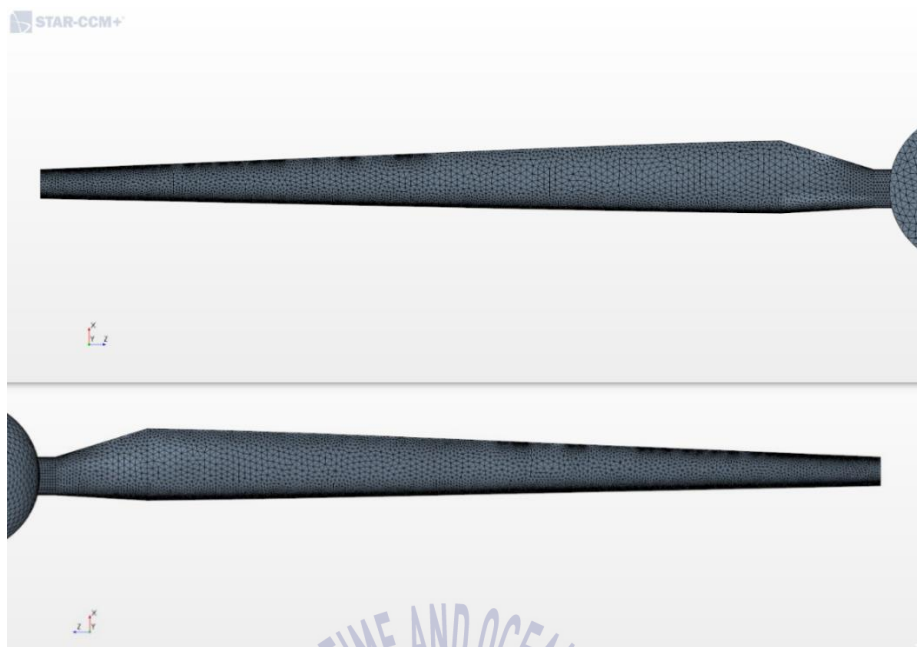


Figure 4.17 Surface mesh of the blade

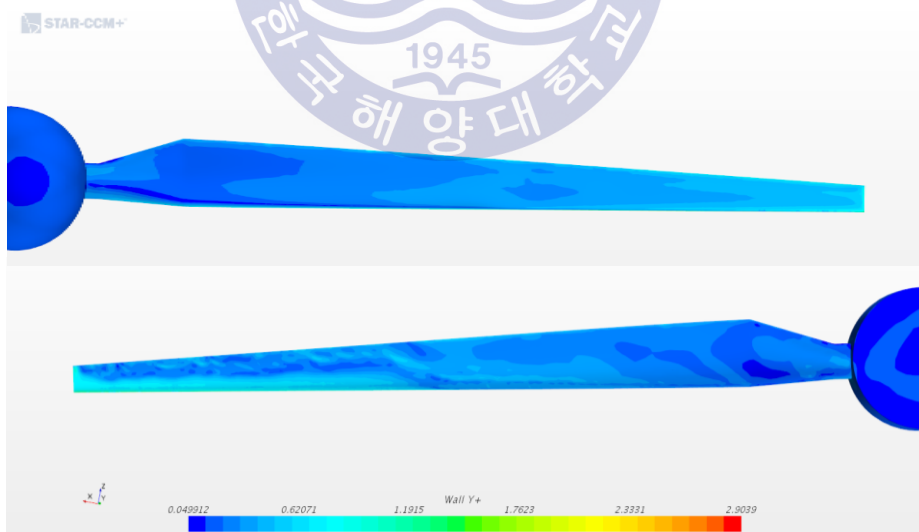


Figure 4.18 Y plus values on blade surface

4.4. Flange type velocity booster analysis

2-D and 3-D drawing of the all four booster models were indicated in the figure 3.15 to figure 3.22 in chapter 3. Those 3-D CAD models were used for these simulations.

Basic setting of the simulation is indicated in table 4.5. Numerical domain and its boundary conditions are indicated in table 4.6 and figure 4.19.

Table 4.5 Basic settings for flange type velocity booster simulations

Item	Specification
Simulation type	Unsteady
Turbulence model	K-Omega SST
Fluid	Air
Domain size	Diameter: 10.455 m, length: 45.305 m
Turbulence intensity	0.01
Turbulence viscosity ratio	10
Reference pressure	101 k Pa
Simulation time	10 s
Tested wind velocities (varies)	7.5 m/s

Table 4.6 Boundary conditions for flange type velocity booster simulations

Condition	Related boundaries
Wall	4 (booster walls)
Symmetry	3 (side walls)
Velocity inlet	1 (inlet)
Pressure outlet	2 (outlet)

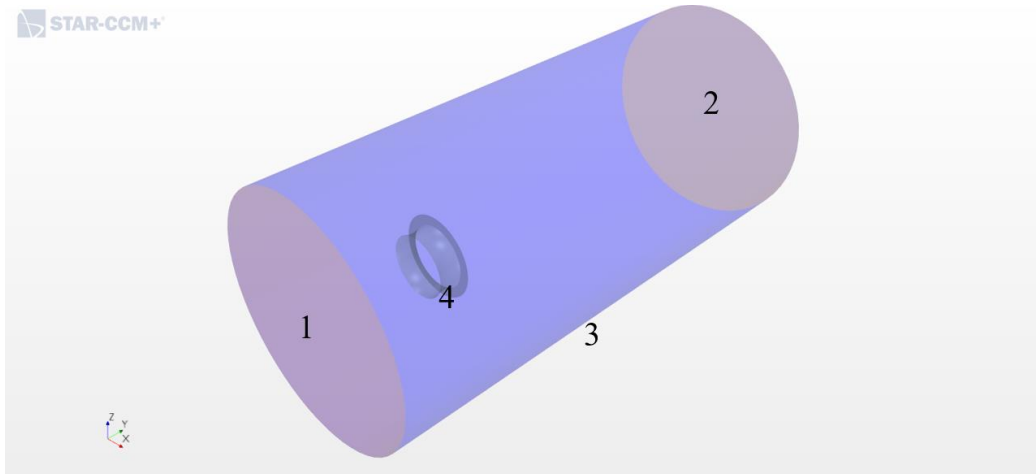


Figure 4.19 Numerical domain of flange type velocity booster analysis

Hexahedral mesh was used as the main type of mesh. It was fined towards the booster and coarsened outwards. 5 layers of prism mesh used near booster wall to capture the boundary layer accurately. Cell count varies according to the booster model. Total cell count in cases of booster model 1 and model 2 are 5,287,878 and 5,708,974 respectively while cases of booster model 3 and model 4, it is 5,673,429 and 5,611,285.

Figure 4.20 indicates the cross sectional view of the volume mesh. Figure 4.21 indicates the zoomed view of the volume mesh close to the booster. Figure 4.22 to figure 4.25 indicates the surface mesh on four booster models.

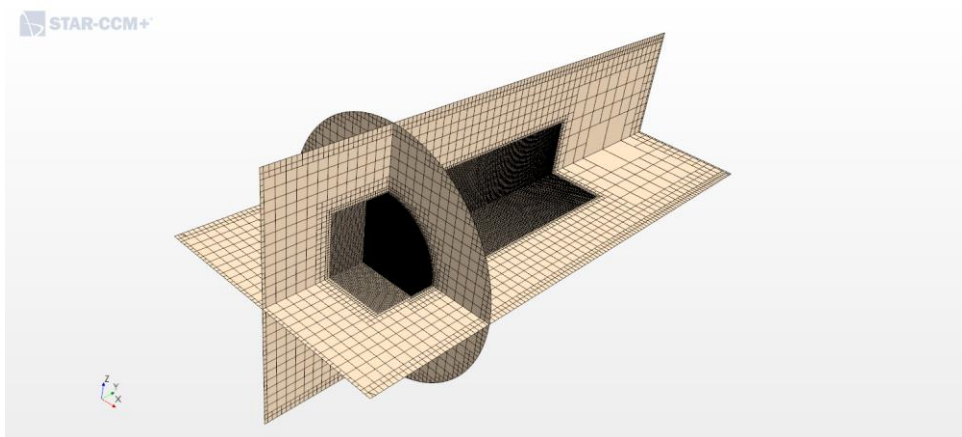


Figure 4.20 Sectional view of the volume mesh

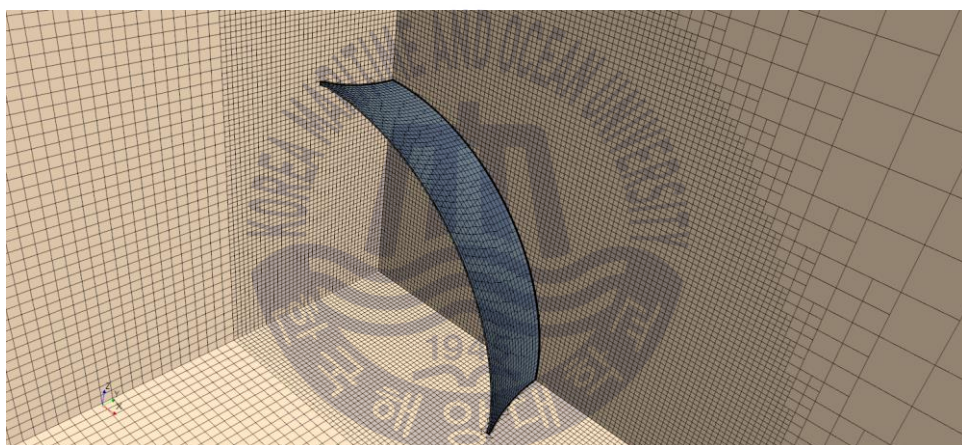


Figure 4.21 Zoomed sectional view of the volume mesh closer to the booster region



Figure 4.22 Surface mesh of the booster model 1



Figure 4.23 Surface mesh of the booster model 2



Figure 4.24 Surface mesh of the booster model 3



Figure 4.25 Surface mesh of the booster model 4

4.5. 2 kW wind turbine analysis with flange type velocity boosters

Same boosters which were previously analyzed were used with the 2 kW wind turbine and indicated below.

Figure 4.26 to figure 4.29 indicates 3-D models of the boosters with 2 kW wind turbine.

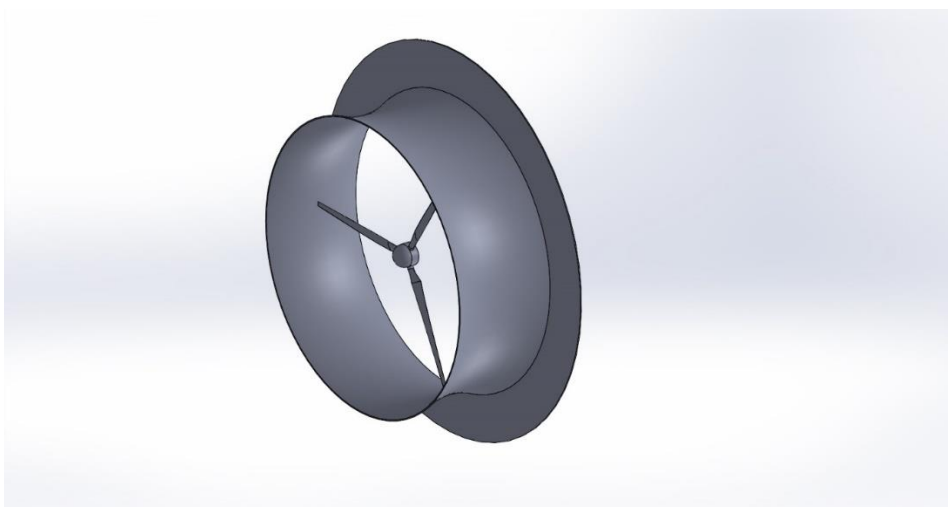


Figure 4.26 2 kW turbine with booster model 1



Figure 4.27 2 kW turbine with booster model 2

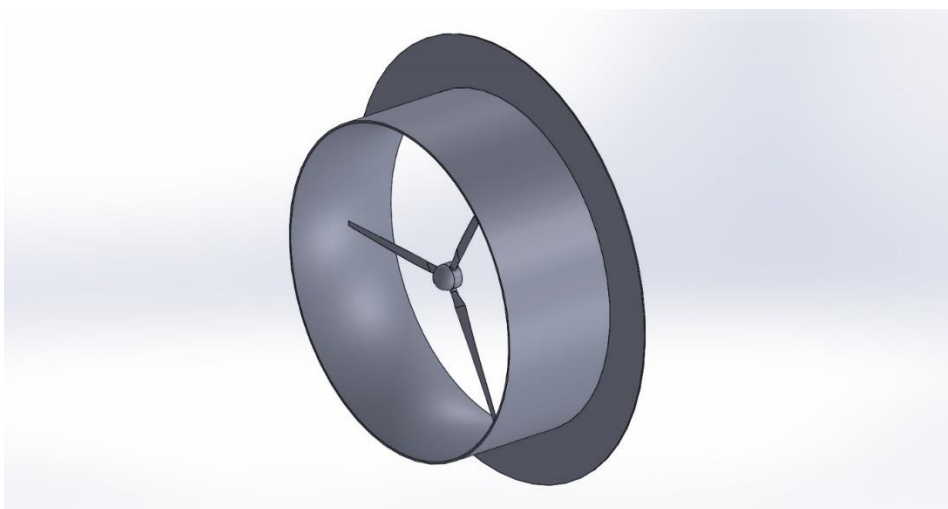


Figure 4.28 2 kW turbine with booster model 3



Figure 4.29 2 kW turbine with booster model 4

Basic setting of the simulation is indicated in table 4.7. Numerical domain and its boundary conditions are indicated in table 4.8 and figure 4.30.

Table 4.7 Basic settings for turbine and booster combine system simulations

Item	Specification
Simulation type	Unsteady
Turbulence model	K-Omega SST
Fluid	Air
Domain size	14.48 m X 107.27 m X 14.48 m
Turbulence intensity	0.01
Turbulence viscosity ratio	10
Reference pressure	101 k Pa
Simulation time	10 s
Tested wind velocities (varies)	2 m/s, 4 m/s, 7.5 m/s, 8 m/s, 10 m/s, 12 m/s, 16 m/s
TSR value (varies)	4, 5, 6, 7, 8, 8.5, 9, 10, 11, 12

Table 4.8 Boundary conditions for turbine and booster combine systems

Condition	Related boundaries
Wall	5 (turbine surface), 6 (booster walls)
Symmetry	3 (side walls)
Velocity inlet	1 (inlet)
Pressure outlet	2 (outlet)
Interface	4 (interfaces between rotating and stationary domains)

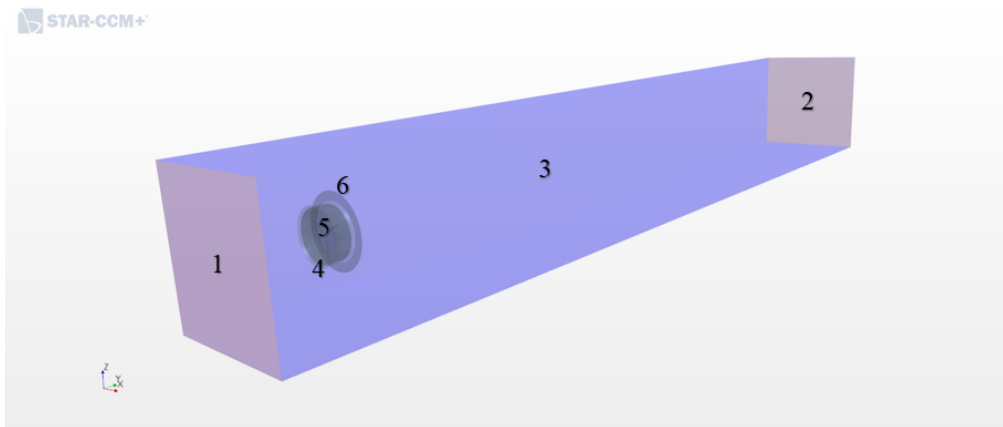


Figure 4.30 Numerical domain of turbine and booster combine systems

Hexahedral mesh was used as the main type of mesh. It was fined towards the turbine and coarsened outwards. 12 layers of prism mesh was used near turbine surface and 5 layers of prism mesh used near booster wall to capture the boundary layer accurately. Cell count varies according to the booster model and indicated below in table 4.9. Figure 4.31 indicates the cross sectional view of the volume mesh. Figure 4.32 indicates the zoomed view of the volume mesh close to the turbine. Interface between the rotational and stationary domains and booster are also visible there. Figure 4.33 to figure 4.40 indicates the surface mesh on 2 kW turbine and booster models and y plus distribution on front and back sides of 2 kW turbine with booster models.

Table 4.9 Cell count in the mesh

Booster model	Cell count		
	Rotating domain	Static domain	Total
Model 1	3,080,082	2,079,429	5,159,511
Model 2	3,072,241	1,519,870	4,592,111
Model 3	3,080,082	1,323,804	4,403,886
Model 4	3,080,082	1,580,657	4,660,739

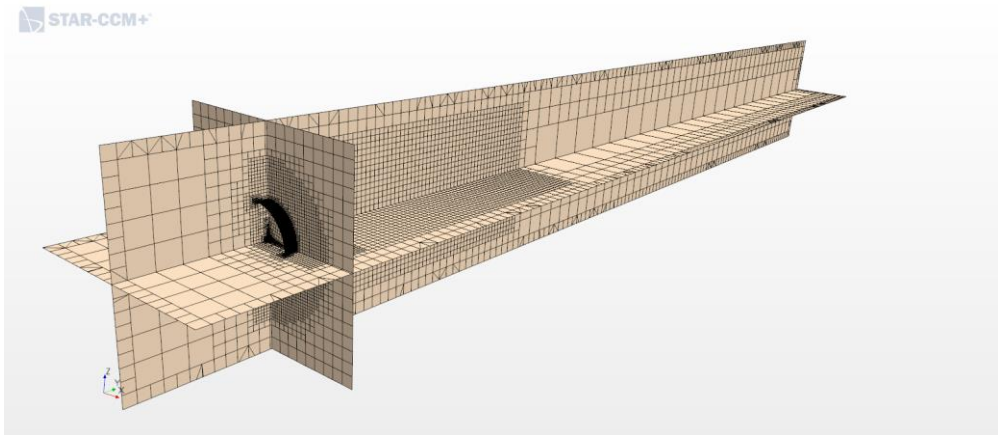


Figure 4.31 Sectional view of the volume mesh

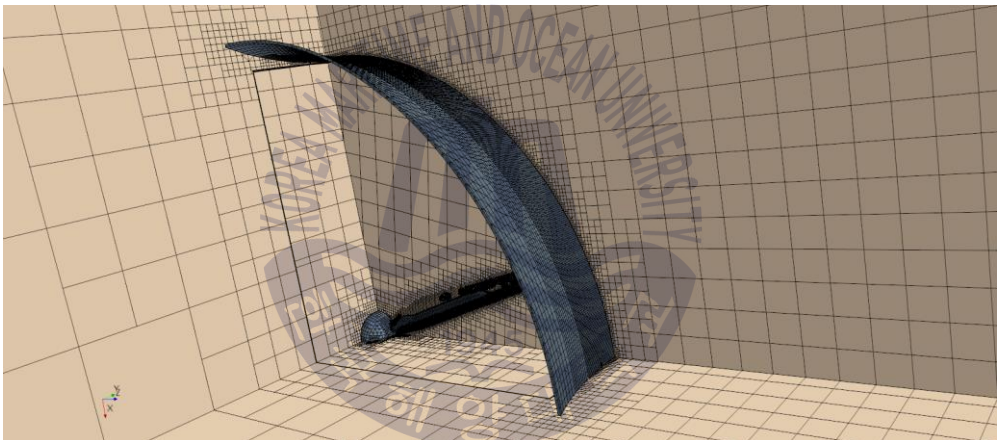


Figure 4.32 Zoomed sectional view of the volume mesh closer to the turbine region



Figure 4.33 Surface mesh of the 2 kW turbine and booster model 1

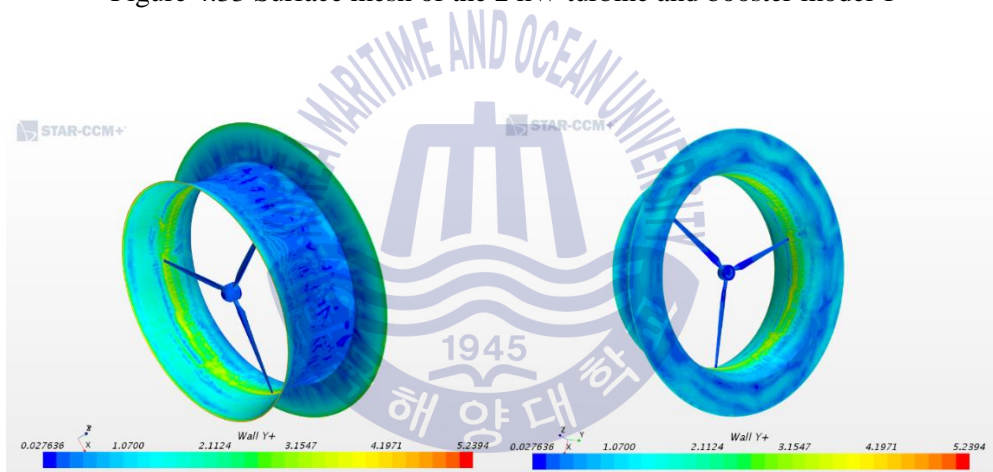


Figure 4.34 Y plus values on 2 kW turbine and booster model 1

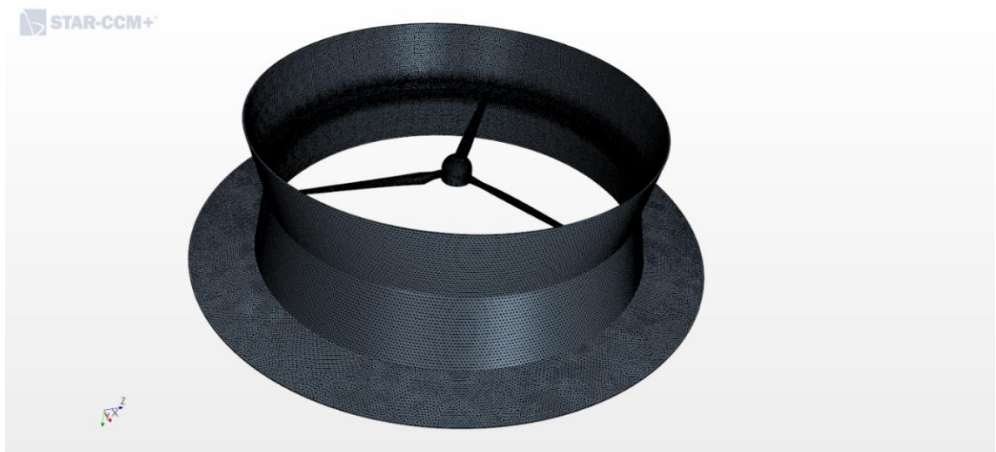


Figure 4.35 Surface mesh of the 2 kW turbine and booster model 2

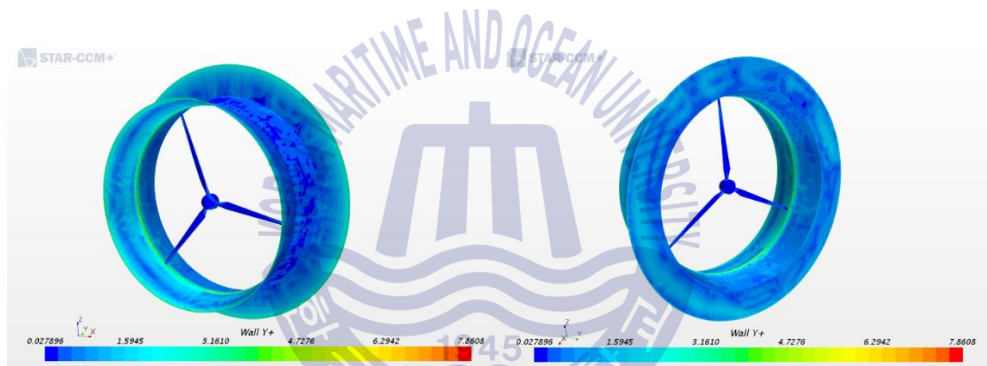


Figure 4.36 Y plus values on 2 kW turbine and booster model 2



Figure 4.37 Surface mesh of the 2 kW turbine and booster model 3

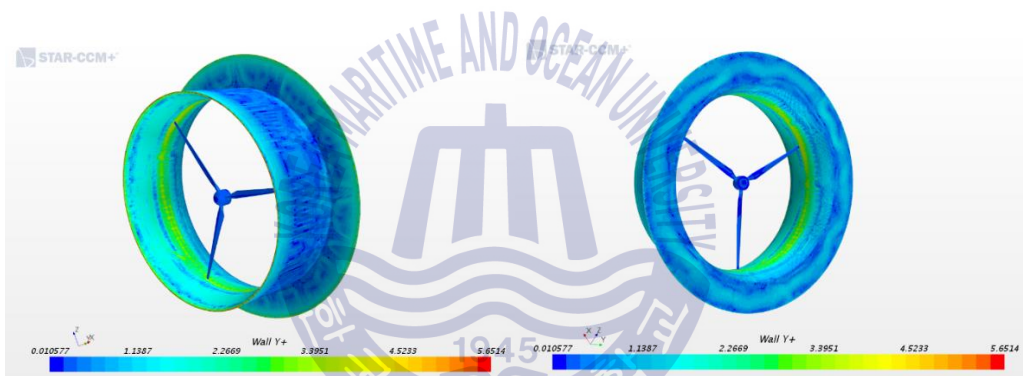


Figure 4.38 Y plus values on 2 kW turbine and booster model 3



Figure 4.39 Surface mesh of the 2 kW turbine and booster model 4

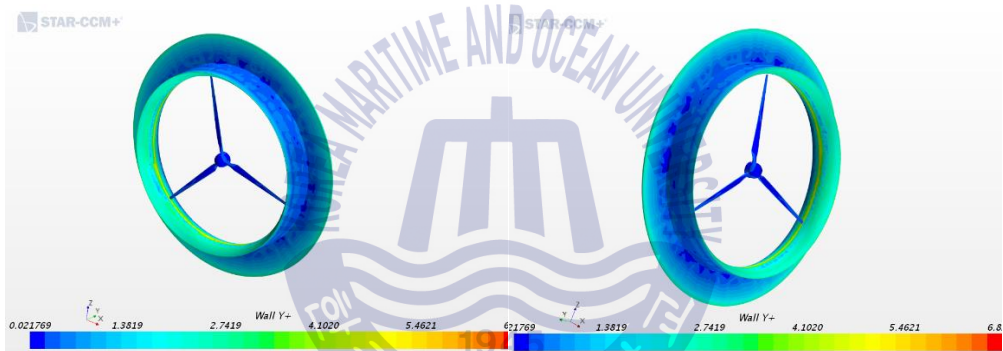


Figure 4.40 Y plus values on 2 kW turbine and booster model 4

Chapter 5. Results and Discussion

Comparison of the NREL phase VI turbine experimental data with the CFD results are done and discussed first in this chapter including power, torque and thrust variation of the turbine with wind velocity. Then 2 kW wind turbine results including power, power coefficient, thrust and torque variation against TSR are analyzed and discussed. Next results of four booster models are analyzed and discussed. Then wind tunnel experimental data and comparison with numerical data is discussed. Next, a total comparison of the data obtained in 2 kW turbine and 2 kW turbine with four different types of boosters are analyzed and discussed. Finally chosen booster model for this application was scaled down to achieve required power output and results are presented in this chapter.

5.1. NREL Phase VI turbine

National Renewable Energy Laboratory of United States has a huge database on experimental data of NREL phase VI wind turbine under different conditions. It is possible to obtain these data to validate numerical models. Upwind baseline test sequence data was requested from the NREL and received. Those were used to compare with the numerical data.

Turbine was in upwind position with blade tip pitch of 3 degrees. Rotational speed was set to 72 rpm. Comparison of the experimental and numerical data is indicated below for these conditions. Four different wind conditions were examined and thrust, torque and power data were examined for those wind conditions.

Table 5.1 and figure 5.1 indicates the comparison of thrust variation with the wind velocity for experimental and numerical cases.

Table 5.1 Thrust comparison

Wind Velocity (m/s)	Thrust (N)	
	Experimental	Numerical
7	1118.75	913.72
10	1631.82	1446.27
13	1986.93	1819.09
15	2247.89	2175.09

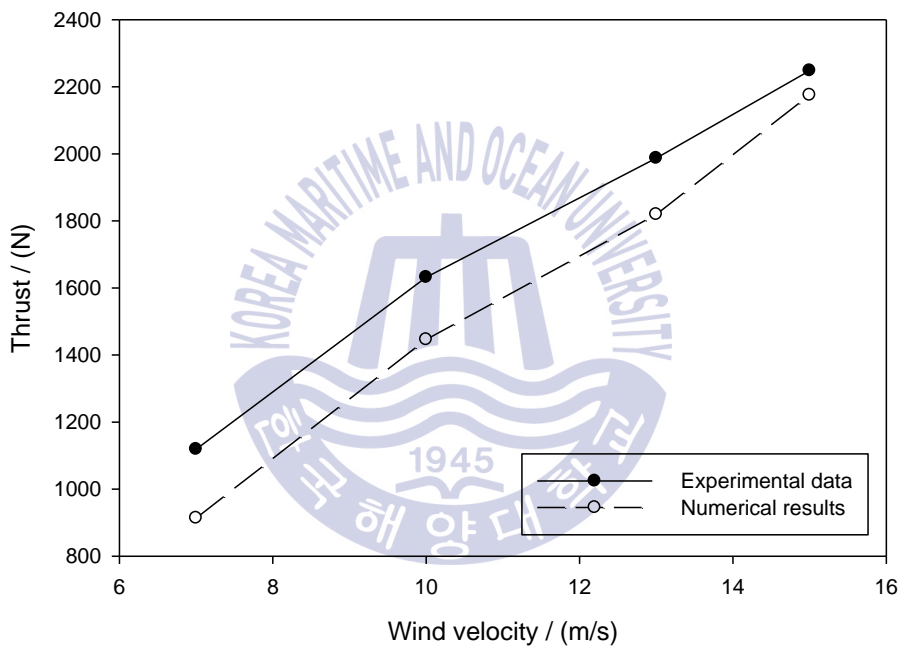


Figure 5.1 Thrust comparison

Thrust values are under predicted in numerical analysis as in figure 5.1. But the variation has a similar pattern in both numerical and experimental values.

Table 5.2 and figure 5.2 indicate the torque comparison of experimental and numerical data.

Table 5.2 Torque comparison

Wind Velocity (m/s)	Torque (Nm)	
	Experimental	Numerical
7	762.4	489.05
10	1305.4	940.93
13	1220.12	912.36
15	1188.31	904.53

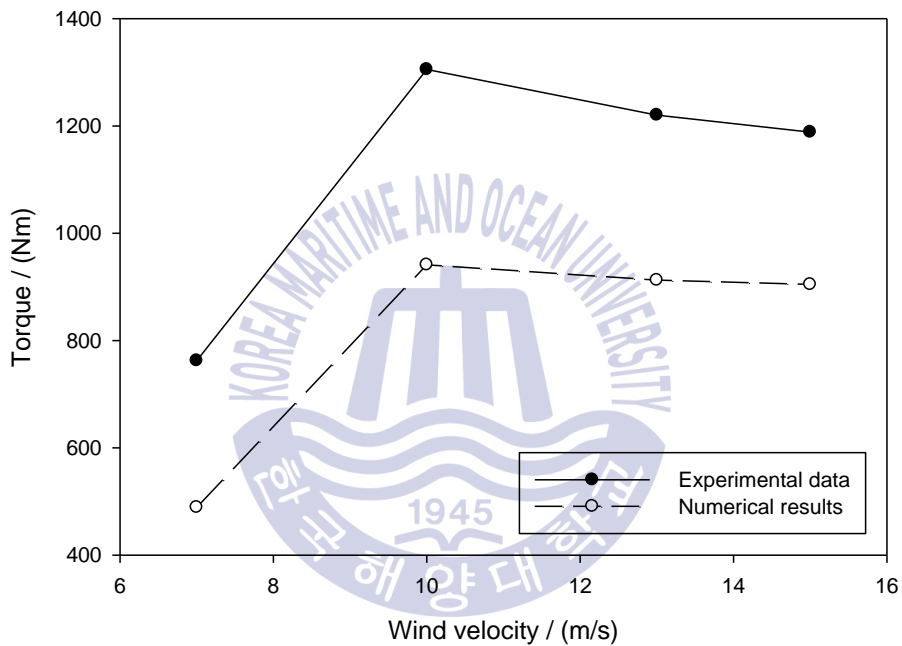


Figure 5.2 Torque comparison

Torque value are seem to be under predicted in numerical analysis according to figure 5.2. This could be improved by a further decrease of y plus values by make the mesh finer.

Table 5.3 and figure 5.3 indicates the power variation with wind velocity in both experimental and numerical analysis cases.

Table 5.3 Power comparison

Wind Velocity (m/s)	Power (kW)	
	Experimental	Numerical
7	3.889	3.682
10	7.35	7.105
13	7.429	6.751
15	7.056	6.826

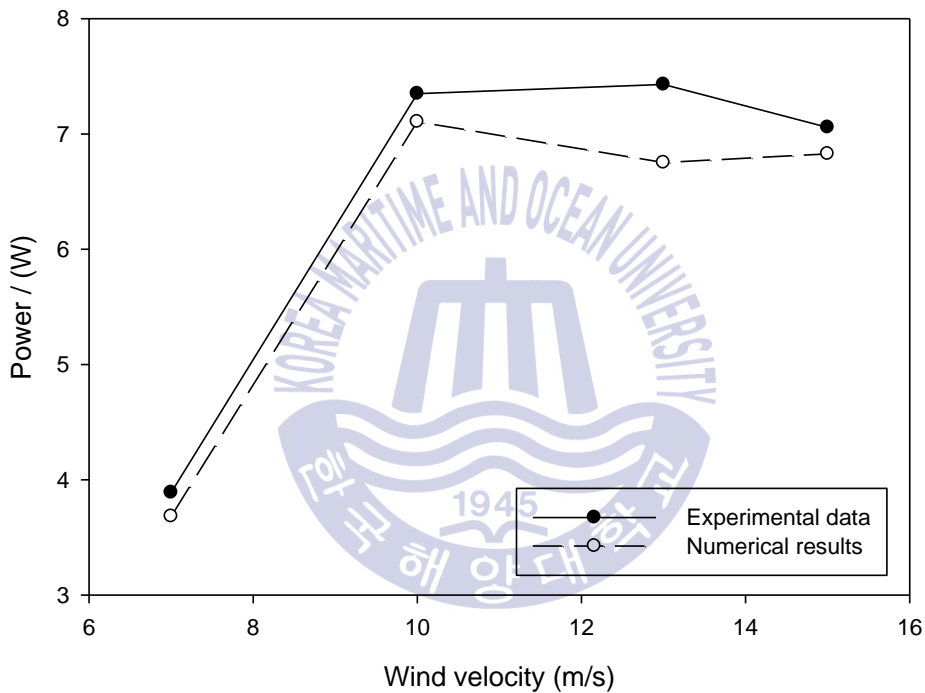


Figure 5.3 Power comparison

Power also under predicted in numerical results due to under predicted results of torque. Overall accuracy could be increased with higher number of cells in a finer grid. But this could not be achieved due to the computational limitations.

Figure 5.4 and figure 5.5 the velocity distribution over planes perpendicular and parallel to the turbine rotational plane respectively.

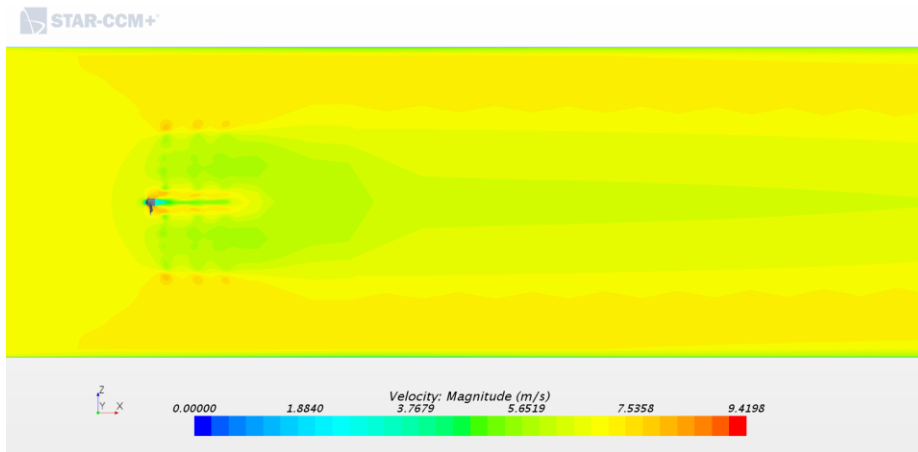


Figure 5.4 Velocity distribution in the plane perpendicular to turbine rotation

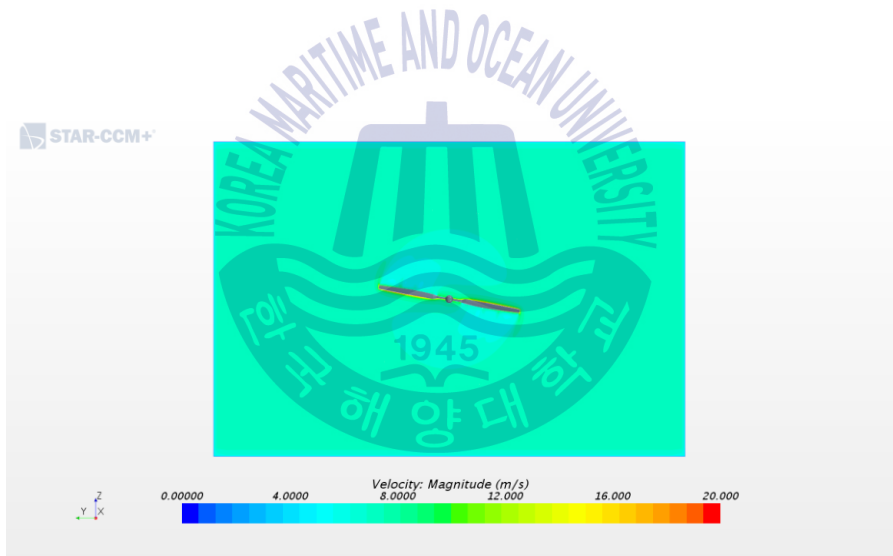


Figure 5.5 Velocity distribution in the plane of the turbine rotation

5.2. 2 kW turbine

2 kW wind turbine was analyzed and obtained results are presented below. Performance of the turbine was checked at wind velocity of 7.5 m/s while varying the TSR. Turbine power, C_p , torque thrust values which were obtained by the numerical calculations are indicated in the table 5.4.

Table 5.4 2 kW turbine overall results

Wind velocity / m/s	TSR	RPM	Turbine Power / W	Cp	Torque / Nm	Thrust / N
7.5	2	59.4	79.7	0.0169	12.81	91.59
7.5	3	89.0	342.53	0.0725	36.74	149.1
7.5	4	118.7	888.56	0.188	71.45	239.83
7.5	5	148.4	1508.63	0.3192	97.04	350.25
7.5	6	178.1	2027.56	0.429	108.73	470.11
7.5	7	207.8	2236.81	0.4732	102.75	564.57
7.5	7.5	222.6	2273.34	0.481	97.48	607.51
7.5	8	237.4	2247	0.4754	90.35	646.92
7.5	9	267.1	2034.32	0.4304	72.7	718.72
7.5	10	296.8	1609.27	0.3405	51.76	779.85

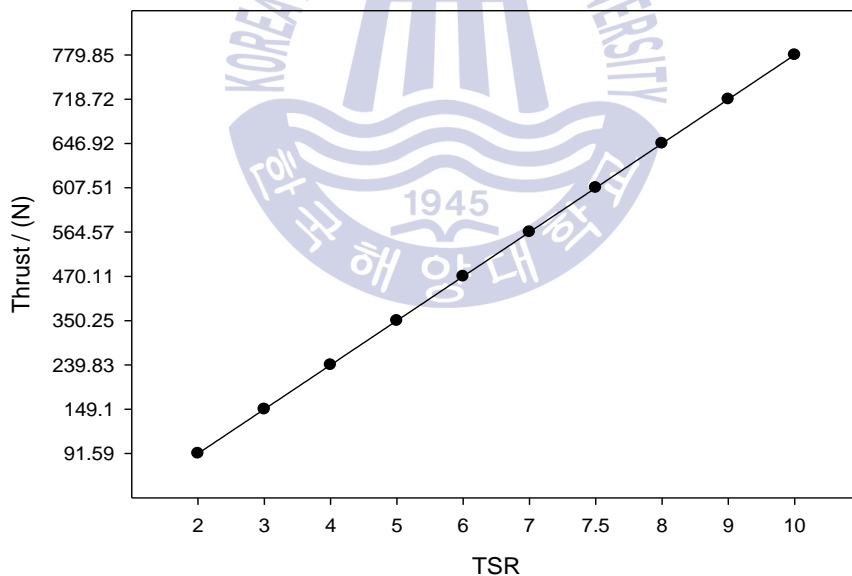


Figure 5.6 Thrust variation with TSR

Turbine thrust is increasing steadily with TSR as indicated figure 5.6.

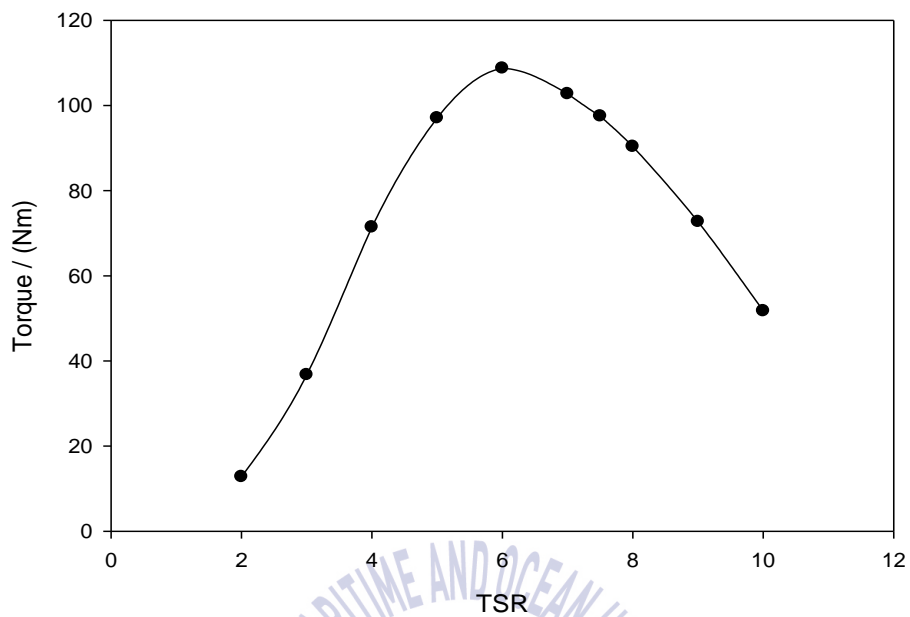


Figure 5.7 Torque variation with TSR

Turbine torque is increasing with the TSR to a maximum value of 108.7 Nm by TSR of 6. Then decreases with the TSR down to 51.7 Nm by TSR of 10 as indicated in figure 5.7.

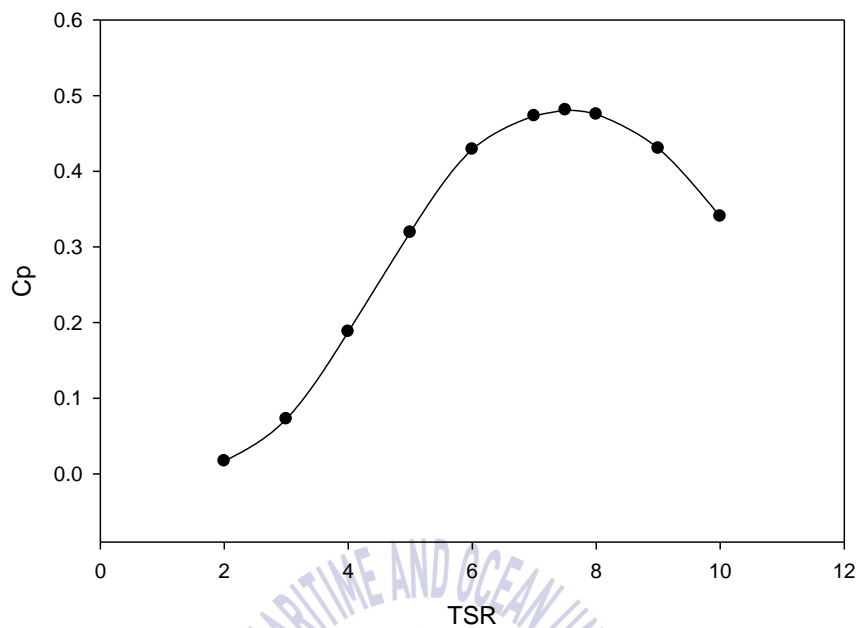


Figure 5.8 C_p variation with TSR

C_p indicates its' maximum value of 0.48 at 7.5 TSR. But has lower values other than 7.6 as in figure 5.8.

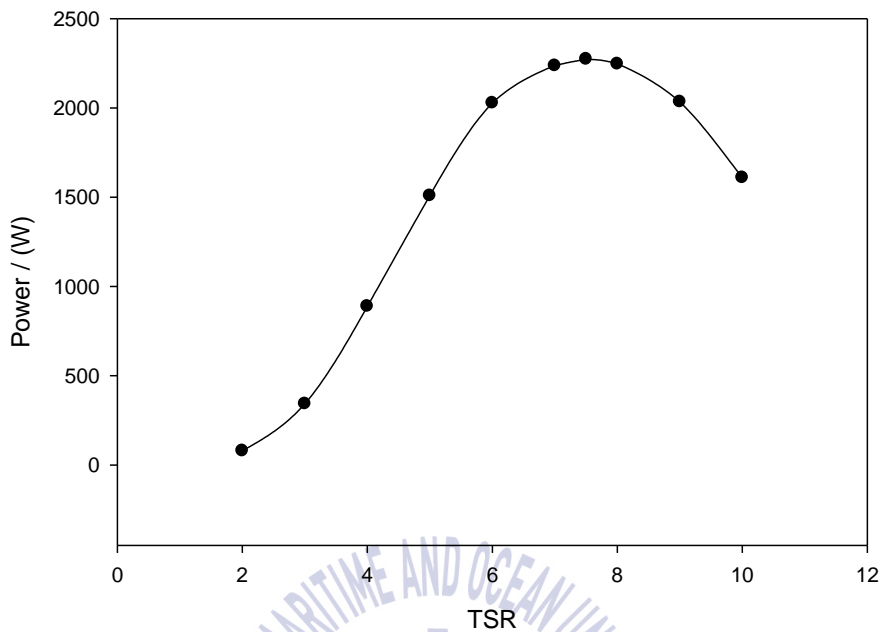


Figure 5.9 Power variation with TSR

Power variation of the turbine is quite similar to its C_p variation graph. Turbine also achieves its design power of 2 kW by TSR 6 and maintain above this design power up to TSR 9. It achieves its maximum power output of 2273.34 W at TSR 7.5. Overall performance of the turbine is up to desired level thus the design can be considered as successful.

Figure 5.10 and figure 5.11 indicate the velocity profile of perpendicular and parallel planes to the wind turbine's rotational plane respectively.

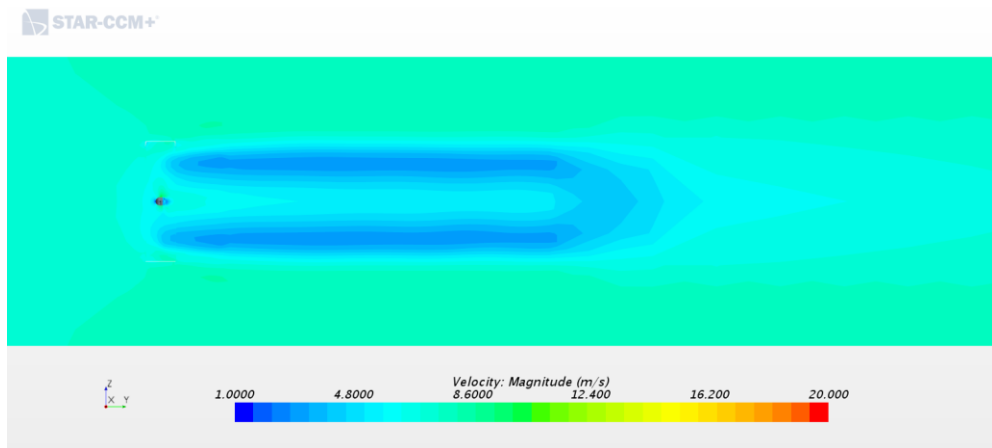


Figure 5.10 Velocity distribution in the plane perpendicular to turbine rotation

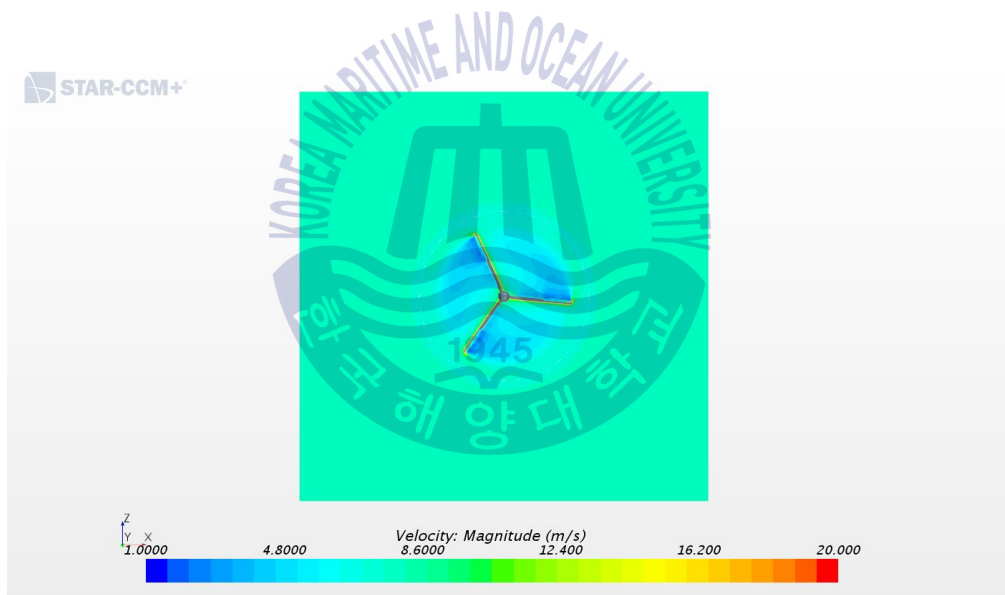


Figure 5.11 Velocity distribution in the plane of the turbine rotation

5.3. Flange type velocity booster models

This section presents the results obtained by the analysis of four booster models.

All four booster models were analyzed for their flow conditions at 7.5 m/s free stream wind velocity, which is the design wind velocity of the turbine. Average wind velocity across the plane where turbine would operate, was measured under three different sectional area conditions. They are, total sectional area inside the booster, area related 0% to 70% of radius and area related to 70% to 90% of radius. Here onwards, area related to 0% to 70% of radius will be referred as middle region and area related to 70% to 90% of radius will be referred as critical region.

Figure 5.12, figure 5.13 and figure 5.14 indicate the velocity distribution over middle region, critical region and total area of four boosters respectively.



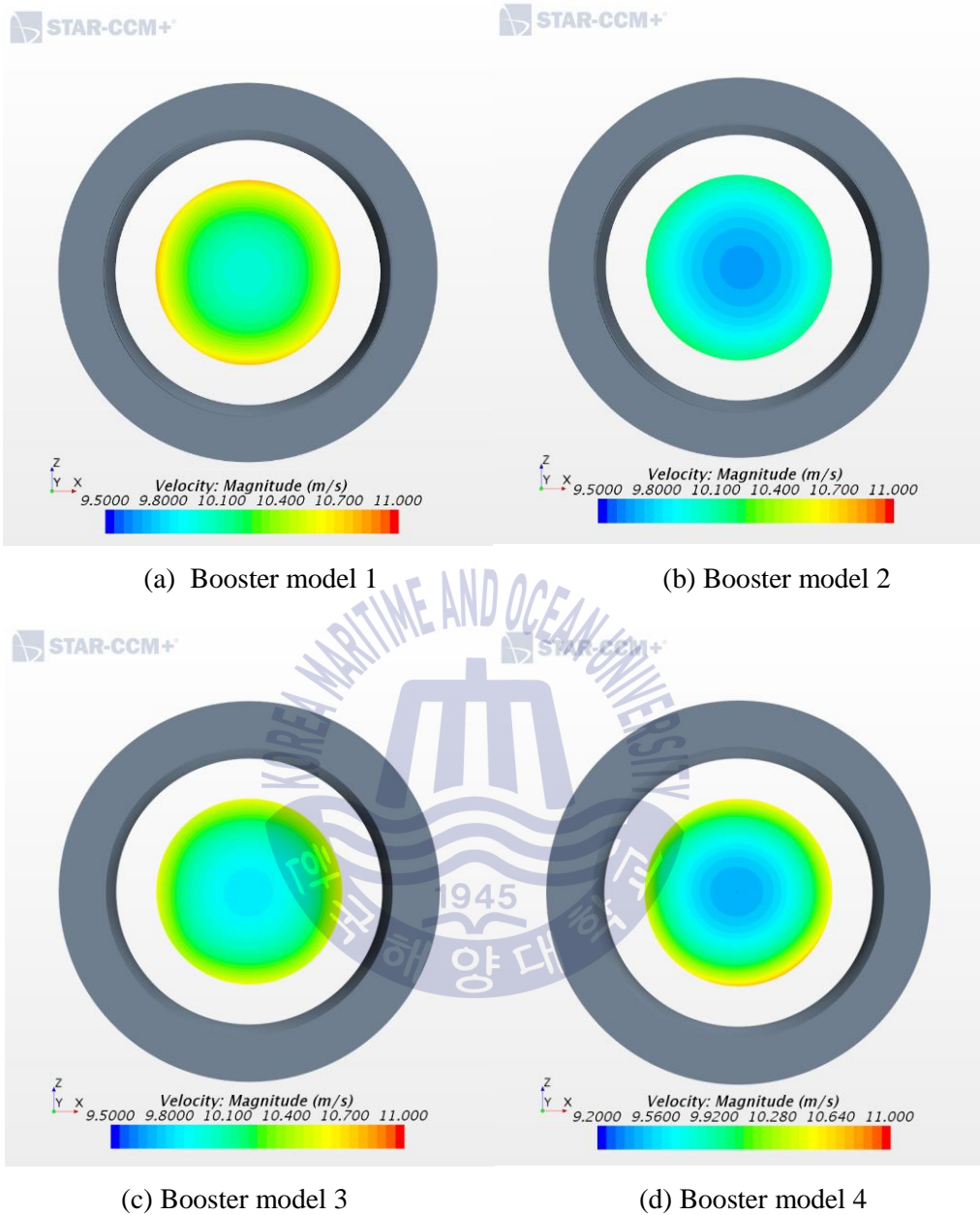
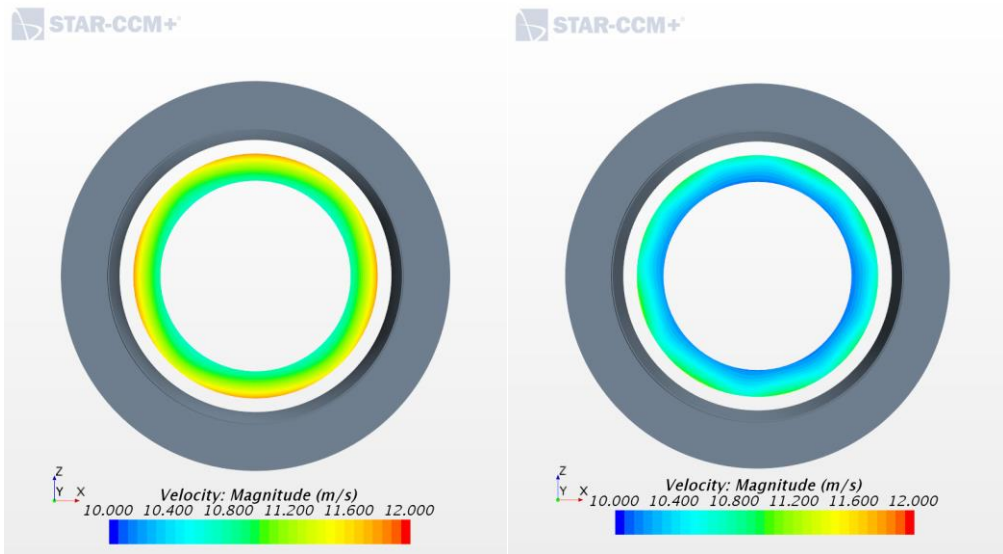
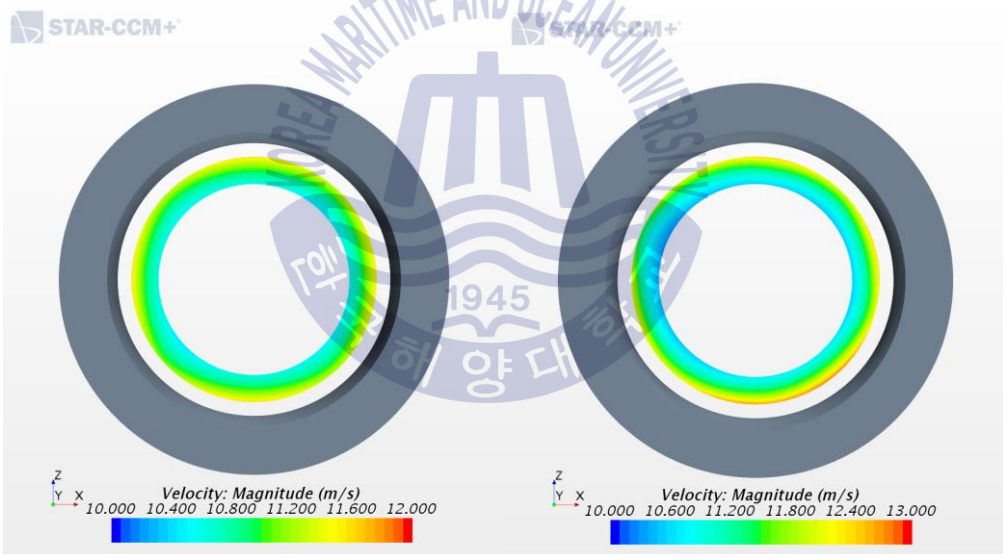


Figure 5.12 Velocity distribution in the middle region



(a) Booster model 1

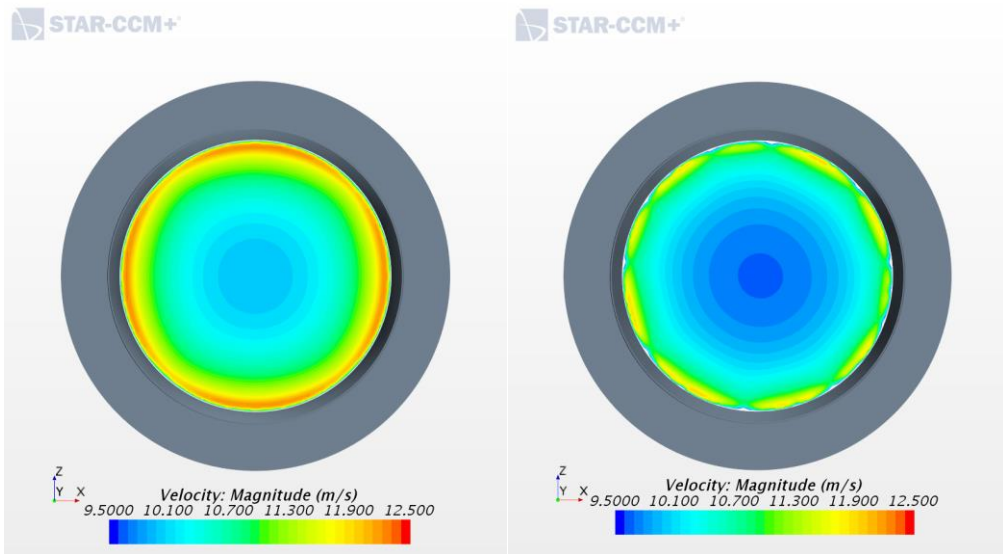
(b) Booster model 2



(c) Booster model 3

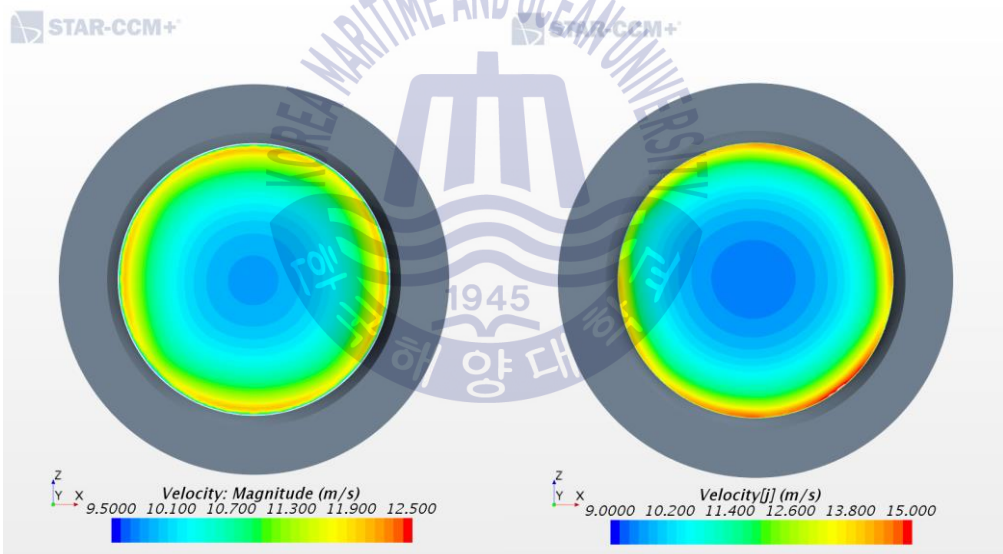
(d) Booster model 4

Figure 5.13 Velocity distribution in the critical region



(a) Booster model 1

(b) Booster model 2



(c) Booster model 3

(d) Booster model 4

Figure 5.14 Velocity distribution in the total area

Table 5.5 Average velocity distribution

Average velocity (m/s)	Booster model 1	Booster model 2	Booster model 3	Booster model 4
Critical region	11.15	10.4	10.94	11.18
Middle region	10.31	9.83	10.15	9.93
Total area	10.84	10.25	10.64	10.89

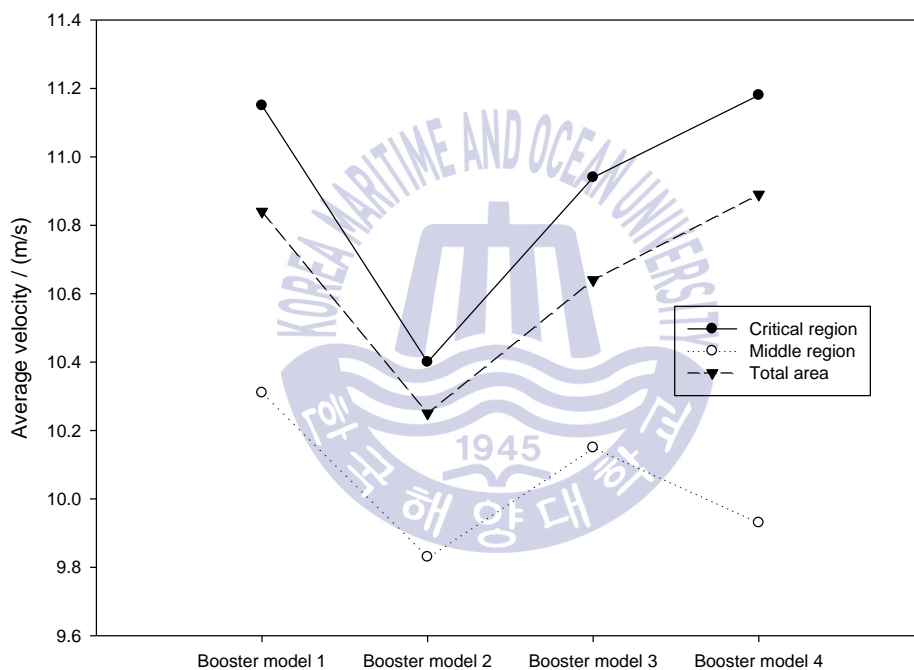


Figure 5.15 Average velocity distribution

Booster model 1 and model 3 indicates similar behavior with best performance. Booster model 2 indicates lower performance compared to above mentioned two models. Booster model 4 which is the compact model indicates higher average velocity in its critical region, but poor average velocity in middle region.

5.4. Wind tunnel experiment

Wind tunnel tests were carried out in the wind tunnel facility in the Korea Maritime and Ocean University. That wind tunnel facility is indicated below in figure 5.16. Wind tunnel test section is 1m X 1m. Booster models were scaled down by a factor of 0.06, in order to minimize the blockage effect. Blockage ratio, which is the ratio of frontal projected area of model upon the cross-sectional area of the test section is 0.16.

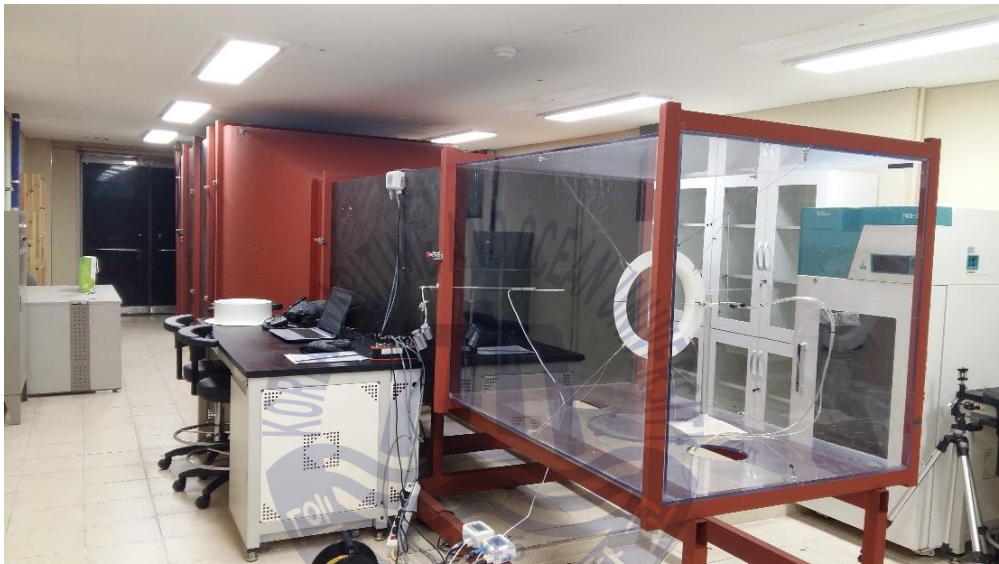


Figure 5.16 Wind tunnel facility

Booster models were placed in the middle of the wind tunnel using cables to minimize the external effects on the flow around booster as indicated in figure 5.17. Wind tunnel velocity was measured at the center of the wind tunnel, 1m ahead of the booster which is closer to 3 diametral lengths respected to booster. Because of this, the readings can be assumed as not getting affected by the flow patterns around the booster. Wind velocity was measured in middle plane of the booster at 10 equally spaced radial positions as well.

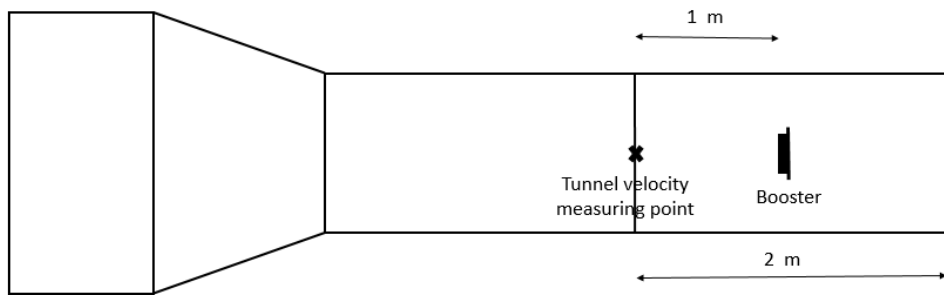


Figure 5.17 Velocity measuring point and booster placement in the wind tunnel

Booster model 3 and booster model 4 were tested in wind tunnel for wind conditions of 5 m/s, 7.5 m/s, 10 m/s and 12.5 m/s. Wind tunnel was again numerically modeled in order to obtain numerical data to compare with the experimental results. Time averaged velocity readings for 30 s were taken in experimental analysis.

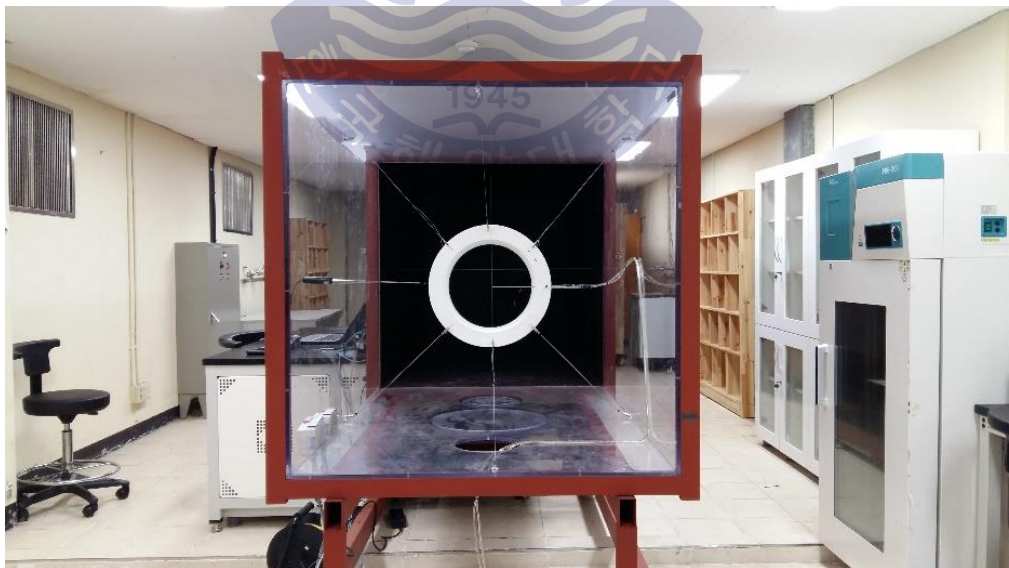


Figure 5.18 Booster orientation in the wind tunnel



Figure 5.19 Velocity measuring points inside the booster

Comparison of the numerical and experimental data is indicated below figure 5.20 to figure 5.27 and table 5.6 to table 5.13.

Table 5.6 Velocity distribution through booster model 3 at free stream wind velocity of 5 m/s

Radial position	Velocity readings / (m/s)		Percentage velocity increase / (%)	
	Num:	Exp:	Num:	Exp:
0.00	6.849	7.005	36.98	38.44
0.10	6.852	7.050	37.04	41.28
0.20	6.868	7.079	37.36	39.90
0.30	6.900	7.089	38.00	40.93
0.40	6.951	7.136	39.02	41.31
0.50	7.027	7.231	40.54	43.19
0.60	7.136	7.359	42.72	47.47
0.70	7.296	7.488	45.92	49.76
0.80	7.533	7.627	50.66	52.85
0.90	7.917	7.824	58.34	57.11

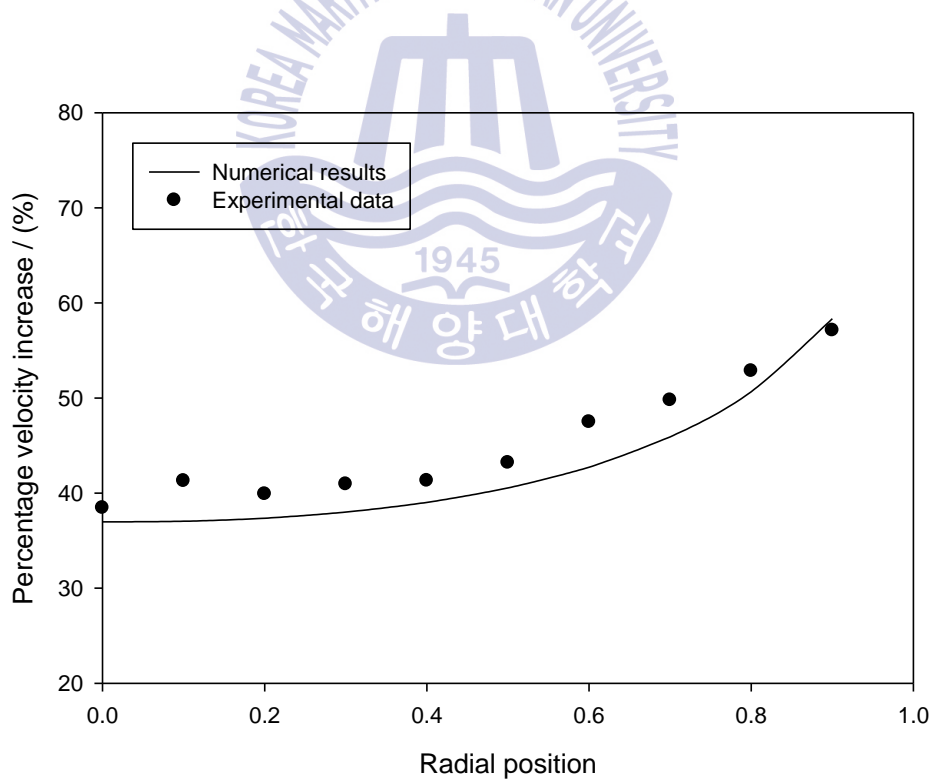


Figure 5.20 Percentage velocity increase through booster model 3 at free stream wind velocity of 5 m/s

Table 5.7 Velocity distribution through booster model 3 at free stream wind velocity of 7.5 m/s

Radial position	Velocity readings / (m/s)		Percentage velocity increase / (%)	
	Num:	Exp:	Num:	Exp:
0.00	10.838	10.680	44.51	42.21
0.10	10.842	10.711	44.56	42.62
0.20	10.875	10.714	45.00	43.62
0.30	10.941	10.896	45.88	45.47
0.40	11.047	11.050	47.29	48.72
0.50	11.200	11.091	49.33	49.07
0.60	11.413	11.224	52.17	49.26
0.70	11.715	11.483	56.20	54.13
0.80	12.143	11.621	61.91	55.78
0.90	12.761	11.911	70.15	60.09

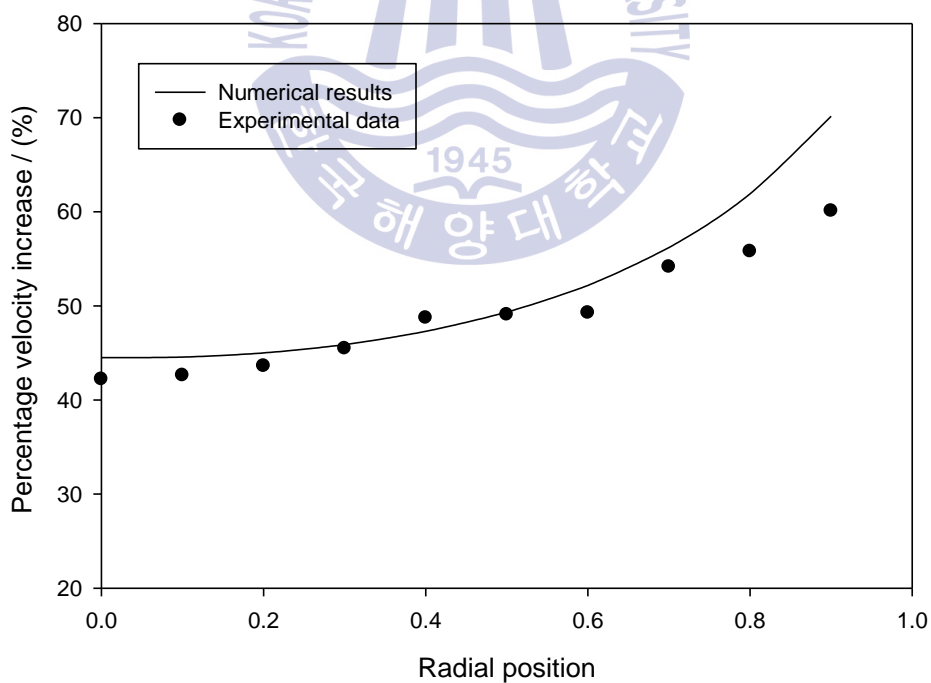


Figure 5.21 Percentage velocity increase through booster model 3 at free stream wind velocity of 7.5 m/s

Table 5.8 Velocity distribution through booster model 3 at free stream wind velocity of 10 m/s

Radial position	Velocity readings / (m/s)		Percentage velocity increase / (%)	
	Num:	Exp:	Num:	Exp:
0.00	14.501	14.545	45.01	44.15
0.10	14.518	14.583	45.18	47.30
0.20	14.577	14.713	45.77	48.77
0.30	14.681	14.781	46.81	48.55
0.40	14.844	14.891	48.44	49.21
0.50	15.075	15.100	50.75	51.76
0.60	15.396	15.204	53.96	51.89
0.70	15.850	15.339	58.50	54.01
0.80	16.499	15.689	64.99	56.58
0.90	17.449	16.197	74.49	62.29

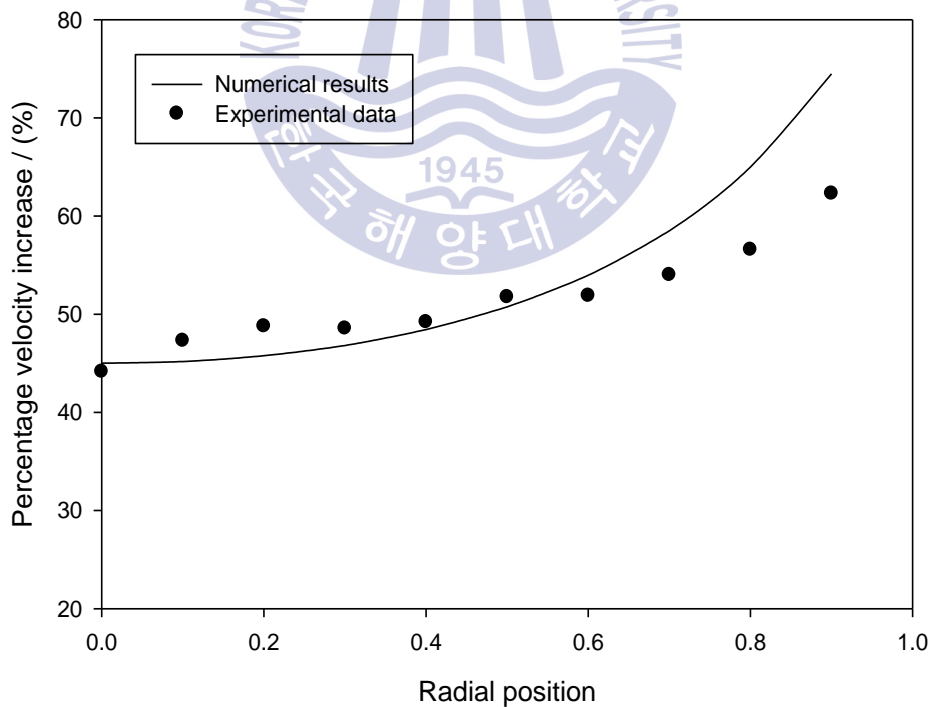


Figure 5.22 Percentage velocity increase through booster model 3 at free stream wind velocity of 10 m/s

Table 5.9 Velocity distribution through booster model 3 at free stream wind velocity of 12.5 m/s

Radial position	Velocity readings / (m/s)		Percentage velocity increase / (%)	
	Num:	Exp:	Num:	Exp:
0.00	17.897	18.191	43.18	45.06
0.10	17.885	18.329	43.08	46.28
0.20	17.919	18.347	43.35	45.96
0.30	18.000	18.632	44.00	49.53
0.40	18.138	18.669	45.10	48.88
0.50	18.343	18.856	46.74	51.21
0.60	18.633	19.100	49.06	53.41
0.70	19.051	19.297	52.41	54.75
0.80	19.659	19.659	57.27	57.65
0.90	20.545	20.320	64.36	61.91

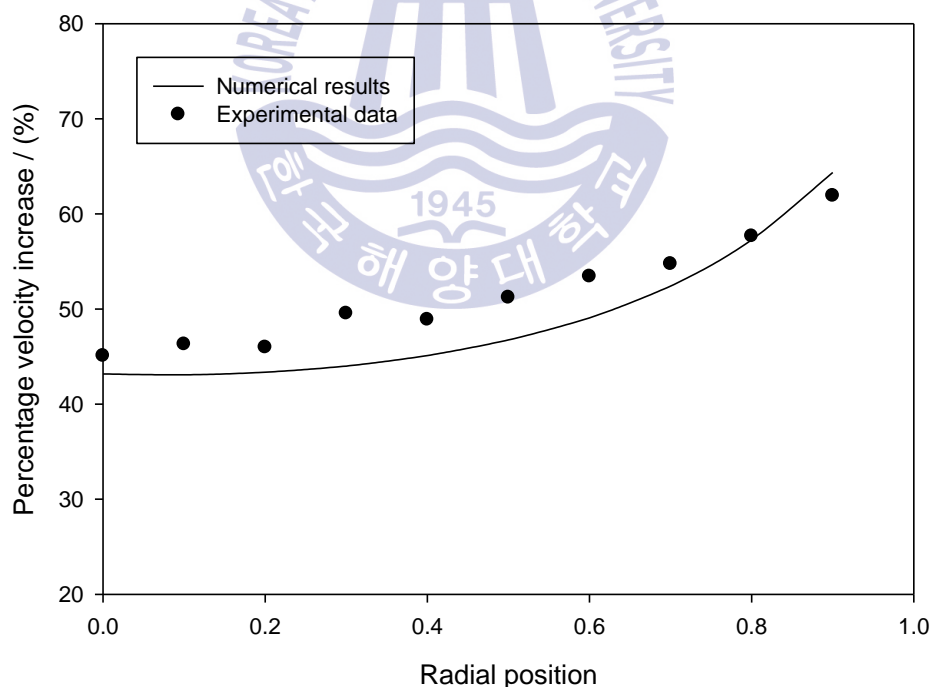


Figure 5.23 Percentage velocity increase through booster model 3 at free stream wind velocity of 12.5 m/s

Table 5.10 Velocity distribution through booster model 4 at free stream wind velocity of 5 m/s

Radial position	Velocity readings / (m/s)		Percentage velocity increase / (%)	
	Num:	Exp:	Num:	Exp:
0.00	6.383	6.311	27.66	25.97
0.10	6.390	6.284	27.80	26.18
0.20	6.403	6.292	28.06	26.35
0.30	6.439	6.306	28.78	28.96
0.40	6.477	6.353	29.54	26.81
0.50	6.531	6.378	30.62	30.43
0.60	6.652	6.413	33.04	33.60
0.70	6.780	6.663	35.60	33.26
0.80	6.977	6.670	39.54	34.75
0.90	7.566	6.858	51.32	36.61

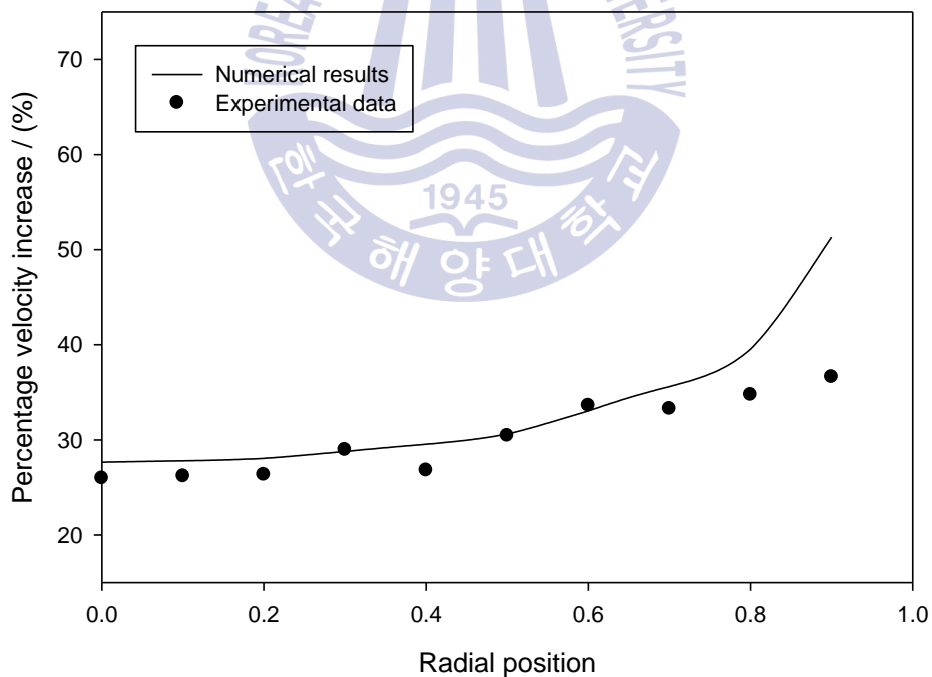


Figure 5.24 Percentage velocity increase through booster model 4 at free stream wind velocity of 5 m/s

Table 5.11 Velocity distribution through booster model 4 at free stream wind velocity of 7.5 m/s

Radial position	Velocity readings / (m/s)		Percentage velocity increase / (%)	
	Num:	Exp:	Num:	Exp:
0.00	9.570	9.486	27.60	25.64
0.10	9.580	9.488	27.73	25.67
0.20	9.605	9.517	28.07	27.74
0.30	9.670	9.631	28.93	28.07
0.40	9.739	9.663	29.85	29.88
0.50	9.833	9.730	31.11	30.60
0.60	10.047	9.819	33.96	32.15
0.70	10.271	9.992	36.95	32.17
0.80	10.606	10.112	41.41	35.01
0.90	11.598	10.426	54.64	39.20

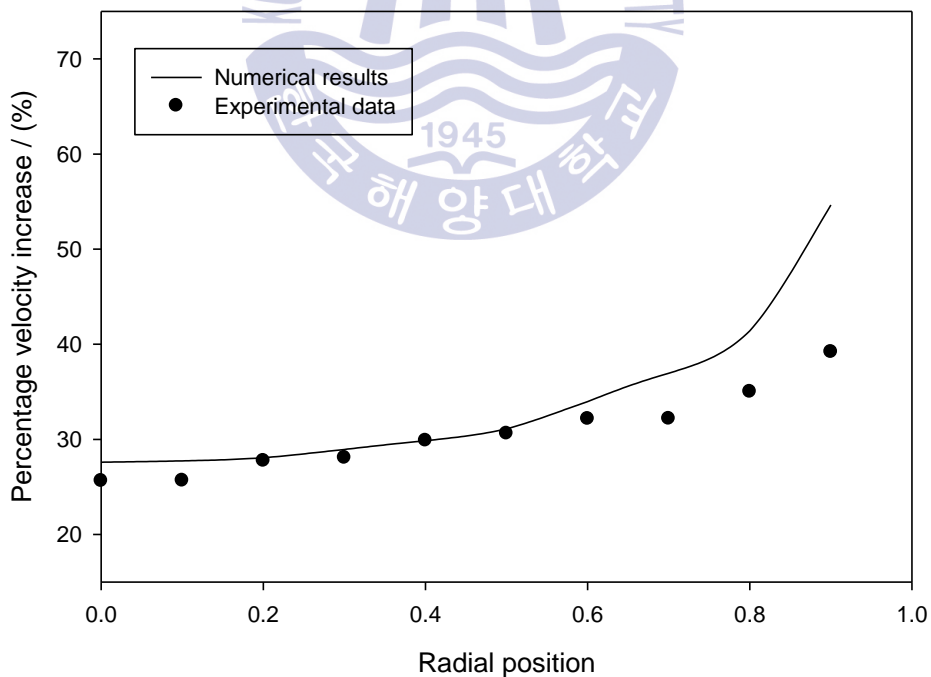


Figure 5.25 Percentage velocity increase through booster model 4 at free stream wind velocity of 7.5 m/s

Table 5.12 Velocity distribution through booster model 4 at free stream wind velocity of 10 m/s

Radial position	Velocity readings / (m/s)		Percentage velocity increase / (%)	
	Num:	Exp:	Num:	Exp:
0.00	12.965	12.940	29.65	27.61
0.10	12.972	13.030	29.72	28.12
0.20	13.017	13.076	30.17	28.57
0.30	13.144	13.105	31.44	30.92
0.40	13.278	13.148	32.78	30.57
0.50	13.464	13.236	34.64	31.05
0.60	13.879	13.396	38.79	32.77
0.70	14.301	13.692	43.01	34.63
0.80	14.930	14.014	49.30	39.30
0.90	16.727	14.356	67.27	42.42

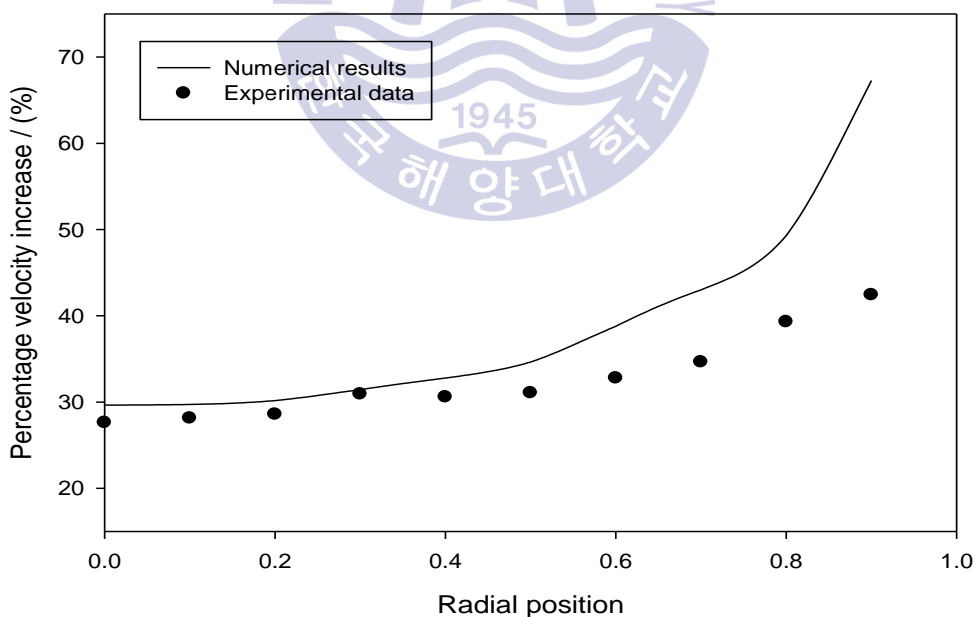


Figure 5.26 Percentage velocity increase through booster model 4 at free stream wind velocity of 10 m/s

Table 5.13 Velocity distribution through booster model 4 at free stream wind velocity of 12.5 m/s

Radial position	Velocity readings / (m/s)		Percentage velocity increase / (%)	
	Num:	Exp:	Num:	Exp:
0.00	16.279	16.065	30.23	28.21
0.10	16.331	16.061	30.65	29.52
0.20	16.401	16.103	31.21	29.13
0.30	16.589	16.238	32.71	29.39
0.40	16.782	16.451	34.26	31.61
0.50	17.043	16.572	36.34	33.54
0.60	17.615	16.790	40.92	34.32
0.70	18.185	17.090	45.48	37.93
0.80	19.022	17.526	52.18	40.66
0.90	21.402	17.957	71.22	43.77

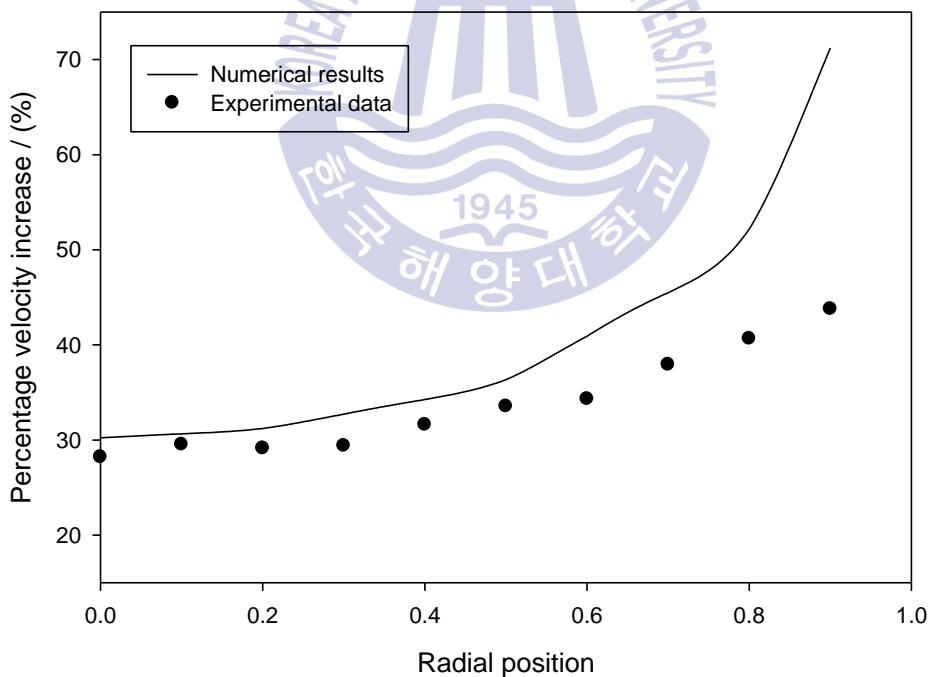


Figure 5.27 Percentage velocity increase through booster model 4 at free stream wind velocity of 12.5 m/s

Considering the booster model 3, 35 to 70 percent of wind velocity increase can be observed. Wind velocity profiles in all four free stream wind velocities indicates similar pattern. But the percentage increase of the wind velocity increases with the increase of free stream wind velocity. Flow throughout the booster indicates quite similar behavior in both numerical and experimental cases.

When consider the booster model 4, 25 to 70 percent of wind velocity increase can be observed. In this case also, wind velocity profile in all four free stream velocities indicates similar pattern. When considering the percentage velocity increase values, region closer to booster wall indicates higher gain when free stream velocity increases but middle region does not indicates such behavior. Flow through the middle region of this booster model indicates quite similar behavior considering numerical and experimental cases. But the flow closer to the booster wall has lower velocity in experimental analysis with compared to the numerical prediction. This might be due to higher turbulence in the region. Velocity fluctuations also could affect this.

When comparing numerical and experimental data, both booster model 3 and booster model 4 indicate considerably good agreement. Thus numerical model can be assumed as good prediction and can be used for further analysis.

5.5. 2 kW turbine with different flange type velocity booster models

This section presents comparison between stand-alone turbine and turbine with four booster models.

Table 5.14 and figure 5.28 indicate the torque variation of stand-alone turbine and turbines with four flange type velocity boosters.

Table 5.14 Torque comparison

TSR	RPM	Torque / Nm				
		Without booster	With booster model 1	With booster model 2	With booster model 3	With booster model 4
2	59.4	12.81	23.58	21.85	23.34	19.27
3	89.0	36.74	30.3	29.86	31.65	28.86
4	118.7	71.45	45.26	46.49	44.99	66.44
5	148.4	97.04	127.96	125.63	128.83	126.03
6	178.1	108.73	189.83	188.16	191.25	155.33
7	207.8	102.75	211.09	202.85	210.96	172.98
8	237.4	90.35	188.86	180.16	188.02	163.28
9	267.1	72.7	149.07	143.53	146.66	129.64
10	296.8	51.76	105.94	105.09	106.02	99.83

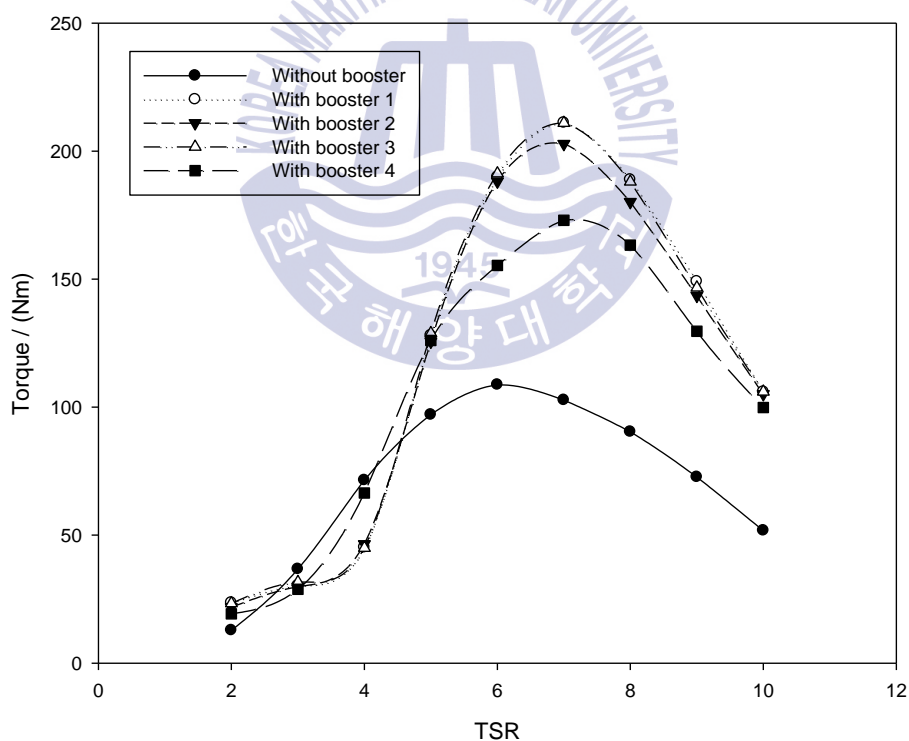


Figure 5.28 Torque comparison

Torque values are lower in turbines with boosters compared to stand alone turbines in lower TSR values, especially under TSR 4.5. All turbines with boosters show higher torque values compared to the stand alone turbine in TSR values beyond 5. Booster model 1 and booster model 3 shows quiet similar behavior while booster model 2 shows slightly lower values compared to booster model 1 and 3. Turbine with booster model 4 shows even lower torque values compared to others. Stand-alone turbine achieves its highest torque values at TSR 6 but turbines with boosters achieve their highest torque values at TSR 7.

Table 5.15 and figure 5.29 indicate the **C_p** variation of stand-alone turbine and four turbines with boosters. **C_p** calculation is based on turbine power output and wind power correspond to turbine swept area and free stream velocity.

Table 5.15 Comparison of power coefficient

TSR	RPM	C _p				
		Without booster	With booster model 1	With booster model 2	With booster model 3	With booster model 4
2	59.4	0.017	0.031	0.029	0.031	0.025
3	89.0	0.073	0.060	0.059	0.063	0.056
4	118.7	0.188	0.119	0.122	0.119	0.175
5	148.4	0.319	0.421	0.413	0.424	0.415
6	178.1	0.429	0.749	0.743	0.755	0.613
7	207.8	0.473	0.972	0.934	0.972	0.797
8	237.4	0.475	0.994	0.948	0.990	0.859
9	267.1	0.430	0.882	0.850	0.868	0.768
10	296.8	0.341	0.697	0.696	0.697	0.657

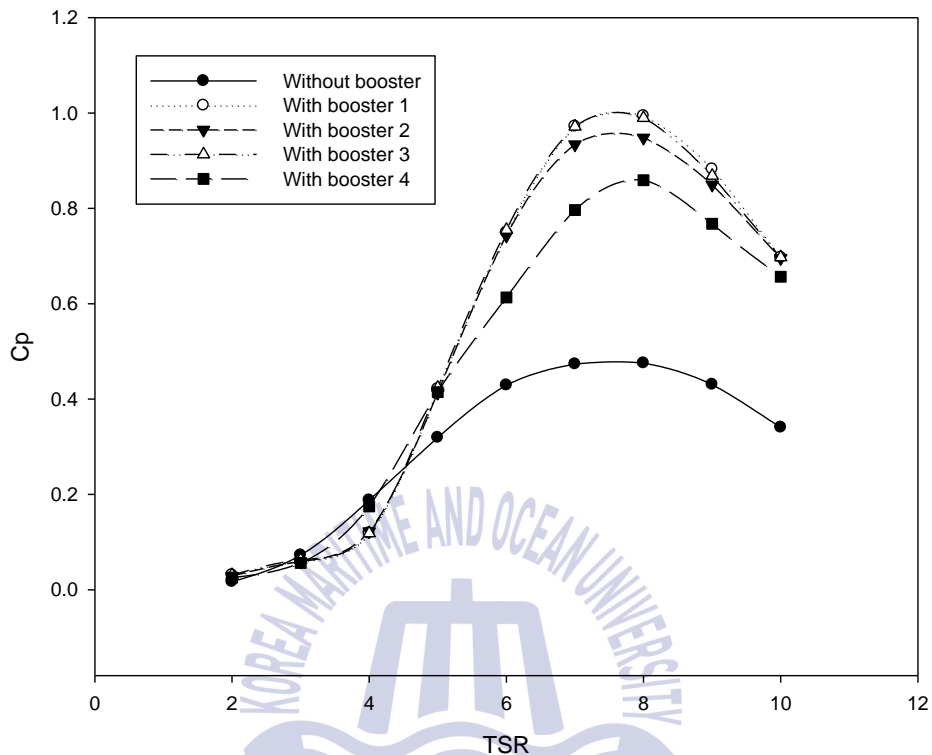


Figure 5.29 Comparison of power coefficient

C_p of turbines with boosters are more similar or lower compared to stand alone turbine below TSR 4.5. But beyond this TSR value turbines with boosters show much higher C_p values compared to the stand alone turbine even though all cases achieve their maximum C_p around 7.5 TSR. Both turbines with booster model 1 and booster model 3 have a similar behavior while turbine with booster model 2 has slightly low C_p values compared to those two. Turbine with booster model 4 has even lower performance. But still indicates better performance compared to stand-alone turbine case.

Table 5.16 and figure 5.30 indicate the power variation of stand-alone turbine and four turbines with boosters.

Table 5.16 Power comparison

Wind velocity / m/s	TSR	RPM	Turbine Power / W				
			Without booster	With booster model 1	With booster model 2	With booster model 3	With booster model 4
2	7.5	59.4	42.40	87.12	83.72	87.08	71.40
3	7.5	89.0	143.09	294.04	282.54	293.88	240.98
4	7.5	118.7	339.17	696.97	669.73	696.62	571.20
5	7.5	148.4	662.43	1361.28	1308.06	1360.58	1115.63
6	7.5	178.1	1144.68	2352.29	2260.33	2351.08	1927.81
7	7.5	207.8	1817.72	3735.35	3589.32	3733.43	3061.29
8	7.5	237.4	2713.32	5575.80	5357.81	5572.93	4569.63



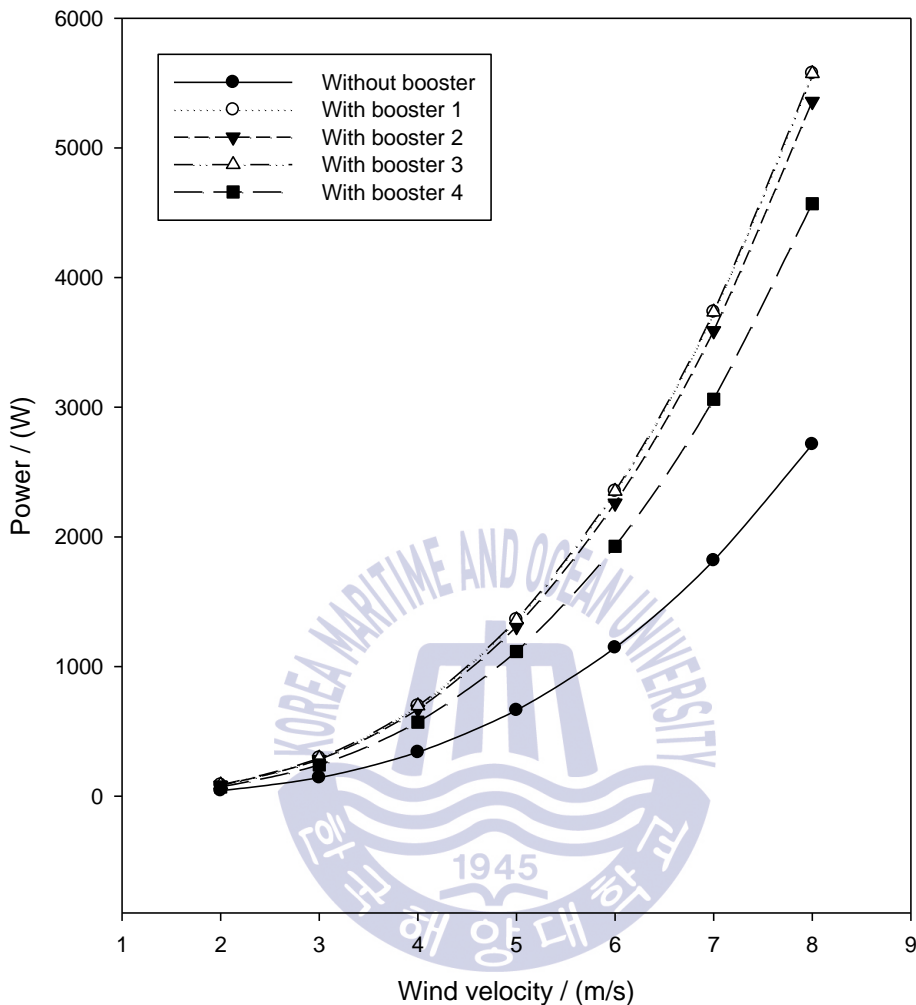


Figure 5.30 Power comparison

Turbines with boosters indicate much higher power output compared to stand-alone turbine. Turbines with first three booster models could improve the power output by a factor of 2 while turbine with booster model 4 improve the power output by a factor of 1.7 compared to stand-alone turbine. Since both booster model 1 and booster model 3 shows similar behavior, it is acceptable to choose either of them considering manufacturing cost. Booster model 4 is also a good choice concerning its' compact size.

Figure 5.31 to figure 5.38 indicate the wind velocity distribution along the plane perpendicular to turbine rotation and Vorticity around the turbine and booster models in all four cases.

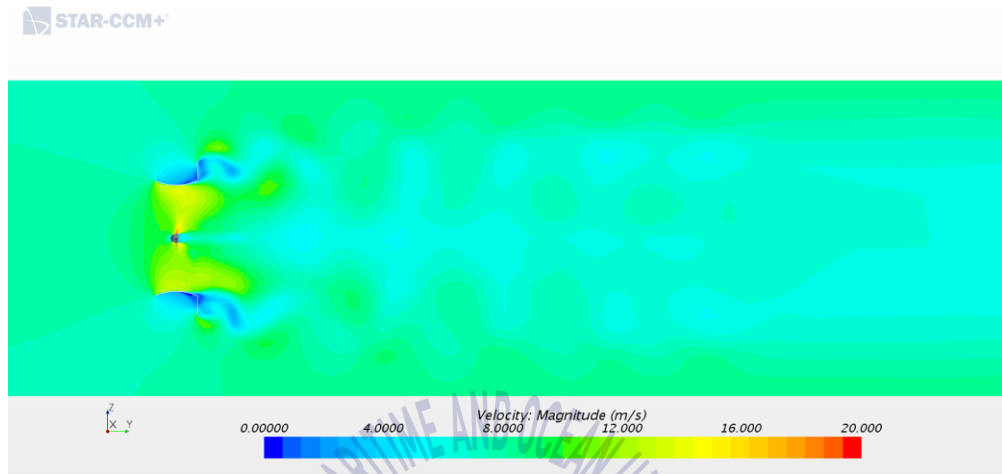


Figure 5.31 Velocity distribution of turbine with booster model 1 in the plane perpendicular to turbine rotation

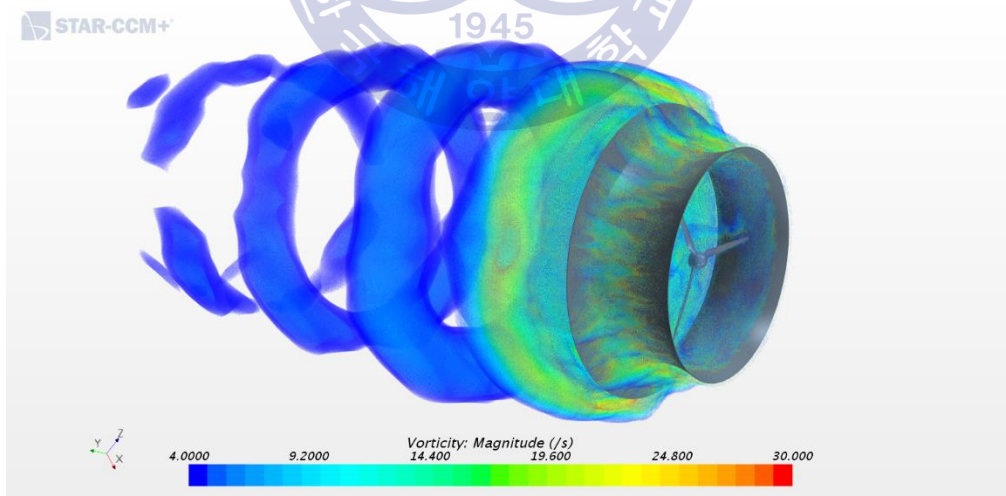


Figure 5.32 Vorticity around booster model 1

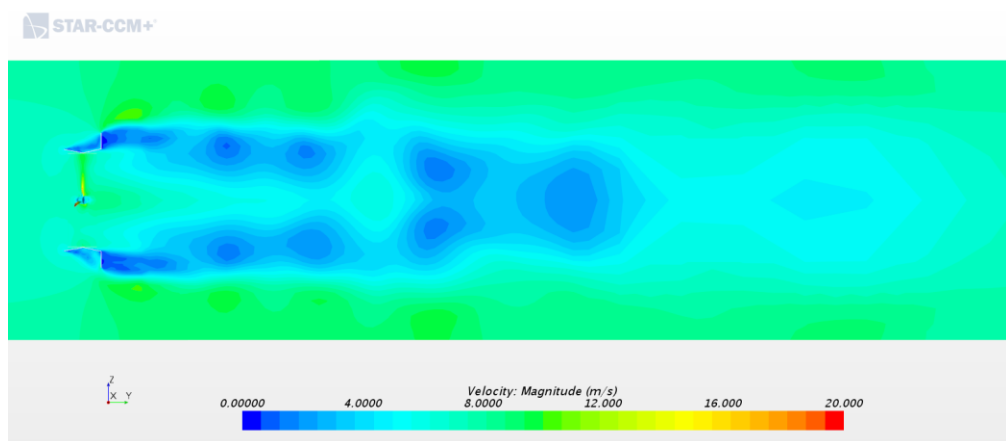


Figure 5.33 Velocity distribution of turbine with booster model 2 in the plane perpendicular to turbine rotation

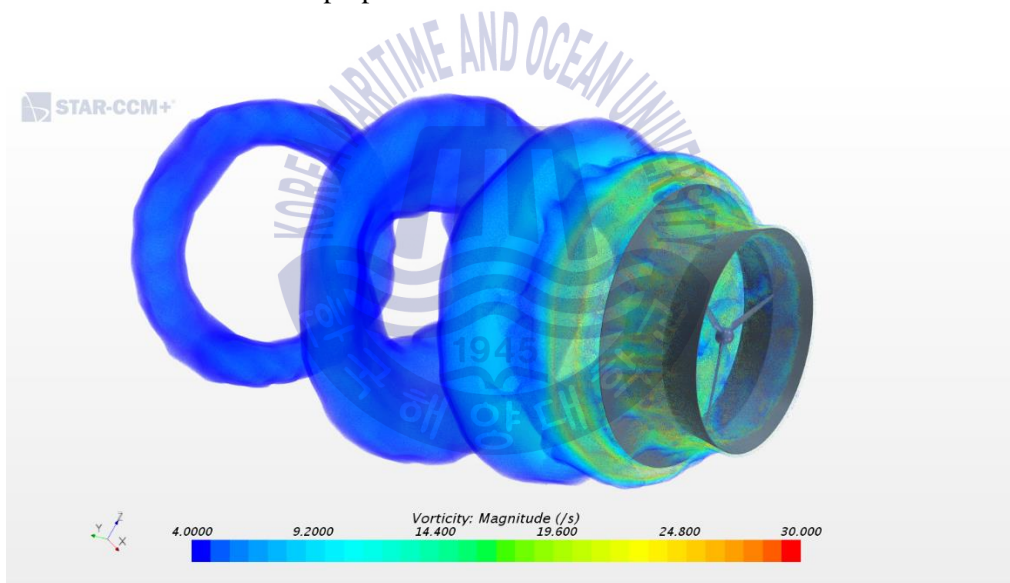


Figure 5.34 Vorticity around booster model 2

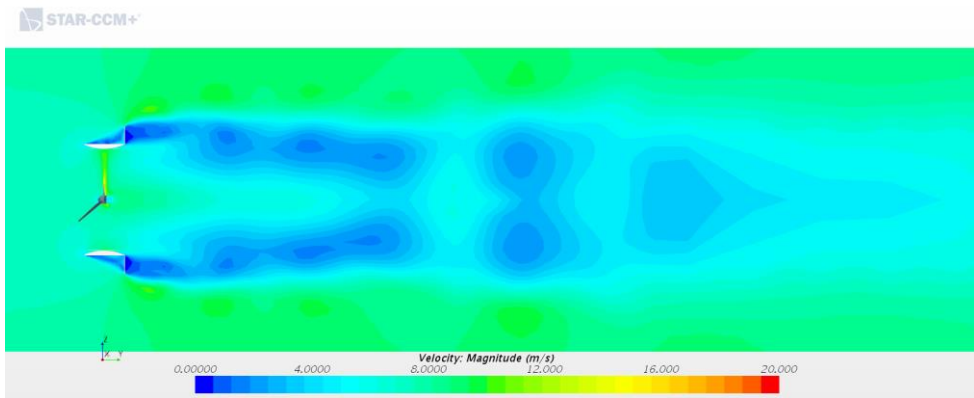


Figure 5.35 Velocity distribution of turbine with booster model 3 in the plane perpendicular to turbine rotation

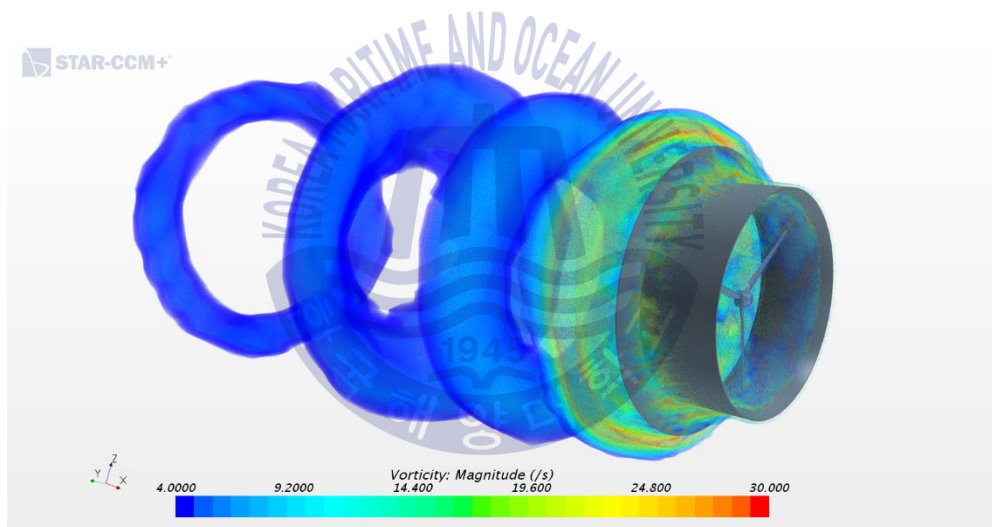


Figure 5.36 Vorticity around booster model 3

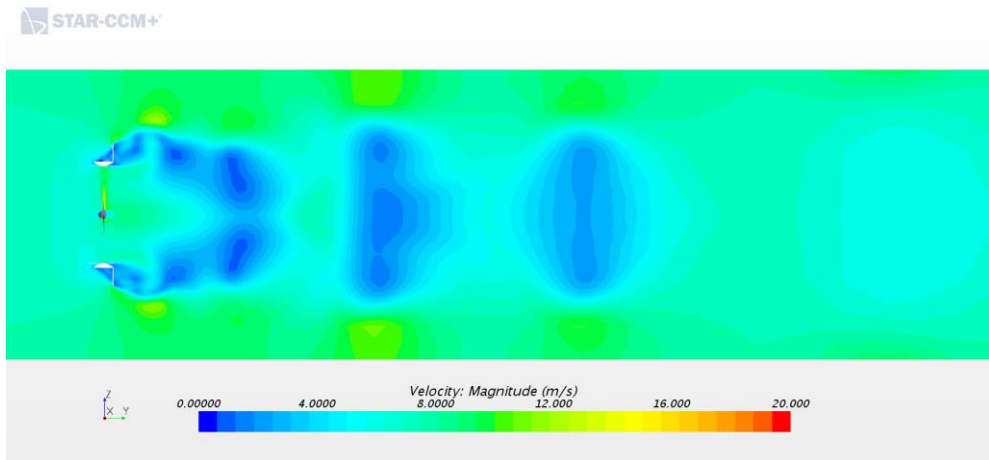


Figure 5.37 Velocity distribution of turbine with booster model 4 in the plane perpendicular to turbine rotation

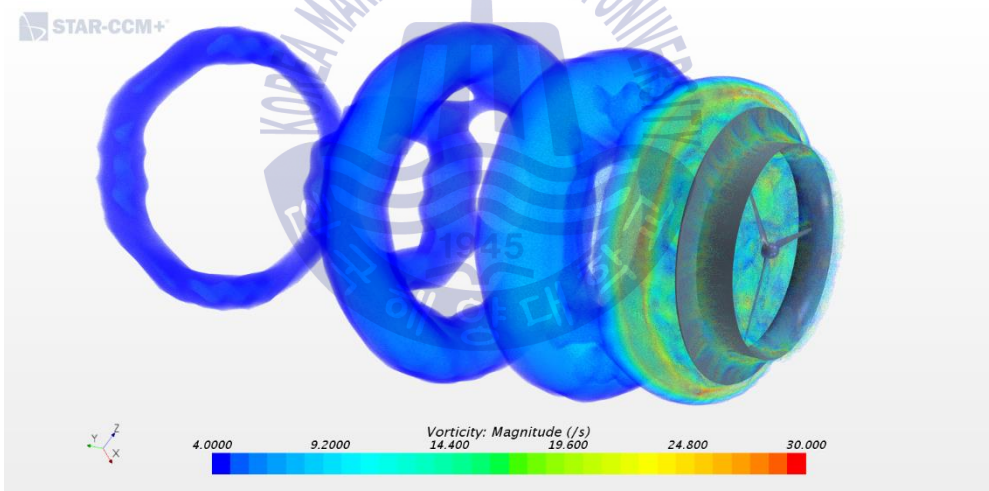


Figure 5.38 Vorticity around booster model 4

It is clear that vortices are generated behind the booster, irrespective to the model. These low pressure regions force to increase wind flow through the boosters which resulted the output power increase of the turbine in all four cases.

5.6. Scaled down turbine-booster system

Considering the size, performance and economical aspects, booster model 4 was chosen for this application, which is a 2 kW wind turbine system. But due to the performance improvement by the booster, originally designed 2 kW turbine is delivering much higher power output than required. So the whole booster-turbine system was scaled down by 25% of its original design size. It is an advantage which gained by the application of booster. Final results are indicated in table 5.17 and figure 5.39 below.

Table 5.17 Power variation with wind velocity

Wind velocity / m/s	TSR	RPM	Turbine Power / W
2	7.5	79.14	40.19
3	7.5	118.71	135.65
4	7.5	158.28	321.55
5	7.5	197.84	628.03
6	7.5	237.41	1085.24
7	7.5	276.98	1723.32
8	7.5	316.55	2572.42
9	7.5	356.12	3662.68
10	7.5	395.69	5024.25
11	7.5	435.26	6687.28

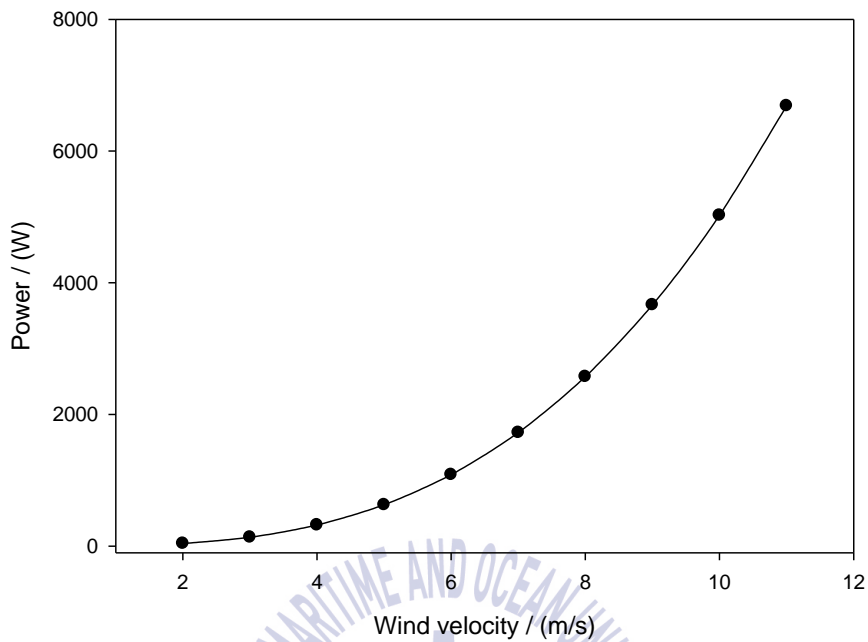


Figure 5.39 Power variation of scaled down turbine with wind velocity

According to these results, final booster-turbine system is capable of delivering required power output of 2 kW at its' design wind velocity of 7.5 m/s and TSR of 7.5.

Chapter 6. Conclusions

This study focused on wind turbine design especially for low wind conditions. Since stand-alone turbine is not sufficient to capture higher output compared to its size, wind condition improving mechanisms were designed and analyzed. Study used finite volume based commercial CFD code star CCM+ to simulate the performance and analyze the results of the simulation.

First Star CCM+ CFD code's ability to predict the wind turbine operation was checked using NREL phase VI wind turbine experimental data. Numerical code's predictions were satisfactory similar to these data, even though it is slightly under predicted. Improving the grid quality will maximize the accuracy of the code which is computationally affordable especially in smaller size wind turbines.

Then a 2 kW wind turbine was designed according to the Blade Element Momentum Theory. NACA 634421 and FX 76MP140 airfoils were used for root region and tip region respectively, considering both structural strength and aerodynamic performances of the turbine blades. Turbine shows higher performance achieving maximum C_p value of 0.48 at its designed wind velocity of 7.5 m/s and TSR of 7.5.

Next, several booster designs were done in order to boost the performances of the turbine. Initially booster sizes were limited by length wise and diameter wise constrains, considering the handling and cost limitations. First booster model was inspired by a similar design for a tidal current turbine. Then internal shape was changed in booster model 2 with aims to reduce the manufacturing complexity. Then the thickness dependence was checked in booster model 3. Final booster model is highly compacted to a half of the length of other three booster models.

All four booster model were first numerically analyzed to check their ability to improve the flow conditions. Booster model 1 and model 3 indicated best performance followed by booster model 2. Booster model 4 indicated higher flow velocity close to its' inner wall but lower flow velocity towards its' middle region compared to other three booster models.

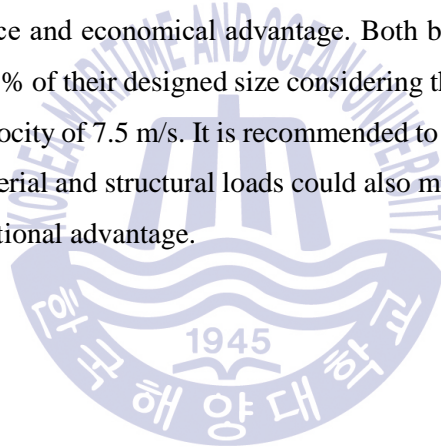
A scaled down models of booster 3 and booster 4 were tested in a wind tunnel and the results were compared with numerical data. Both booster models indicated good

agreement between numerical and experimental data. Thus, numerical model can be considered as accurate.

Finally, turbine was numerically analyzed with four booster models. Those were indicated a significant power boost compared to stand alone turbine case. Turbine with booster model 1 and booster model 3 shows a similar behavior with highest power output around 4.7 kW which is more than twice as much as stand-alone turbines maximum power output of 2.273 kW. These two models are suitable for smaller wind turbines.

Turbine with booster model 2 shows slightly lower performance compared to first two booster models. Turbine with booster model 4 indicates even lower performance compared to first three models. But considering its' compact size and power output increase by a factor of 1.7, it is a good choice to implement.

Booster model 4 was chosen for this application, which is a 2 kW system. It is because of both its' performance and economical advantage. Both booster model 4 and turbine was scaled down by 25% of their designed size considering the required power output of 2 kW at rated wind velocity of 7.5 m/s. It is recommended to maintain 7.5 TSR value for best performance. Material and structural loads could also minimized due to this scaling down which is an additional advantage.



Acknowledgement

First and foremost, I would like to express my sincere gratitude to my supervisor Prof. Dr. Young-Ho Lee for his guidance not only for my studies but also for all other aspects of my life in Korea which aided me a lot. I could not have imagined having a better supervisor and mentor for my studies in Korea.

Beside my supervisor, I would like to thank to thesis committee chairperson Prof. Dr. Dong-Woo Sohn and thesis committee co-chairperson Dr. Byung-Ha Kim for their encouragement, valuable comments and suggestions.

Similarly, I am deeply thankful to Dr. Prasanna Gunawardane, who introduced me to Prof. Dr. Young-Ho Lee and supporting me throughout the time. If not, I would not be able to gain all these.

Next, I would like to thank all my lab mates, Dr. Chang-Goo Kim, Dr. Ji-Hoon Park, Dr. In-Cheol Kim, Mr. Joji Wata, Mr. Ayham Amin, Mr. Batbeleg Tuvshintugs, Ms. Enkhtaivan Batmunkh, Mr. Mesake Navunava, Mr. Ho-Seong Yang, Mr. Hyeon-Soo Park, Mr. Watchara Tongphong and Mr. Ali Azzam for their support and companionship.

Then, I am heartily thankful for my lovely wife Ms. Muthumini Karunarathne who was encouraging me and being with my side through all times. If not, I may not be able to achieve all these.

At last but not least, I'm great full for my parents, sister and brother. For being with me and supporting me in my whole life.

References

- [1] IEA Renewable Energy Working Party. Renewable Energy... into the mainstream. The Netherlands, 2002
- [2] Global Wind Energy Council. Global Wind Statistics – 2017 report. From http://gwec.net/wp-content/uploads/vip/GWEC_PRstats2017_EN-003_FINAL.pdf. Retrieved March 30, 2018
- [3] Wind Power Engineering and Development. Global Wind Report 2016 – Annual market update. From <https://www.windpowerengineering.com/business-news-projects/global-wind-report-2016-annual-market-update>. Retrieved January 16, 2018
- [4] Manwell, J.F., Mc Gowan, J.G. and Rogers, A.L., *Wind Energy Explained*. John Wiley & Sons Ltd, England, Chapter 2, 2002.
- [5] Montessorimuddle.org. (2018). Global Atmospheric Circulation and Biomes | Montessori Muddle. From <http://montessorimuddle.org/2011/04/21/global-atmospheric-circulation-and-biomes>. Retrieved February 23, 2018
- [6] Spera D.A., *Wind Turbine Technology, Fundamental Concepts of Wind Turbine Engineering*, ASME Press; New York, 1994
- [7] Reuk.co.uk. (2018). Savonius Wind Turbines | REUK.co.uk. From <http://www.reuk.co.uk/wordpress/wind/savonius-wind-turbines>. Retrieved January 18, 2018
- [8] Hau, E., *Wind Turbines: Fundamentals, Technologies, Application, Economics*. 2nd edition. New York: Springer-Verlang, 2007, p.86.
- [9] Gasch, R. and Twele, J. Wind power plants. Berlin: Solarpraxis AG, 2002

- [10] Burton, T., Jenkins, N., Sharpe, D. and Bossanyi, E., *Wind energy handbook*. 2nd ed. Chichester: Wiley, 2011
- [11] Schubel, P. and Crossley, R., Wind Turbine Blade Design Review. *Wind Engineering*, 2012, pp 365-388
- [12] Ohya, Y., Karasudani, T., Sakurai, A., Abe, K. and Inoue, M. Development of a shrouded wind turbine with a flanged diffuser. *Journal of Wind Engineering and Industrial Aerodynamics*, 2008, pp 524-539
- [13] Abe, K., Nishida, M., Sakurai, A., Ohya, Y., Kihara, H., Wada, E. and Sato, K. Experimental and numerical investigations of flow fields behind a small wind turbine with a flanged diffuser. *Journal of Wind Engineering and Industrial Aerodynamics*, 2005, pp 951-970
- [14] Kanya, B. and Visser, K. Experimental Validation of a Ducted Wind Turbine Design Strategy. *Wind Energy Science Discussions*, 2017, pp 1-22
- [15] Statistics.gov.lk. (2018). Cow and Buffalo Milk Production. From <http://www.statistics.gov.lk/agriculture/Livestock/MilkProduction.html>. Retrieved April 23, 2018
- [16] Betz .A, Das Maximum der theoretischmoglichen Ausnutzung des Windesdurch Windmotoren, Zeitschrift fur das gesamte Turbinewesen, German, 1920
- [17] Hau, E. Wind turbines: Fundamentals, Technologies, Application, Economics. 2nd edition. New York: Springer- Verlang, 2006, p 84
- [18] Manwell .J.F, Mc Gowen. J.G, Rogers .A.L. Wind Energy, Theory, Design and Applications, Sandia National Laboratories, Wind Turbine Blade Workshop, 2004

[19] Elliott, D., Schwartz, M., Scott, G., Haymes, S., Heimiller, D. and George, R. Wind Energy Resource Atlas of Sri Lanka and the Maldives, 2018

[20] Prandtl, Betz, Vier Abhandlungen zur Hydrodynamik und Aerodynamik, Gottinger Nachr, Gottingen; 1927, pp 88-92

[21] Hand .M.M, Simms .D.A, Fingersh .L.J, Jager .D.W, Cotrell .J.R, Schereck. S, Larwood. S.M. Technical Report – Unsteady Aerodynamics Experimental Phase VI: Wind Tunnel Test Configurations and Available Data Campaigns, National Renewable Energy Laboratory, 2001

[22] User Guide STAR-CCM+ Version 8.06. 2013

[23] Kim, I.C., Ph.D. Thesis, Korea Maritime and Ocean University, 2018

